5. SITE 1051[1]

Shipboard Scientific Party[2]

HOLE 1051A

Position: 30°03.1740′N, 76°21.4580′W

Date occupied: 1915 hr, 21 January 1997

Spud hole: 2230 hr, 21 January 1997

Date departed: 0200 hr, 27 January 1997

Time on hole: 126.75 hr (5 day, 6 hr, 45 min)

Seafloor (drill pipe measurement from rig floor, mbrf): 1994.0

Distance between rig floor and sea level (m): 11.3

Water depth (drill pipe measurement from sea level, m): 1982.7

Total depth (drill pipe measurement from rig floor, mbrf): 2630.3

Penetration (m): 644.6

Number of cores (including cores having no recovery): 73

Total core recovered (m): 599.89

Core recovery (%): 94.3

Oldest sediment cored:
    Depth (mbsf): 644.6
    Nature: claystone
    Age: late early Paleocene

Comments: Drilled through chert interval 381.6 to 389.9 mbsf.

HOLE 1051B

Position: 30°03.1860′N, 76°21.4712′W

Date occupied: 0200 hr, 27 January 1997

Spud hole: 0315 hr, 27 January 1997

Date departed: 1315 hr, 30 January 1997

Time on hole: 83.25 hr (3 day, 11 hr, 15 min)

Seafloor (drill pipe measurement from rig floor, mbrf): 1992.0

Distance between rig floor and sea level (m): 11.4

Water depth (drill pipe measurement from sea level, m): 1980.6

Total depth (drill pipe measurement from rig floor, mbrf): 2518.6

Penetration (m): 526.6

Number of cores (including cores having no recovery): 61

Total core recovered (m): 508.18

Core recovery (%): 96.9

Oldest sediment cored:
    Depth (mbsf): 526.6

    Nature: chalk
    Age: late Paleocene

Comments: Drilled from 374.1 to 376.1 mbsf.

Principal results: The location of Site 1051 was chosen to recover a thick Paleogene and Upper Cretaceous sequence. We anticipated that the Paleogene sequence would be much more expanded than at the other sites along the Blake Nose transect, as indicated by multichannel seismic (MCS) profile Line TD-5 (Fig. 3, "Introduction" chapter, back-pocket foldout, this volume). We also expected to recover the Cretaceous/Paleogene (K/T) boundary at intermediate water depths along the Blake Nose as well as a more expanded sequence of Upper Cretaceous sediments than at Site 1049. The drilling results demonstrate that the Paleogene section at Site 1051 is substantially thicker and includes younger Eocene sediments that are not found in the deeper water sites on the Leg 171B transect. The detailed shipboard biostratigraphy indicates that an almost complete sequence was recovered from the lowermost part of the upper Eocene to the upper part of the lower Paleocene. Unfortunately, we had to stop drilling in the lower Paleocene section because our drilling rate became too slow to justify continued extended core barrel (XCB) coring.

We recovered a 630-m-thick sequence from two holes drilled at Site 1051. The lowermost upper Eocene–lower Paleocene sequence contains mainly oozes and chalks composed predominantly of nannofossils, siliceous microfossils, and clay. The siliceous component consists of generally well-preserved radiolarians, sponge spicules, and diatoms. The clay content increases downhole in the lower Eocene and Paleocene. More than 25 ash layers were identified, spanning the majority of the Eocene sequence.

The sequence at Site 1051 is divided into four lithologic units based on color, microfossil content, and lithology. The top of Unit I consists of several meters of manganese nodules and phosphatic foraminifer sand, representing the present seafloor (Subunit IA). The 63.95-m-thick Subunit IB is characterized by yellow middle Eocene siliceous nannofossil ooze with foraminifers and clay. A sharp transition from yellow to green is used to divide Subunits IB and IC. This transition is not marked by any change in microfossil or lithologic components and is clearly diachronous relative to a similar color change observed at Sites 1050 and 1052. We interpret the color change as a downhole diagenetic change in oxidation state. Subunit IC consists of a 66-m-thick section of predominantly siliceous greenish gray nannofossil oozes. The transition between Subunits IC and ID occurs at the ooze to chalk transition. Subunit ID is a 257-m-thick sequence of siliceous nannofossil chalk and nannofossil chalk with siliceous microfossils.

Unit II is 6.6 m thick (376.1–382.7 meters below seafloor [mbsf]) and was only partly recovered. It consists of strongly altered, dark green, porcellanitic smectite clay and several interbeds of white silicified, foraminifer porcellanite. Several distinctive firmgrounds are present in the recovered material and display white foraminifer sand infilling burrows in the green clay. The entire interval of clay and silicified foraminifer porcellanite appears to coincide with a hiatus of about 2 m.y. in which bottom currents were episodically sufficient to thoroughly winnow the silt and clay fraction.

Lithologic Unit III is a 144.2-m-thick dark siliceous nannofossil chalk with clay. An apparently complete Paleocene–Eocene transition was recovered at Site 1051 and is partly laminated in the lowermost Eocene and in parts of the upper Paleocene, indicating decreased bioturbation. There

is also a distinctive soft-sediment breccia about 10 cm thick, 10 m below the Paleocene/Eocene boundary. The breccia occurs just above Chron C25n and may represent part of a small slump. The slump appears to be within or just below the stratigraphic interval at which many Paleocene benthic foraminifers became extinct. Benthic foraminifers are very rare for more than 10 m within the extinction interval, and the fauna is reduced from about 40 taxa to only 7. An impoverished benthic fauna is present for a least 50 m above the onset of the extinction interval.

Scattered crossbedded foraminifer sands occur at 450–470 mbsf. Unit IV is the oldest unit (lower Paleocene) and was recovered only in Hole 1051A. It is a 76.4-m-thick sequence of dark green siliceous nannofossil chalk to siliceous claystone or clayey spiculite.

Excellent age control was provided by biostratigraphy. Planktonic foraminifers and nannofossils are well preserved in the upper and middle Eocene. Preservation of both groups is variable in the lower Eocene and becomes poor near the Paleocene/Eocene boundary, where foraminifers are infilled with calcite and recrystallized. Nannofossil preservation improves in the upper Paleocene and is moderate throughout the lower Paleocene. Planktonic foraminifers are overgrown in the lower Paleocene but are still useful for biostratigraphy. Almost all lower upper Eocene to lower Paleocene nannofossil and planktonic foraminifer zones were recognized, indicating that the sequence is complete except for two hiatuses, each 1–2 m.y. long. The first hiatus coincides with the Unit II claystone and foraminifer packstone in the lowermost middle Eocene. A second hiatus occurs in the upper Paleocene where calcareous nannofossil Zone CP5 is missing.

The shipboard magnetostratigraphy is noisy, but a useful polarity pattern emerged from post-cruise analysis of discrete samples. Polarity interpretations are straightforward for the middle Eocene through upper Paleocene portions of the section (Chrons C17n–C26) and corroborate the biostratigraphic information. A well-defined magnetostratigraphy was obtained for the lower Paleocene, but the sequence of polarity zones does not match the nannofossil biostratigraphy.

Color cycles are visible in nearly the entire sequence, with the exception of lithologic Subunits IA and IB and Unit II. The lower half of Subunit ID (between 300 and 380 mbsf) is badly biscuited by XCB coring, and the record of color cycles is incomplete. The cycles in the middle and lower Eocene may represent the 41-k.y. obliquity periodicity, as judged from sedimentation rates determined by the biostratigraphy. In contrast, the Paleocene color records correspond more closely to a 23-k.y. precessional periodicity. The combination of lithologic cycles in the core and downhole log data should provide a high-quality cyclostratigraphy that could enhance both the magnetochronology and biochronologies as well as improve correlation between sites in the depth transect.

Hole 1051A was logged with three tool strings: the triple-combo (natural gamma ray, resistivity, and formation density), the Formation MicroScanner (FMS), and the geological high-sensitivity magnetic tool (GHMT). The sonic digital tool was not used because of an apparent electrical incompatibility between the sonic and FMS tools that we were not able to fix during the time available for logging. Hole conditions were excellent, with an average diameter of 11 in and sporadic washouts of as much as 15 cm. The hole was logged between 120 and 643 mbsf. Most of the logs clearly define the structure and depth of the lower to middle Eocene unconformity, as well as a prominent interval of soft-sediment deformation in the lower Eocene between 455 and 475 mbsf. Likewise, there are pronounced increases in gamma ray, thorium, and magnetic susceptibility at about 510 mbsf that correspond to the depth of the benthic foraminifer extinction interval, lithologic evidence for soft-sediment deformation, and an increase in clay content. The transition from the upper Paleocene siliceous nannofossil chalk to diatomaceous nannofossil claystones (lithologic Unit IV) is associated with a gradual drop in magnetic susceptibility as well as increases in gamma-ray attenuation and uranium content. The FMS produced high-quality logs in two separate runs. The resistivity and magnetic susceptibility data from the FMS tool should help produce a complete cyclostratigraphy for the Paleocene to lower middle Eocene that will complement and check the cyclostratigraphies compiled from core measurements.

Sediments at Site 1051 are very low in organic matter, and gas samples consist largely of small quantities of methane and ethane. Both the inorganic chemistry of the pore waters and analysis of gas samples detected marked changes in composition above and below the claystone and foraminifer packstone at about 380 mbsf. For example, strontium, lithium, calcium, and magnesium all show a clear shift in concentration across the hiatus. Apparently, the claystone acts as a seal that prevents the upward flow of gas and pore waters. The same level also corresponds to an abrupt drop in carbonate content from about 75% to about 50%.

BACKGROUND AND OBJECTIVES

Background

Site 1051 is located on an erosional remnant of the Paleogene sedimentary cover of the Blake Nose. The Paleogene section at Site 1051 is more expanded and includes younger sediments than at the deeper water sites on the Leg 171B transect. The location of Site 1051 was chosen to drill through the Paleogene and Maastrichtian–Campanian sediments to recover an expanded Paleogene and Upper Cretaceous section correlative with those at other sites on the Leg 171B transect. The present depth of 1983 meters below sea level (mbsl) is 317 m shallower than Site 1050 and about 690 m shallower than Site 1049. This depth transect will allow studies of the vertical structure of the Paleogene and Cretaceous oceans.

Objectives

MCS profile Line TD-5 (see Figs. 3 [back-pocket foldout] and 4 in the "Introduction" chapter, this volume) suggests that the Eocene interval is more expanded at Site 1051 than at Sites 1049 and 1050. Reflectors in the MCS line indicate that the substantial thickness of middle Eocene and younger sediments at Site 1051 was either eroded or never deposited at the deeper water sites. The upper Eocene and younger section is expected to contain a high-temporal-resolution record of ocean structure, magnetic reversals, and biological evolution, particularly during times of rapid climate change, such as the Eocene–Oligocene onset of glaciation and the early to middle Eocene cooling.

Another objective of drilling at Site 1051 was to recover the K/T boundary at intermediate water depths along the Blake Nose. Comparisons could then be made between the tektite layer of this interval and that observed at Site 1049. In addition, Site 1051 was selected to drill through a more expanded sequence of Upper Cretaceous sedimentary rocks than was drilled at Site 1049. Recovering the Cretaceous interval would provide benthic foraminifers for the reconstruction of intermediate-water conditions within the Cretaceous as well as plankton for refining the biochronology and surface-water conditions.

Finally, we believed that climate-controlled color and lithologic cycles would be pronounced at Site 1051 because of its more landward position and possibly higher clay content relative to the deeper water sites. The combination of lithologic cycles in cores and logs should provide a high-quality cyclostratigraphy to enhance both the magnetochronology and biochronology as well as to improve correlation among sites along the depth transect.

OPERATIONS

Hole 1051A

After the transit from Site 1050, we deployed a beacon at 1915 hr on 21 January 1997 at the Global Positioning System (GPS) position at Site 1051 (proposed site BN-3). The bottom-hole assembly (BHA) was made up with a $10^1/_8$-in polycrystalline diamond compact (PDC) fixed-cutter bit in the hope of improving upon the performance (rate of penetration [ROP]) of the roller cone bit used at the previous two

sites. We decided to spud Hole 1051A with the XCB coring system because of the potential for damage if we spudded into the surficial layer of manganese nodules with the advanced hydraulic piston corer (APC). The driller gently lowered the bit, and, based on a reduction in drill-string weight, determined that the seafloor was at 1994.0 meters below rig floor (mbrf). The rig floor was 11.3 and 11.4 mbsl for Holes 1051A and 1051B, respectively. Core 171B-1051A-1X was taken to 5.8 mbsf. APC coring continued from 5.8 to 138.8 mbsf with excellent recovery. Core 16H advanced from 138.8 to 148.3 mbsf with a full stroke. However, when 100,000 lb of overpull failed to retrieve the barrel, we had to drill over the stuck core barrel to release it from the formation. Cores 4H through 16H were oriented using the tensor tool.

We then resumed XCB coring and proceeded with excellent recovery until Core 41X advanced only 2.3 m when it encountered a hard chert layer at 381.6 mbsf. The only practical manner of advancing beyond this depth with the XCB was to drop a core barrel with a center bit and to drill ahead 8.3 m to 389.9 mbsf. Although the chert layer was only ~1 m thick, the extra advance was necessary to verify that we had completely penetrated the chert layer and to push the tungsten carbide inserts (TCI) that had been stripped from the XCB cutting shoe while attempting Core 41X into the borehole wall. The extreme hardness of the TCIs could damage the main PDC bit.

We resumed XCB coring at 389.9 mbsf and advanced past the original objective of 600 mbsf to a total depth of 644.6 mbsf (Table 1), where coring operations were terminated because of the slow ROP (2.0 m/hr for the last core). The K/T boundary was assumed to lie perhaps another 30–40 m beneath total depth. To attain this depth with the present ROP would have taken another 12 hr of rotation.

At 0815 hr on 25 January, the bit was raised back to 105 mbsf for logging. Raising the drill pipe to logging depth was complicated by the discovery that more than 400 m of monofilament fishing line was wrapped around eight joints of drill pipe. As each joint was lifted past the dual-elevator stool, the rig crew cut off small sections of the fishing line. This process was made more difficult by the presence of large, sharp fishing hooks. Because there were no fishing boats in the area, we assumed that the line drifted in the Gulf Stream for some distance before adhering to the drill string.

By 2030 hr on 25 January, the logging equipment was being rigged up. This took longer than the normal 30 min because of the extra rigging required to compensate for the absence of the wireline heave compensator. The first log was the triple-combo, which logged the entire hole. The data are of good quality and indicate that the hole was in excellent condition, with a smooth bore that ranged in diameter from just under 10 in to a maximum of 14 in. The second log was the FMS, which required extensive troubleshooting before it was eventually run successfully without the sonic tool. The heave of the ship and the lack of the wireline heave compensator will require considerable reprocessing to remove the effect of the tool's vertical motion. The last tool run was the GHMT, which provided good-quality magnetic susceptibility data.

Once logging was finished and the tools were recovered, the borehole was displaced with 35 bbl of 10.5 lb/gal mud. At 0200 hr on 27 January, the bit cleared the mudline and the vessel offset 30 m northwest to start Hole 1051B.

Hole 1051B

The driller tagged the seafloor at 1992 mbrf and spudded Hole 1051B with the XCB at 0315 hr on 27 January. After passing through a 2-m-thick hard crust and advancing to 4.8 mbsf, the XCB barrel was recovered, and APC coring was initiated. We APC cored to 135.0 mbsf, just above the depth of the last APC core on the first hole; this avoided consuming an extra hour drilling over another stuck core barrel. APC Cores 171B-1051B-4H through 15H were oriented with the tensor tool, and Adara temperature measurements were obtained at 33, 62, and 87 mbsf (Cores 4H, 7H, and 11H, respectively).

We advanced XCB coring to 374.1 mbsf with excellent recovery. At this depth, we drilled through the chert layer with a center bit. After 70 min of rotation and only 2 m of advancement, we finally penetrated the chert layer, and the center bit was retrieved. We resumed XCB coring to a total depth of 526.6 mbsf (Table 1).

After we displaced the hole with 35 bbl of 10.5 lb/gal mud, we retrieved the drill string. The PDC XCB bit was missing 8 of the 13 cutting elements. Although the bit body was in gauge, the bit was too worn and was retired from service. At 1315 hr on 31 January, the drilling equipment had been secured and the vessel began the transit to Site 1052.

LITHOSTRATIGRAPHY

Description of Lithologic Units

The sediment recovered from two holes drilled at Site 1051 is 630 m thick and comprises a lowermost upper Eocene–lower Paleocene ooze and chalk composed predominantly of nannofossils, siliceous microfossils, and clay. The siliceous component consists of radiolarians, sponge spicules, and diatoms. The clay content increases downhole in the lower Eocene–Paleocene section. Alternations of dark and lighter intervals, which we infer to represent Milankovich-type climate cycles, are visible in nearly the entire sequence. A striking component is the more than 25 volcanic ash layers in the Eocene–upper Paleocene sequence (Fig. 1).

The sequence was divided into four lithologic units based on color, microfossil content, and lithology (Fig. 2; Table 2). Unit I consists of an uppermost layer containing manganese nodules that represents the present seafloor (Subunit IA). The 61-m-thick Subunit IB is characterized by yellow middle Eocene siliceous nannofossil ooze with foraminifers and clay. A sharp transition from yellow to green is used to divide Subunits IB and IC. This transition is not marked by any change in microfossil, lithologic, or physical characteristics (see "Biostratigraphy," "Physical Properties," "Inorganic Chemistry," "Organic Geochemistry," and "Downhole Logging" sections, this chapter) and is clearly diachronous relative to a similar color change observed at Site 1050 (Fig. 3). This color change is also observed at Sites 1052 and 1053. It is probably related to a downhole diagenetic change in oxidation state, as manganese oxide specks are present in the yellowish Subunit IB and pyrite occurs farther downhole in the greenish Subunit IC. The sediment of Subunit IC is ~56 m thick and is predominantly greenish gray, siliceous nannofossil ooze.

The transition between Subunits IC and ID occurs at the change from ooze to chalk, which coincides with both a *P*-wave velocity change (see "Physical Properties" section, this chapter) and the switch from APC to XCB coring. Subunit ID is an ~260-m-thick sequence of siliceous nannofossil chalk and nannofossil chalk with siliceous microfossils. The lower parts of Subunit IC and Subunit ID display cyclic light–dark alternations (Fig. 4), presumably related to the 40-k.y. obliquity cycle (see "Physical Properties" and "Core-Core Integration" sections, this chapter). The transition from light to dark intervals is usually sharp and conspicuously burrowed.

Lithologic Unit II represents a condensed section in the lower to middle Eocene transition and contains a strongly altered dark green porcellanitic smectite clay (Fig. 5) overlying a silicified foraminifer porcellanite. The clay is interpreted as a bentonite, whereas the silicified foraminifers of the porcellanite suggest strong winnowing. Unit II is 6.8 m thick (376.1–382.9 mbsf) and was poorly recovered. The transition between Units I and II was not recovered. The transition from Unit II to Unit III is marked by a change from interbedded wavy laminated chert to a siliceous nannofossil chalk at Section 171B-1051B-45X-1, 7 cm. This transition corresponds to a significant change in chemistry and physical properties downhole (see "Physical Properties," "Inorganic Geochemistry," "Organic Geochemistry," and "Downhole Logging" sections, this chapter).

Table 1. Site 1051 coring summary.

Core, interval (cm)	Date (January 1997)	Time (UTC)	Depth (mbsf)	Length cored (m)	Length recovered (m)	Recovery (%)
171B-1051A-						
1X	22	0440	0.0-5.8	5.8	0.00	0.0
2H	22	0500	5.8-15.3	9.5	9.47	99.7
3H	22	0535	15.3-24.8	9.5	10.04	105.7
4H	22	0625	24.8-34.3	9.5	9.76	103.0
5H	22	0710	34.3-43.8	9.5	9.83	103.0
6H	22	0745	43.8-53.3	9.5	9.85	103.0
7H	22	0830	53.3-62.8	9.5	9.63	101.0
8H	22	0910	62.8-72.3	9.5	9.82	103.0
9H	22	0940	72.3-81.8	9.5	8.80	92.6
10H	22	1020	81.8-91.3	9.5	9.26	97.5
11H	22	1100	91.3-100.8	9.5	8.76	92.2
12H	22	1130	100.8-110.3	9.5	9.59	101.0
13H	22	1215	110.3-119.8	9.5	9.65	101.0
14H	22	1300	119.8-129.3	9.5	10.03	105.6
15H	22	1340	129.3-138.8	9.5	9.69	102.0
16H	22	1530	138.8-148.3	9.5	10.10	106.3
17X	22	1630	148.3-158.2	9.9	8.55	86.3
18X	22	1715	158.2-167.8	9.6	9.02	93.9
19X	22	1800	167.8-177.4	9.6	9.76	101.0
20X	22	1840	177.4-187.0	9.6	9.78	102.0
21X	22	1945	187.0-196.6	9.6	9.82	102.0
22X	22	2030	196.6-206.2	9.6	6.07	63.2
23X	22	2105	206.2-215.8	9.6	9.80	102.0
24X	22	2145	215.8-225.4	9.6	9.65	100.0
25X	22	2220	225.4-235.0	9.6	9.87	103.0
26X	22	2300	235.0-244.6	9.6	9.65	100.0
27X	22	2340	244.6-254.2	9.6	9.89	103.0
28X	23	0005	254.2-263.8	9.6	9.80	102.0
29X	23	0110	263.8-273.4	9.6	9.64	100.0
30X	23	0210	273.4-283.0	9.6	7.07	73.6
31X	23	0315	283.0-292.6	9.6	9.82	102.0
32X	23	0430	292.6-302.2	9.6	7.83	81.5
33X	23	0600	302.2-311.8	9.6	5.57	58.0
34X	23	0730	311.8-321.5	9.7	9.93	102.0
35X	23	0905	321.5-331.1	9.6	9.02	93.9
36X	23	1045	331.1-340.7	9.6	9.81	102.0
37X	23	1300	340.7-350.4	9.7	6.39	65.9
38X	23	1420	350.4-360.1	9.7	9.44	97.3
39X	23	1545	360.1-369.7	9.6	9.65	100.0
40X	23	1710	369.7-379.3	9.6	7.50	78.1
41X	23	1900	379.3-381.6	2.3	1.30	56.5
*****Drilled 381.6 to 389.9 mbsf *****						
42X	23	2140	389.9-399.5	9.6	9.91	103.0
43X	23	2250	399.5-409.1	9.6	9.98	104.0
44X	23	2355	409.1-418.7	9.6	9.89	103.0
45X	24	0115	418.7-428.3	9.6	9.90	103.0
46X	24	0210	428.3-437.9	9.6	9.88	103.0
47X	24	0340	437.9-447.5	9.6	9.88	103.0
48X	24	0450	447.5-457.1	9.6	9.80	102.0
49X	24	0630	457.1-460.2	3.1	3.38	109.0
50X	24	0845	460.2-466.8	6.6	7.21	109.0
51X	24	1100	466.8-476.5	9.7	9.78	101.0
52X	24	1245	476.5-486.1	9.6	9.93	103.0
53X	24	1400	486.1-495.7	9.6	9.87	103.0
54X	24	1525	495.7-505.3	9.6	8.48	88.3
55X	24	1640	505.3-514.9	9.6	5.57	58.0
56X	24	1800	514.9-524.5	9.6	9.84	102.0
57X	24	1910	524.5-534.1	9.6	9.90	103.0
58X	24	2030	534.1-543.7	9.6	9.83	102.0
59X	24	2150	543.7-553.3	9.6	9.44	98.3
60X	24	2320	553.3-556.4	3.1	2.88	92.9
61X	25	0125	556.4-562.9	6.5	5.75	88.4
62X	25	0330	562.9-572.5	9.6	9.75	101.0
63X	25	0450	572.5-582.1	9.6	9.82	102.0
64X	25	0610	582.1-591.8	9.7	10.09	104.0
65X	25	0720	591.8-601.5	9.7	9.87	102.0
66X	25	0845	601.5-611.1	9.6	9.83	102.0
67X	25	1040	611.1-620.7	9.6	9.01	93.8
68X	25	1225	620.7-624.3	3.6	4.15	115.0
69X	25	1450	624.3-630.4	6.1	1.02	16.7
70X	25	1630	630.4-634.5	4.1	0.81	19.7
71X	25	1900	634.5-640.0	5.5	0.29	5.3
72X	25	2050	640.0-641.6	1.6	2.46	154.0
73X	25	2255	641.6-644.6	3.0	2.75	91.6

Core, interval (cm)	Date (January 1997)	Time (UTC)	Depth (mbsf)	Length cored (m)	Length recovered (m)	Recovery (%)
Coring totals:				636.3	599.86	94.3
Drilled:				8.3		
Total:				644.6		
171B-1051B-						
1X	27	0845	0.0-4.8	4.8	0.00	0.0
2H	27	0920	4.8-14.3	9.5	10.03	105.6
3H	27	1000	14.3-23.8	9.5	9.66	101.0
4H	27	1115	23.8-33.3	9.5	9.92	104.0
5H	27	1240	33.3-42.8	9.5	10.04	105.7
6H	27	1340	42.8-52.3	9.5	9.79	103.0
7H	27	1455	52.3-61.8	9.5	10.35	108.9
8H	27	1540	61.8-71.3	9.5	9.77	103.0
9H	27	1630	71.3-80.8	9.5	10.05	105.8
10H	27	1735	80.8-87.3	6.5	9.91	152.0
11H	27	1830	87.3-96.8	9.5	9.12	96.0
12H	27	1910	96.8-106.3	9.5	9.36	98.5
13H	27	1955	106.3-115.8	9.5	9.62	101.0
14H	27	2030	115.8-125.3	9.5	9.75	102.0
15H	27	2115	125.3-134.8	9.5	9.46	99.6
16X	27	2215	134.8-143.3	8.5	9.14	107.0
17X	27	2255	143.3-152.9	9.6	9.62	100.0
18X	27	2330	152.9-162.5	9.6	9.77	102.0
19X	28	0030	162.5-172.1	9.6	6.19	64.5
20X	28	0100	172.1-181.7	9.6	9.58	99.8
21X	28	0200	181.7-191.2	9.5	8.77	92.3
22X	28	0240	191.2-200.8	9.6	9.78	102.0
23X	28	0355	200.8-210.5	9.7	9.74	100.0
24X	28	0440	210.5-220.1	9.6	9.70	101.0
25X	28	0550	220.1-229.7	9.6	9.83	102.0
26X	28	0700	229.7-239.4	9.7	9.82	101.0
27X	28	0810	239.4-249.0	9.6	7.11	74.0
28X	28	0925	249.0-258.6	9.6	9.81	102.0
29X	28	1040	258.6-268.2	9.6	9.83	102.0
30X	28	1200	268.2-277.8	9.6	9.79	102.0
31X	28	1315	277.8-287.4	9.6	9.78	102.0
32X	28	1400	287.4-293.6	6.2	7.58	122.0
33X	28	1505	293.6-303.2	9.6	9.83	102.0
34X	28	1620	303.2-308.9	5.7	3.89	68.2
35X	28	1735	308.9-312.9	4.0	6.58	164.0
36X	28	1840	312.9-322.5	9.6	9.69	101.0
37X	28	2000	322.5-332.1	9.6	9.81	102.0
38X	28	2100	332.1-341.7	9.6	5.73	59.7
39X	28	2215	341.7-351.3	9.6	9.75	101.0
40X	28	2325	351.3-360.9	9.6	9.90	103.0
41X	29	0025	360.9-370.5	9.6	9.82	102.0
42X	29	0120	370.5-374.1	3.6	3.13	86.9
*****Drilled 374.1 to 376.1 mbsf*****						
43X	29	0415	376.1-380.1	4.0	0.91	22.7
44X	29	0540	380.1-382.7	2.6	0.85	32.7
45X	29	0750	382.7-389.7	7.0	3.16	45.1
46X	29	0950	389.7-399.3	9.6	8.80	91.6
47X	29	1130	399.3-409.0	9.7	9.80	101.0
48X	29	1305	409.0-418.6	9.6	9.83	102.0
49X	29	1445	418.6-428.3	9.7	9.84	101.0
50X	29	1645	428.3-437.9	9.6	9.84	102.0
51X	29	1830	437.9-447.6	9.7	9.83	101.0
52X	29	2025	447.6-457.3	9.7	9.89	102.0
53X	29	2155	457.3-466.9	9.6	0.80	8.3
54X	29	2340	466.9-476.5	9.6	9.85	102.0
55X	30	0115	476.5-486.1	9.6	9.87	103.0
56X	30	0225	486.1-495.7	9.6	9.50	98.9
57X	30	0340	495.7-502.3	6.6	6.99	106.0
58X	30	0545	502.3-506.3	4.0	6.16	154.0
59X	30	0800	506.3-510.9	4.6	4.76	103.0
60X	30	1015	510.9-516.9	6.0	6.80	113.0
61X	30	1320	516.9-526.6	9.7	9.90	102.0
Coring totals:				524.6	508.18	96.9
Drilled:				2.0		
Total:				526.6		

Note: An expanded version of this coring summary table that includes lengths and depths of sections and comments on sampling is included on CD-ROM (back pocket, this volume).

Lithologic Unit III is a 178-m-thick dark siliceous nannofossil chalk with clay. An apparently complete Paleocene/Eocene transition recovered in both holes at Site 1051 is laminated in the lowermost Eocene, indicating decreased bioturbation. Sporadic foraminifer cross-bedded sands occur at 450–470 mbsf. Some upper Paleocene sediment is evidently slumped.

Unit IV is the oldest unit (lower Paleocene) and was recovered only in Hole 1051A. Unit IV is an ~76-m-thick sequence of dark green siliceous claystone and siliceous nannofossil chalk. The top of Unit IV is placed at the downhole change to darker colors.

Units I through IV include more than 25 vitric ash layers in the upper middle Eocene–upper Paleocene interval from 6.5 to 456.4 mbsf. The ash layers are fine grained and contain biotite in varying amounts (Table 3; Fig. 1). They range in thickness from a few millimeters to 3 cm. A thick 2-cm ash layer found in both Holes 1051A and 1051B at 189.2 mbsf and 187.2 mbsf, respectively, apparently correlates to
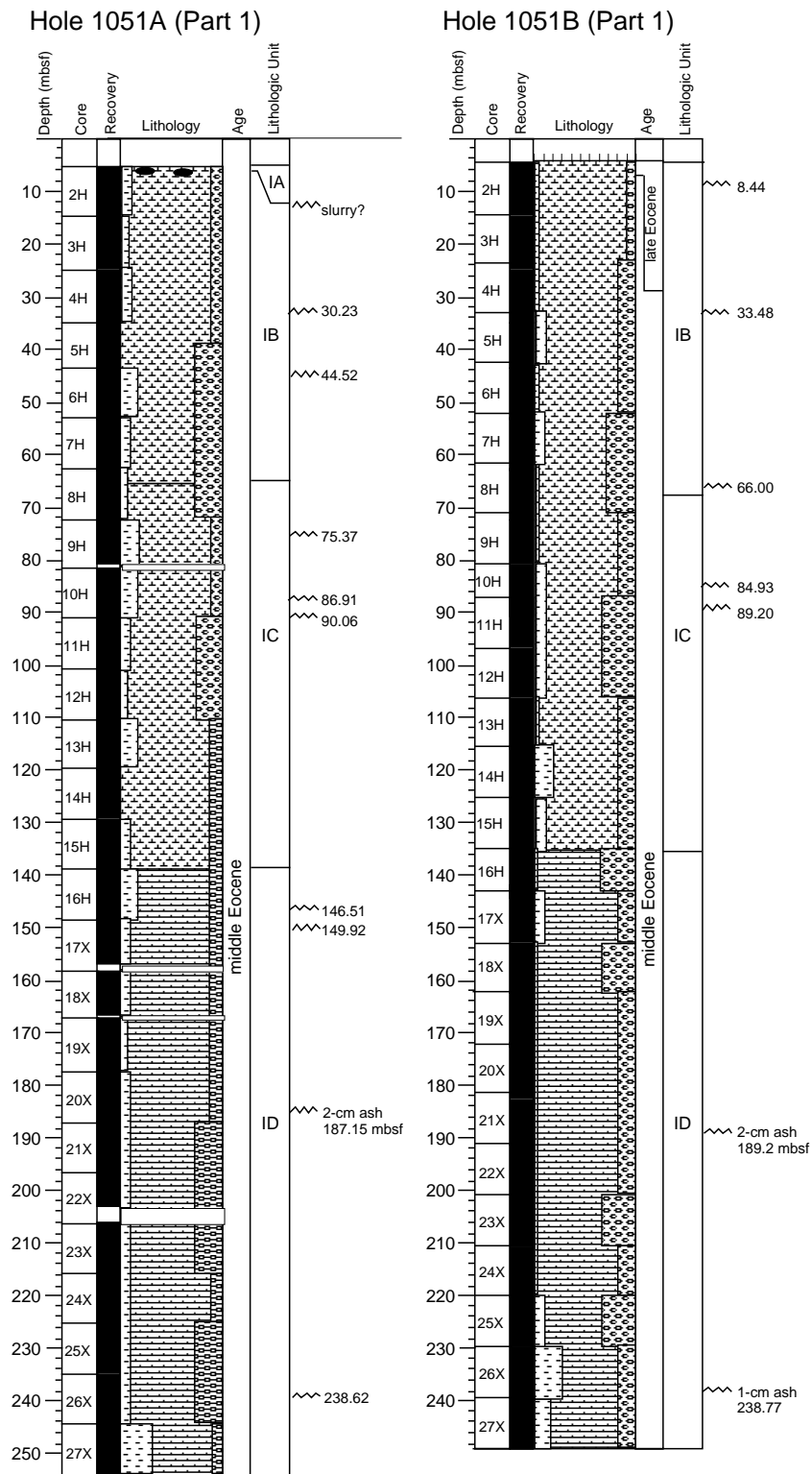
Figure 1. Summary of lithology, core recovery, age for sediment recovered, and correlation of ash layers in Holes 1051A and 1051B. Symbols are the same as those used in Figure 1, "Site 1049" chapter (this volume).

an ash layer of similar thickness at Site 1050 in interval 171B-1050A-1H-5, 11–13 cm. About 460 m of section at Site 1051 is age equivalent to about 320 m of section at Site 1050.

Unit I

Description: Manganese oxide nodules, nannofossil ooze with siliceous microfossils to siliceous nannofossil ooze, and siliceous nannofossil chalk to nannofossil chalk with siliceous microfossils

Intervals: 171B-1051A-2H-1, 0 cm, through 40X-CC; 171B-1051B-2H-1 through 41X-CC
Depth: 0–379.3 mbsf, Hole 1051A; 4.8–374.1 mbsf, Hole 1051B
Thickness: 379.3 m, Hole 1051A; 369.3 m, Hole 1051B
Age: Pleistocene to middle Eocene

Lithologic Unit I is divided into four subunits. The uppermost Subunit IA is a 2.6-m-thick layer with Mn nodules similar to lithologic Subunit IA at Sites 1049 and 1050. Below this, Subunit IB is
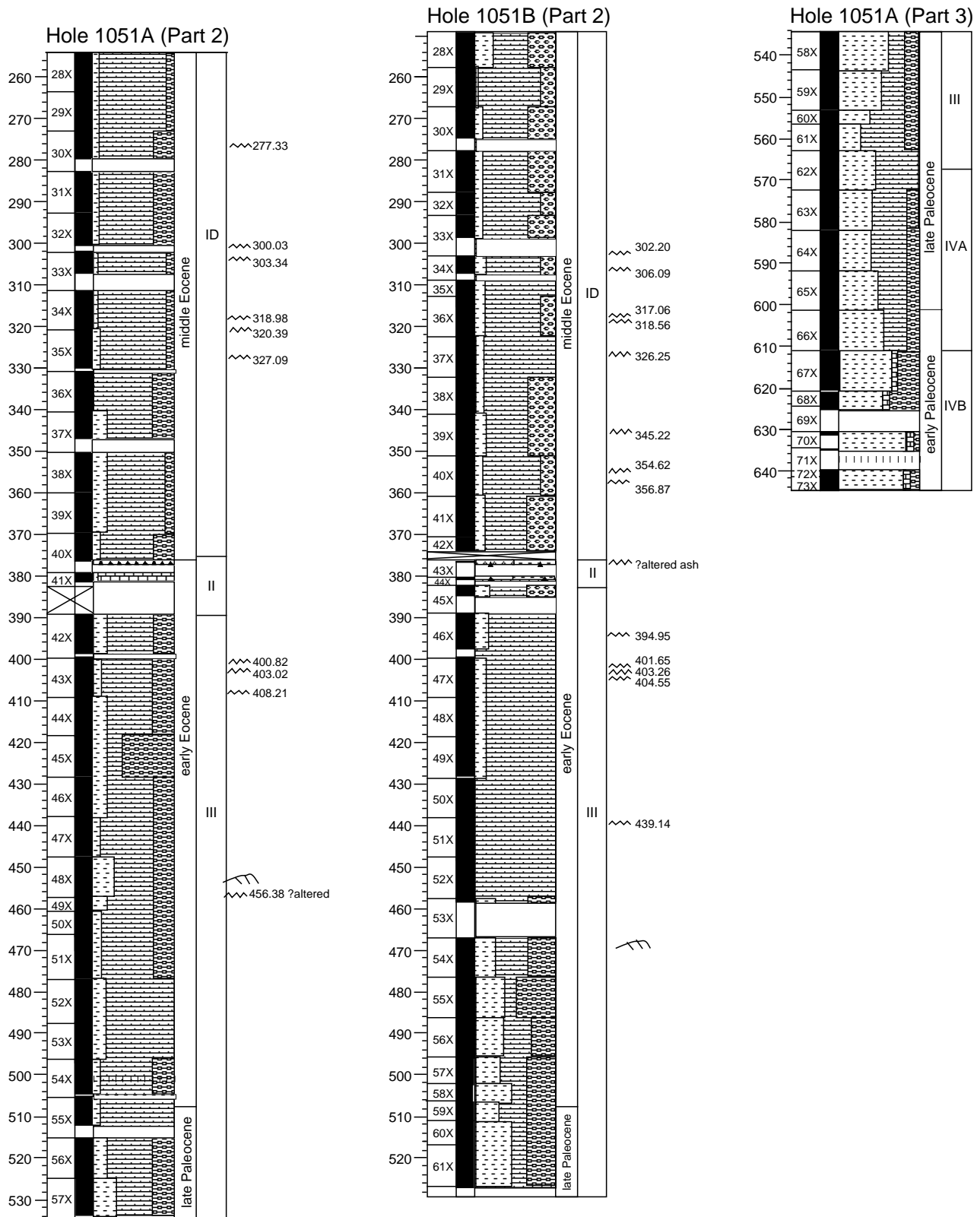
Figure 1 (continued).
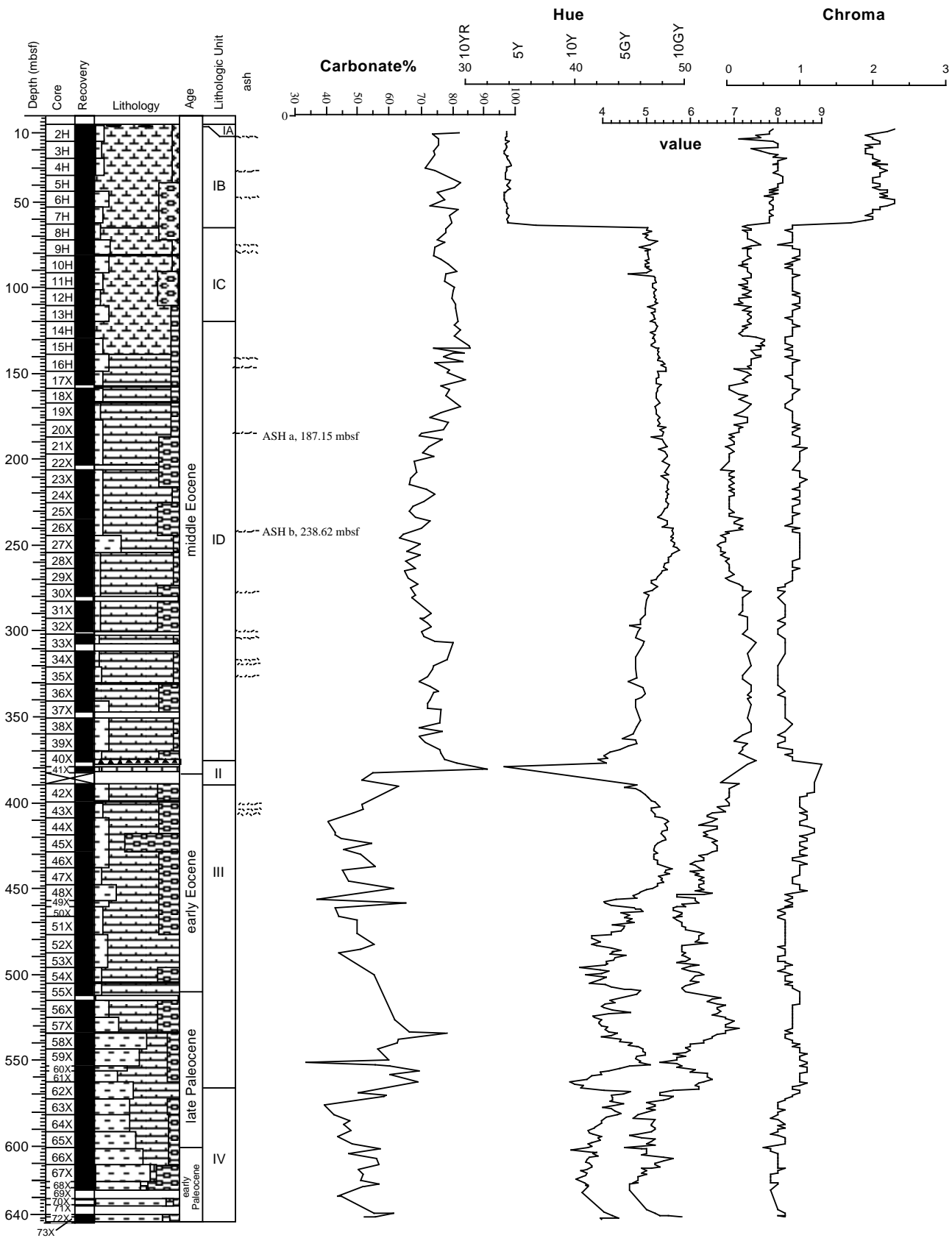
Figure 2. Carbonate content (see "Organic Geochemistry" section, this chapter), hue, value, and chroma measured with the Minolta spectrophotometer for Hole 1051A.

Table 2. Summary of Site 1051 lithologic units.

Lithologic unit/subunit	Hole 1051A	Hole 1051B	Age	Lithology
IA	Interval 2H-1, 0 cm, to 2H-2, 115 cm 0-2.65 mbsf	Not recovered	Pleistocene?	Mn oxide nodules
IB	Interval 2H-2, 115 cm, to 8H-2, 55 cm 2.65-63.64 mbsf	Interval 2H-1, 0 cm, to 8H-5, 95 cm 4.8-68.75 mbsf	middle Eocene to late Eocene (1051B)	Nannofossil ooze with siliceous microfossils to siliceous nannofossil ooze
IC	Interval 8H-2, 55 cm, to 13H-CC 63.64-119.18 mbsf	Interval 5H-2, 79 cm, to 15H-CC 68.75-134.8 mbsf	middle Eocene	Nannofossil ooze with siliceous microfossils to siliceous nannofossil ooze
ID	Interval 14X-1 to 40X-CC 119.18-379.3 mbsf	Interval 16X-1, 0 cm, to 42X-CC 134.8-374.1 mbsf	middle Eocene	Siliceous nannofossil chalk to nannofossil chalk with siliceous microfossils
II	Interval 41X-1, 0 cm, to 41X-CC 379.3-381.6 mbsf (381.6-389.9 mbsf drilled without coring)	Interval 43X-1, 0 cm, to 45X-1, 20 cm 376.1-382.9 mbsf	middle Eocene	Porcellanized foraminifer packstone, olive green claystone, clay-rich firmground
III	Interval 42X-1, 0 cm, to 62X-5, 104 cm 389.9-567.94 mbsf	Interval 45X-1, 20 cm, to 61X-CC 382.9-526.7 mbsf	early Eocene to late Paleocene	Siliceous nannofossil chalk to siliceous nannofossil chalk with clay
IV	Interval 62X-5 104 cm, to 73X-CC 567.94-644.6 mbsf	Not recovered	early to late Paleocene	Siliceous claystone with nannofossils, clayey spiculite with carbonate grains, and clayey nannofossil chalk with siliceous microfossils
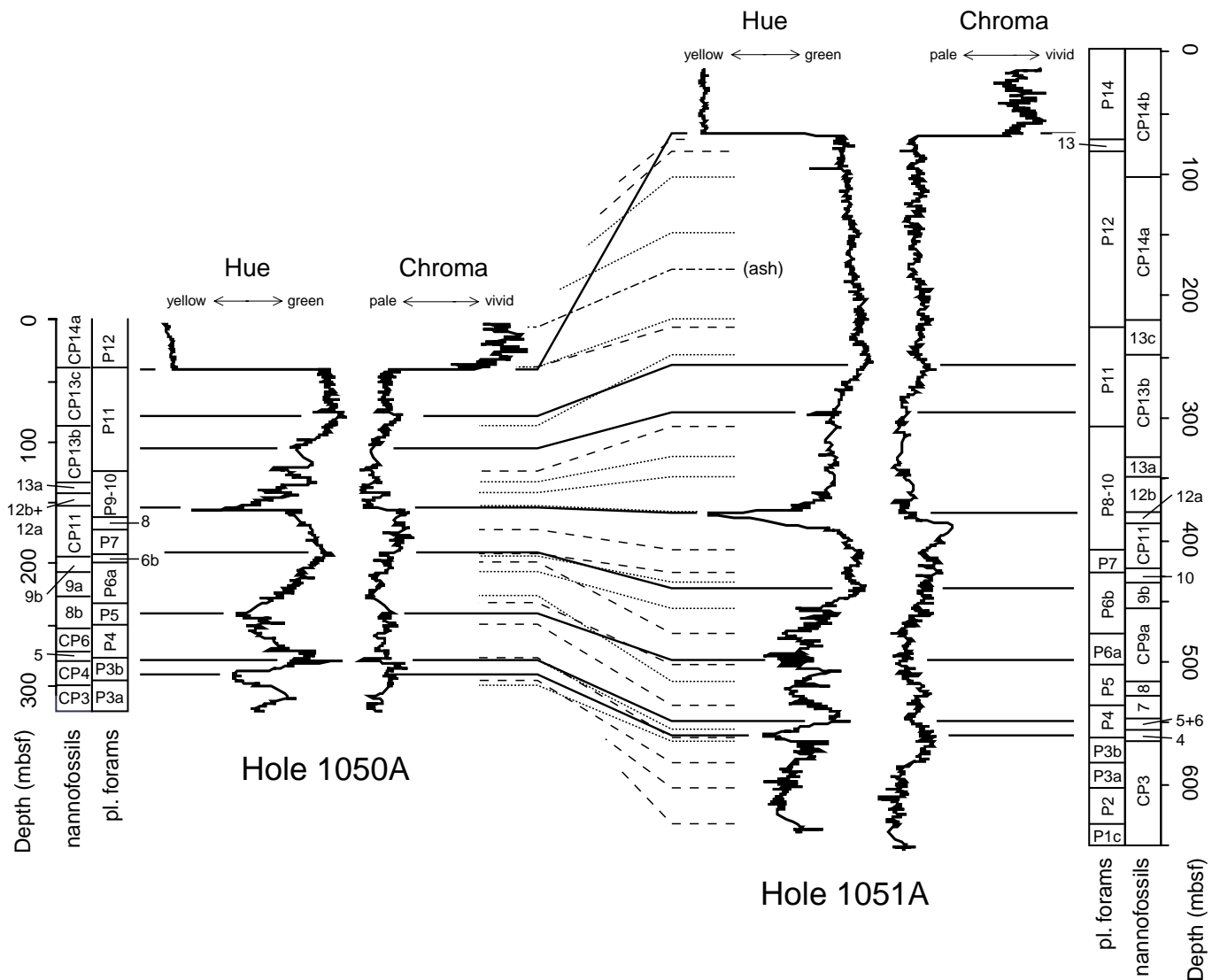
Figure 3. Comparison of the correlation between Holes 1050A and 1051A, based on nannofossil datums (dotted lines), planktonic foraminifer datums (dashed lines), and sediment color, expressed as Munsell hue and chroma (solid lines). Color was measured with a Minolta CM-2002 spectrophotometer. Because of limitations in the plotting hardware and software, the color data are plotted at 10-point averages through the sections. Small-scale disagreement can be attributed to sampling resolution in the paleontologic studies. Larger scale disagreement occurs only in intervals where the fossils are poorly preserved.
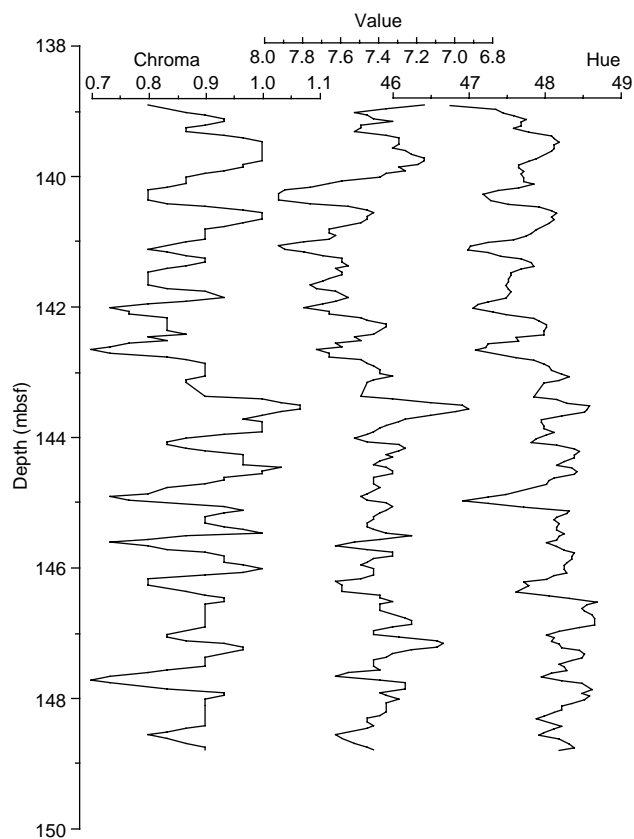
Figure 4. Profiles of spectrophotometer measurements (three-point moving average) in Core 171B-1051A-16H. The cycles of chroma have an average cycle length of about 100 cm and, when calibrated against the average sedimentation rate of 24 m/m.y. (see "Biostratigraphy" section, this chapter), are compatible with the obliquity cycle (±40 k.y.).

~61 m thick and is composed of pale yellow middle Eocene nannofossil ooze with siliceous microfossils to siliceous nannofossil ooze (see Section 5 on CD-ROM, back pocket, this volume). A distinctive color change from pale yellow to light greenish gray marks the top of Subunit IC in Core 171B-1051A-8X. Subunit IC is ~56 m thick and, like Subunit IB, consists of nannofossil ooze with siliceous microfossils to siliceous nannofossil ooze. The downhole transition from ooze to chalk is gradual, and the last occurrence (LO) of ooze constitutes the upper boundary of Subunit ID. This middle Eocene subunit is ~260 m thick and consists of chalk with varying amounts of nannofossils, siliceous microfossils, and clay. Ash layers identified in Unit I are summarized in Table 3.

Subunit IA

Description: Manganese oxide nodules
Interval: 171B-1051A-2H-1, 0 cm, to 2H-2, 115 cm
Depth: 0–2.6 mbsf, Hole 1051A
Thickness: 2.6 m, Hole 1051A
Age: ?Pleistocene

This subunit was recovered as a 2.6-m-thick drilling slurry of pale yellow nannofossil ooze with manganese nodules up to 5 cm in diameter. Large (medium- to coarse-sand sized) gooseneck barnacle plates, and brown and black foraminifers are common throughout. This Mn-rich interval most likely corresponds to the Mn oxide layer recovered at the top of the sections at Sites 1049 and 1050, where it was also designated as lithologic Subunit IA.
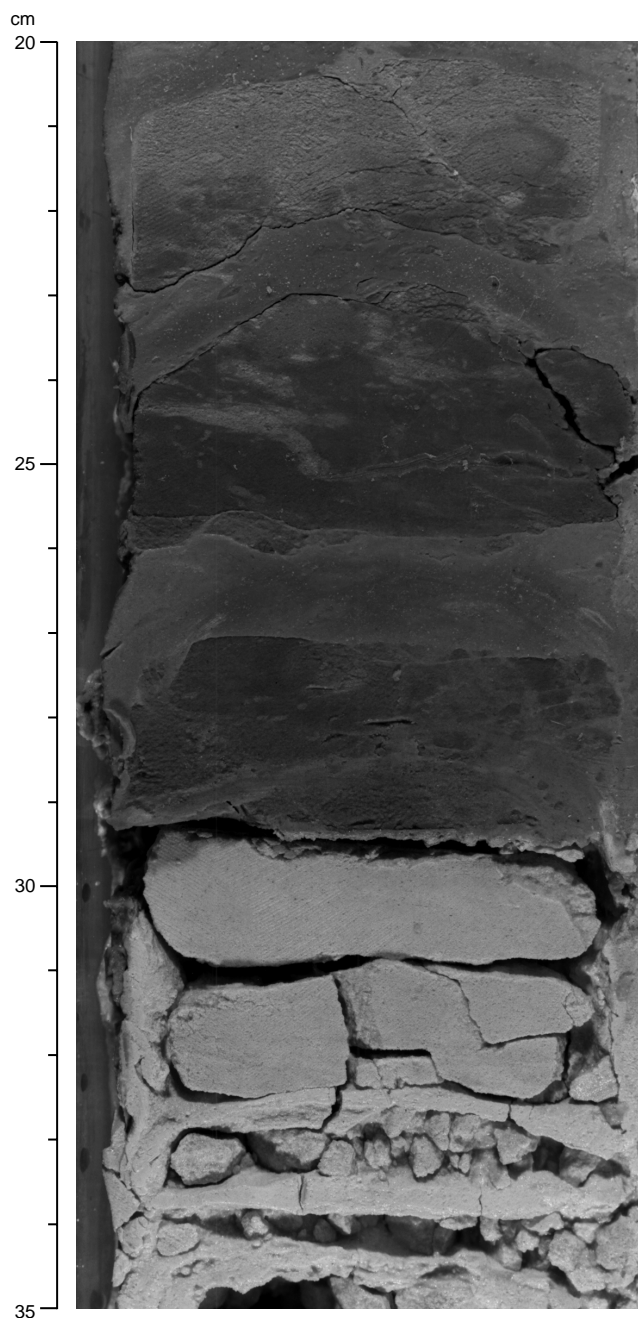
Figure 5. Interval 171B-1051B-43X-1, 20–35 cm. Two types of lithology are present in lithologic Unit II: a slightly bioturbated olive green smectitic clay overlying silicified foraminifer porcellanite with rare quartz silt.

Subunit IB

Description: Nannofossil ooze with siliceous microfossils to siliceous nannofossil ooze
Intervals: 171B-1051A-2H-2, 115 cm, to 8H-2, 55 cm; 171B-1051B-2H-1 to 8H-5, 95 cm.
Depth: 2.6–63.6 mbsf, Hole 1051A; 4.8–68.8 mbsf, Hole 1051B
Thickness: 61.0 m, Hole 1051A; 64.0 m, Hole 1051B
Age: upper to middle Eocene

Subunit IB is primarily a middle Eocene nannofossil ooze with siliceous microfossils (diatoms, radiolarians, and sponge spicules) to siliceous nannofossil ooze. The uppermost part of this subunit in

Table 3. Vitric ash layers in the upper middle Eocene to lower Eocene interval.

Core, section, interval (cm)	Depth (mbsf)	Comments
171B-1051A-		
2H		Ash component throughout core
3H		Ash component throughout core
4H-4, 93	30.23	
171B-1051B-		
2H-3, 64-67	8.44-8.47	
5H-1, 117-124	34.47-34.54	Ash patches
171B-1051A-		
9H-3, 7	75.37	
9H-6, 119-120	80.99-81.00	
10H-4, 61-62	86.91-86.92	
10H-6, 76	90.06	
171A-1051B-		
10H-4, 111-113	88.61-88.63	
171A-1051A-		
16H-6, 21	146.51	
17X-2, 12	149.92	
20X-7, 34-37	186.74-186.77	
26X-3, 62-62.5	238.62	
30X-3, 93	277.33	
32X-5, 143	300.03	
33X-1, 134	303.44	
34X-5, 118	318.98	
34X-7, 9	320.39	
35X-4, 109	327.09	
43X-1, 132-133	400.82-400.83	
43X-3, 51-53	403.01-403.03	
43X-6, 120-122	408.20-408.40	
171B-1051B-		
21X-6, 2-4	189.22-189.24	
26X-7, 7-8	238.77-238.78	
33X-6, 109-111	302.19-302.21	
34X-2, 139-140	306.09-306.10	
36X-3, 126-128	317.16-317.18	
36X-4, 116-117	318.56-318.57	
37X-3, 75-78	326.25-326.28	
39X-4, 101-103	347.21-347.23	
40X-3, 31	354.62	
40X-6, 105	359.87	
47X-2, 84-85	401.63-401.65	
47X-3, 96	403.26	
47X-4, 73-75	404.53-404.55	

Core 171B-1051B-2H is late Eocene in age. Bedding is poorly defined and the sediment is homogeneous. Sporadic burrow-mottled intervals are recognizable. Mn oxide flecks are disseminated throughout. Drilling slurry in the upper few centimeters of most cores indicates that the sediment of lithologic Subunit IB was only slightly disturbed by drilling. The base of lithologic Subunit IB is defined by a sharp change in color from pale yellow (5Y 8/1–8/2) to the light greenish gray (5G 8/1) of the underlying Subunit IC sediments.

Subunit IC

Description: Nannofossil ooze with siliceous microfossils to siliceous nannofossil ooze
Intervals: 171B-1051A-8H-2, 55 cm, through 13H-CC; 171B-1051B-8H-5, 95 cm, through 15H-CC
Depth: 63.6–119.8 mbsf, Hole 1051A; 68.8–134.8 mbsf, Hole 1051B
Thickness: 56.2 m, Hole 1051A; 66.0 m, Hole 1051B
Age: middle Eocene

The top of Subunit IC is defined by a sharp color change from the overlying pale yellow (5Y 8/1–8/2) sediment to the light greenish gray (5G 8/1) sediment of Subunit IC. Like Subunit IB, Subunit IC contains generally homogeneous sediment that is composed of middle Eocene nannofossil ooze with siliceous microfossils to siliceous nannofossil ooze. There are sporadic burrow-mottled intervals, and pyrite flecks are disseminated throughout. The downhole transition from ooze to chalk is gradual; the last downhole occurrence of ooze constitutes the lower boundary of Subunit IC.

Subunit ID

Description: Siliceous nannofossil chalk to nannofossil chalk with siliceous microfossils
Intervals: 171B-1051A-14H-1, 0 cm, through 40X-CC; 171B-1051B-16X-1, 0 cm, through 42X-CC
Depth: 119.8–379.3 mbsf, Hole 1051A; 134.8–376.1 mbsf, Hole 1051B
Thickness: 259.5 m, Hole 1051A; 241.3 m, Hole 1051B
Age: middle Eocene

Middle Eocene Subunit ID consists of light greenish gray to light gray siliceous nannofossil chalk alternating with more calcareous nannofossil chalk with siliceous microfossils. Bioturbation is prevalent in this subunit including *Chondrites, Planolites, Zoophycos,* and unidentified burrows. Pyrite is scattered throughout Subunit ID and is commonly concentrated in burrows. Drilling disturbance is moderate, with biscuiting through most of Subunit ID; nonetheless, the burrows are continuous from one biscuit to the next. The base of this subunit was not recovered.

Unit II

Description: Silicified foraminifer porcellanite, olive green claystone, and clay-rich firmground
Intervals: 171B-1051A-41X-1, 0 cm, to 41X-CC, 18 cm; 171B-1051B-43X-1, 0 cm, to 45X-1, 20 cm
Depth: 379.3–381.6 mbsf, Hole 1051A; 376.1–382.9 mbsf, Hole 1051B
Thickness: 2.3 m, Hole 1051A; 6.8 m, Hole 1051B
Age: early to middle Eocene

Lithologic Unit II is a thin, but significant, interval that marks a distinct shift from typical Paleogene sedimentation at this site. There is a large discontinuity in the concentrations of major and minor ions in interstitial water across this unit (see "Inorganic Geochemistry" section, this chapter), an increase in magnetic susceptibility and velocity (see "Physical Properties" section, this chapter), and high natural gamma-ray values (see "Downhole Logging" section, this chapter). There is a hiatus of ~2 m.y. between lithologic Units I and III (see "Biostratigraphy" section, this chapter). The sediment is a slightly bioturbated green clay overlying a silicified foraminifer porcellanite. This sediment consists of nearly pure foraminifers, but all have been silicified. The foraminifers are cemented together with opal, but there is still considerable porosity (as much as 40%). Although in hand the sediment appears to be composed entirely of foraminifers, it gives almost no reaction to HCl. In addition, pieces of chert with porcellanite rims occur within the sediment and indicate why coring though this interval was difficult. Only the foraminifer porcellanite was recovered in Hole 1051A; both the clay and more of the foraminifer porcellanite were recovered over a 6.8-m interval in Hole 1051B.

The clay is at least 30 cm thick but was compacted by drilling (Fig. 5). A better estimate of the true thickness will be provided by logging results. It is slightly bioturbated with *Phycoides* and a few *Planolites*-like burrows. Its deep olive green color turned white with a faint greenish tint after it dried. X-ray diffraction (XRD) results indicate that the clay is a smectite-group mineral (Fig. 6). Its waxy feel is reminiscent of bentonite.

Underlying the clay is ~80 cm (in Hole 1051A) of silicified foraminifer porcellanite that is locally cross-laminated with green clay drapes (Fig. 7). Two fine-grained interbeds are rich in clay and exhibit wavy lamination (Fig. 7). In the coarser intervals, thin-section samples indicate that the sediment is composed of ~90% foraminifers, most of which have been replaced by silica. The remaining 10% is interstitial clay. There is 5%–10% angular quartz silt in intervals with clay-rich wavy laminae. The porcellanite contains a thin limonitic clay in Hole 1051A. Zeolites are abundant both above and below the porcellanite.

Near the base of the recovered interval is a 5-cm-thick firmground of brown clay with abundant burrows (Fig. 8). A few thin laminae of

a blue clay exhibit wavy lamination at the base of the firmground. More silicified foraminifer porcellanite was recovered below the firmground (Fig. 8). Pieces of brown glassy chert with white porcellanite rims and ghosts of radiolarians and burrows occur at the base of the unit in each hole (Fig. 8).

Unit II represents a significant break in normal pelagic sedimentation at this site. During part of its deposition, currents winnowed away the finer grained material and molded the remaining foraminifers and quartz silt into ripples. Several clay-rich intervals indicate repeated interruptions in current activity. This is the only interval at Site 1051 with chert. The >30-cm-thick clay unit at the top of the interval serves as an aquiclude (see "Inorganic Geochemistry" section, this chapter) that has affected subsequent diagenesis. Opal-A dissolution is concentrated in the more porous and permeable foraminifer sand, causing the foraminifers to be replaced by silica and allowing the formation of chert.

Unit III

Description: Siliceous nannofossil chalk to siliceous nannofossil chalk with clay
Intervals: 171B-1051A-42X-1, 0 cm, to 62X-5, 104 cm; 171B-1051B-45X-1, 20 cm, through 61X-CC
Depth: 389.9–569.9 mbsf, Hole 1051A; 382.9–526.6 mbsf, Hole 1051B
Thickness: 180.0 m, Hole 1051A; 143.7 m, Hole 1051B
Age: late Paleocene to early Eocene

The top of Unit III is placed at the LO of chert in the overlying lithologic Unit II and corresponds with a marked drop in carbonate percentage from ~75% in lithologic Unit I to average values of about 50% (Fig. 2). The dominant lithology in lithologic Unit III is a siliceous nannofossil chalk with clay. The color varies from light grayish green (10GY 8/1) to dark greenish gray (2G 6/1), with the darker lithology being more clay rich. Light–dark color banding is apparent throughout the unit (Fig. 9) at a scale of ~1 m or less in Cores 171B-1051A-47X through 57X and 171B-1051B-55X through 60X. Drilling-induced biscuiting of the cores occurs throughout Unit III but is generally limited to large pieces with thin bands of slurry in between. Biscuiting decreases in intensity downhole. Lamination, cross-stratification, soft-sediment deformation, and microfaulting are observed in Cores 171B-1051A-48X through 50X and 171B-1051B-54X through 60X (Figs. 10–15). Burrows that cut through the deforma-

tional structures imply that the convolute bedding is the result of nearly syndepositional soft-sediment deformation.

The Paleocene/Eocene boundary occurs within an interval of greenish gray, clayey, calcareous chalk. Cores 171B-1051B-59X through 61X consist of alternations of lighter and darker greenish gray, burrow-mottled chalk. The color cycles correspond to pronounced cyclicity in magnetic susceptibility (see "Synthesis" chapter, this volume) and generally have gradational contacts. The chalk is darker green in the lower Eocene sediment than in the Paleocene sediment and is partly laminated. An intraformational mud clast horizon containing partly compacted clasts as much as 5 cm long occurs in the uppermost Paleocene sediment in Section 171B-1051B-60X-2. The entire bed is 23 cm thick (Fig. 14).

Bioturbation is moderate to heavy in Unit III with *Zoophycos, Planolites, Chondrites,* and *Teichichnus,* as well as numerous unidentified burrows. Three closely spaced vitric ash layers occur in Unit III, all within Core 171B-1051A-43X. These ash layers tentatively correlate with three ash layers in Core 171B-1051B-47X. The thicknesses of the ash layers vary from 1 to 2 cm. The base of lithologic Unit III is placed at the color change from dominantly light greenish gray (5GY 7/1) to darker greenish gray (5GY 6/1 to 10GY5/1) at Section 171B-1051A-62X-5, 105 cm.

Unit IV

Description: Siliceous claystone with nannofossils, clayey spiculite with carbonate grains, and clayey nannofossil chalk with siliceous microfossils
Intervals: 171B-1051A-62X-5, 104 cm, through 73X-CC
Depth: 567.9–644.6 mbsf, Hole 1051A
Thickness: 76.7 m, Hole 1051A
Age: early to late Paleocene

Lithologic Unit IV comprises lithologic types with variable amounts of siliciclastic, siliceous, and carbonate components. Clay, in particular, is much more abundant in Unit IV than in Unit III and gives the sediment a darker color. The boundary between lithologic Units III and IV corresponds with a downhole increase in clay percentage, a decrease in carbonate content (see "Organic Geochemistry" section, this chapter), and increases in bulk density and gamma-ray intensity (see "Physical Properties" and "Downhole Logging" sections, this chapter). Sediments above the boundary generally contain about 50% carbonate, whereas sediments in Unit IV have an average carbonate content of 37.5%.
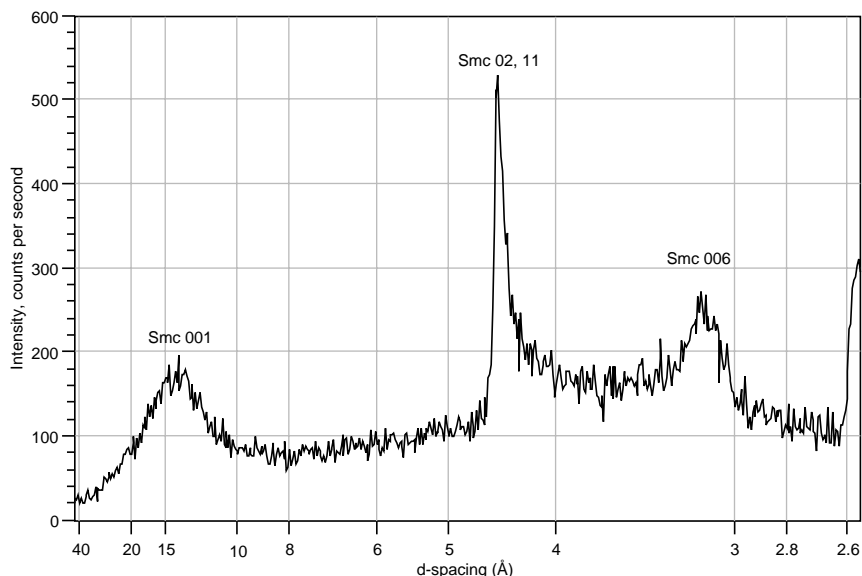
Figure 6. X-ray diffractogram of Sample 171B-1051B-43X-1, 28–30 cm. Smc = smectite group mineral; numbers = the Miller index for the peak.

cm
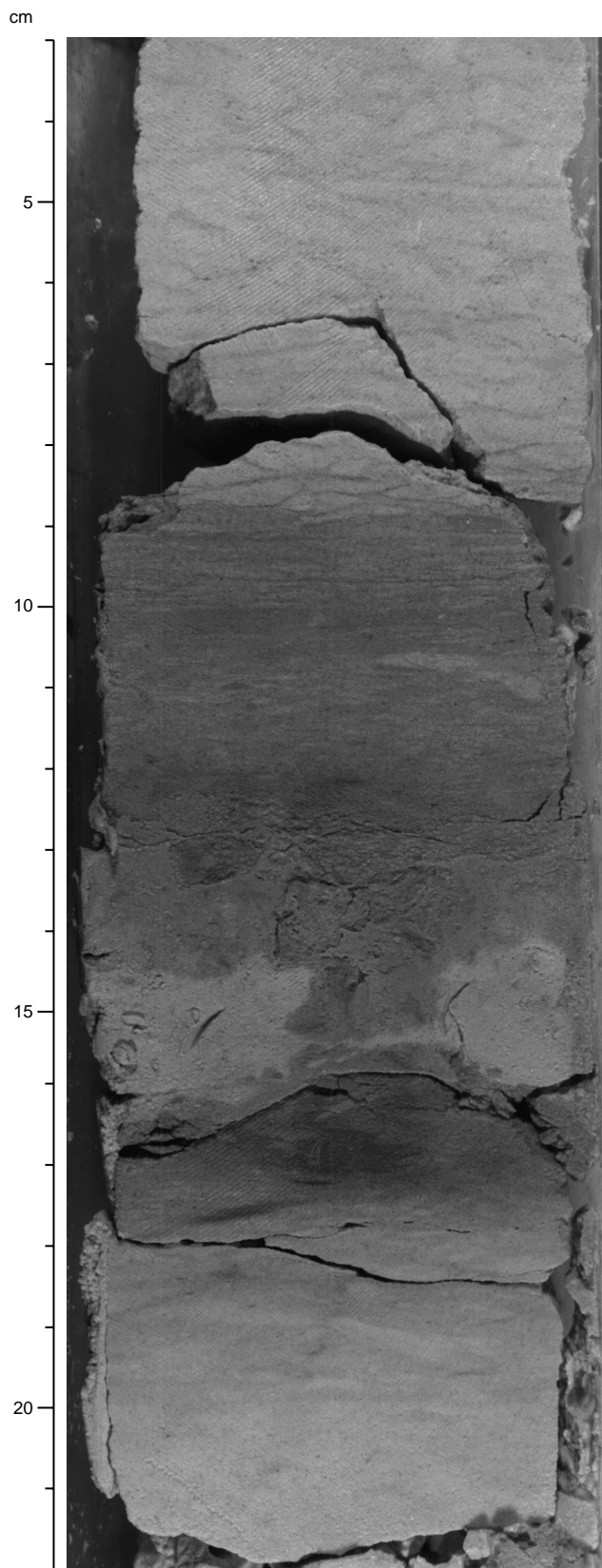
Figure 7. Interval 171B-1051B-43X-CC, 3−22 cm. Wavy lamination in the silicified foraminifer porcellanite of lithologic Unit II (3−8 cm) and a clay-rich, wavy-laminated interbed within the unit.

cm
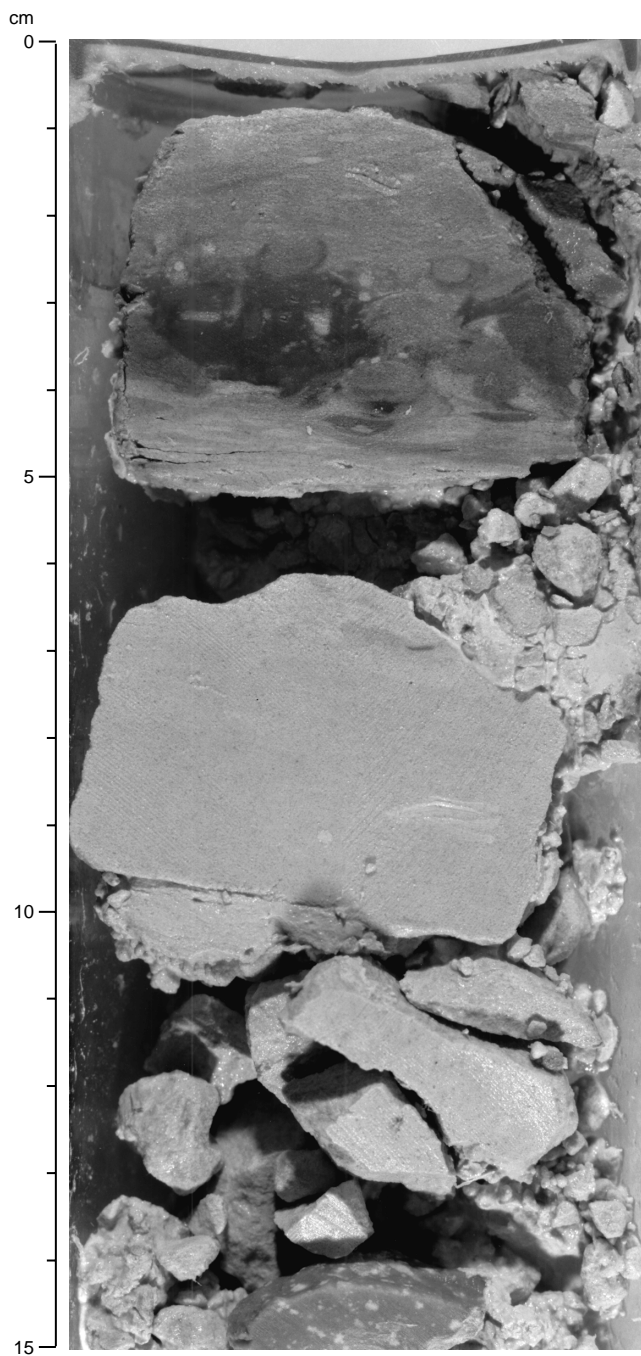
Figure 8. Interval 171B-1051B-44X-CC, 0−15 cm. A brown clay firmground (0−5 cm) occurs within the silicified foraminifer porcellanite with quartz silt of lithologic Unit II.

Microfaults occur in Cores 171B-1051A-62X and 63X, and a small-scale slump fold was found in interval 171B-1051A-65X-3, 135−145 cm (Fig. 16). Geometric relationships between deformational structures, ichnofossils, and sedimentary structures can be used to infer the relative timing of these events (Figs. 17−20). The reverse microfault in interval 171B-1051A-62X-6, 83.5−84 cm (Fig. 16), cuts a horizontal glauconitic lamina, whereas the oblique gray lamina just above it is not offset. This implies that sediment was removed above the fault before the inclined lamina was deposited. The curved
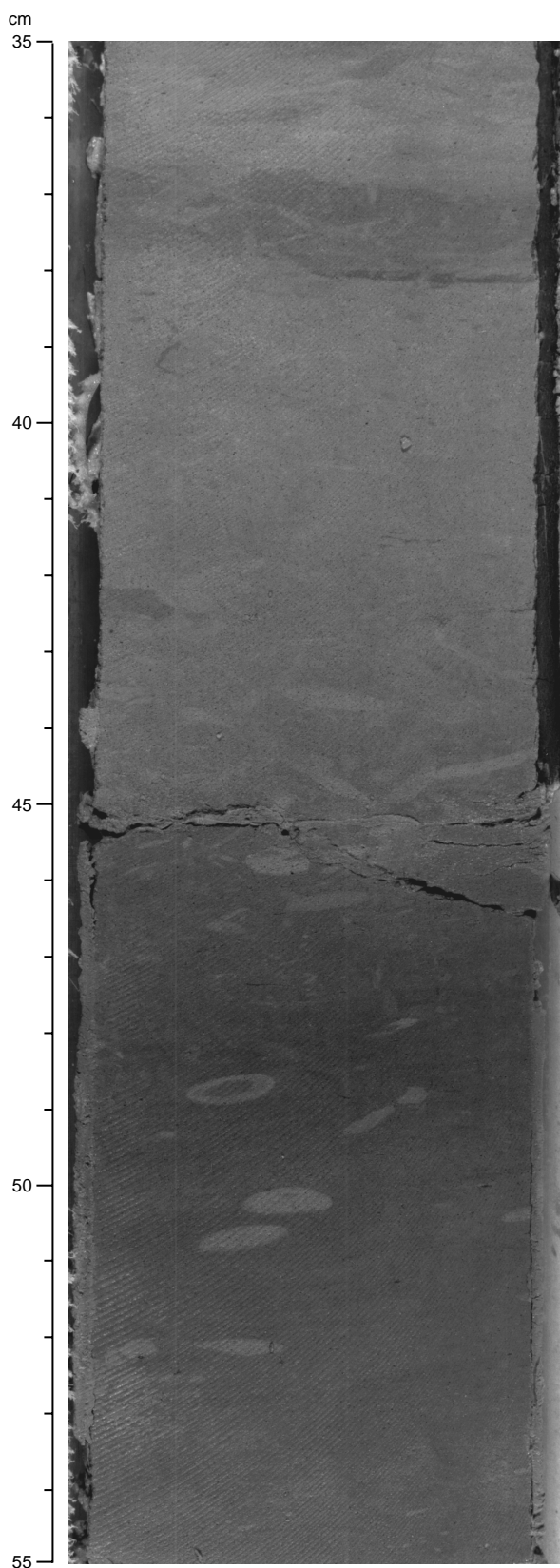
Figure 9. Interval 171B-1051A-48X-6, 35−55 cm. Bioturbated interval showing alternating light–dark lithology typical of lithologic Unit III.
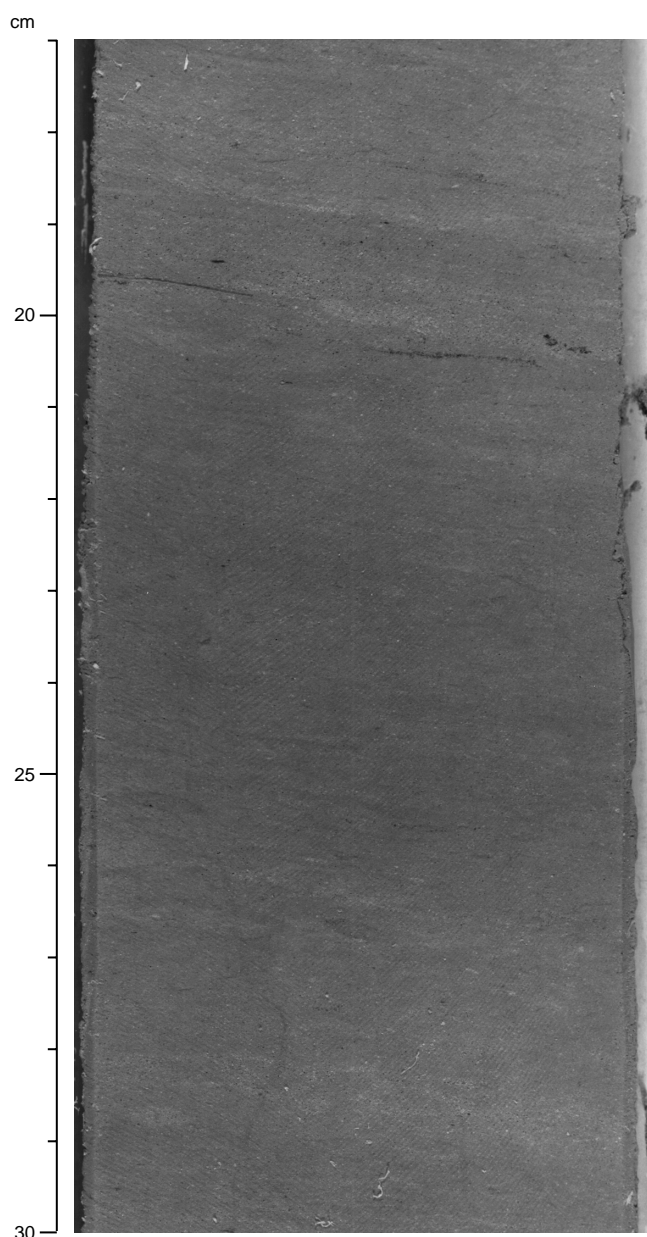
Figure 10. Interval 171B-1051A-48X-7, 17−30 cm. Interval of dipping laminae in lithologic Unit III.

laminae in this interval between 79.5 and 80.5 cm overlie an interval of oblique laminae from 80.5 to 83.5 cm. The curved laminae are truncated by glauconitic laminae parallel to the laminae below 81 cm. Because bedding above and below is horizontal, the interval between 78.5 and 83.5 cm probably belongs to a single depositional event and represents foresets of current-induced ripples, with variation in current shear expressed by the different size of the foresets. Because it was slightly consolidated, the interval of faulted glauconite laminae may have remained unaffected by the erosional event.

Discussion

Correlation using color cycles among sites has provided a data set that supplements (especially in intervals of poor preservation) biostratigraphic and paleomagnetic datums (Fig. 3). We measured color
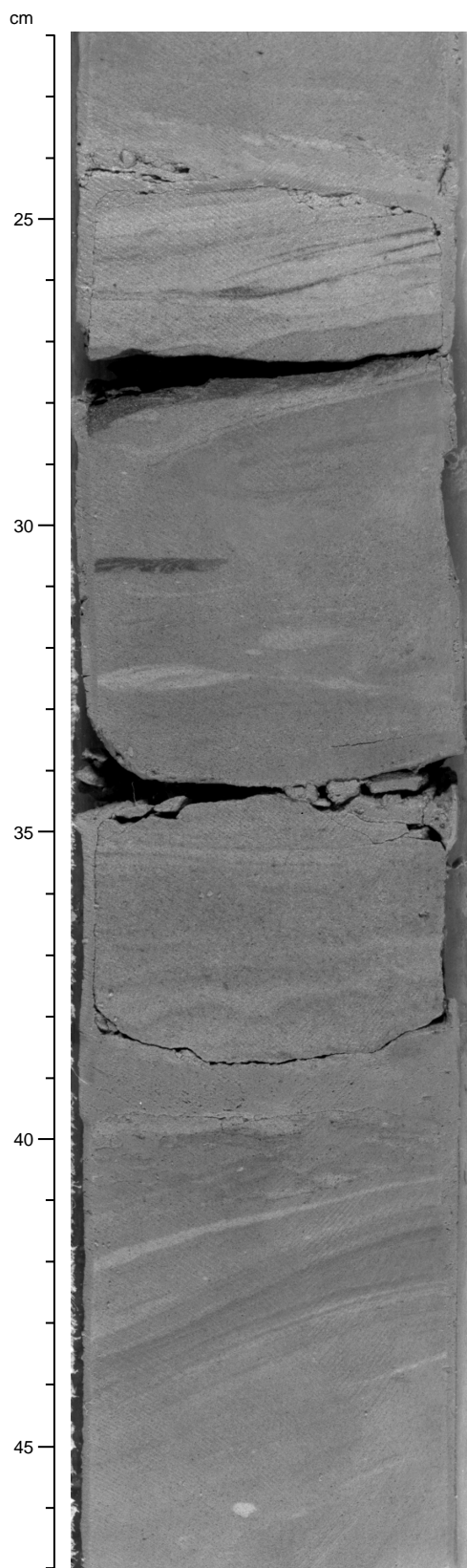
Figure 11. Interval 171B-1051A-48X-CC, 22–47 cm. Cross-bedding occurs in a foraminifer-rich interval in lithologic Unit III at 24–27 and 40–45 cm. A small slump fold occurs at 28–30 cm.
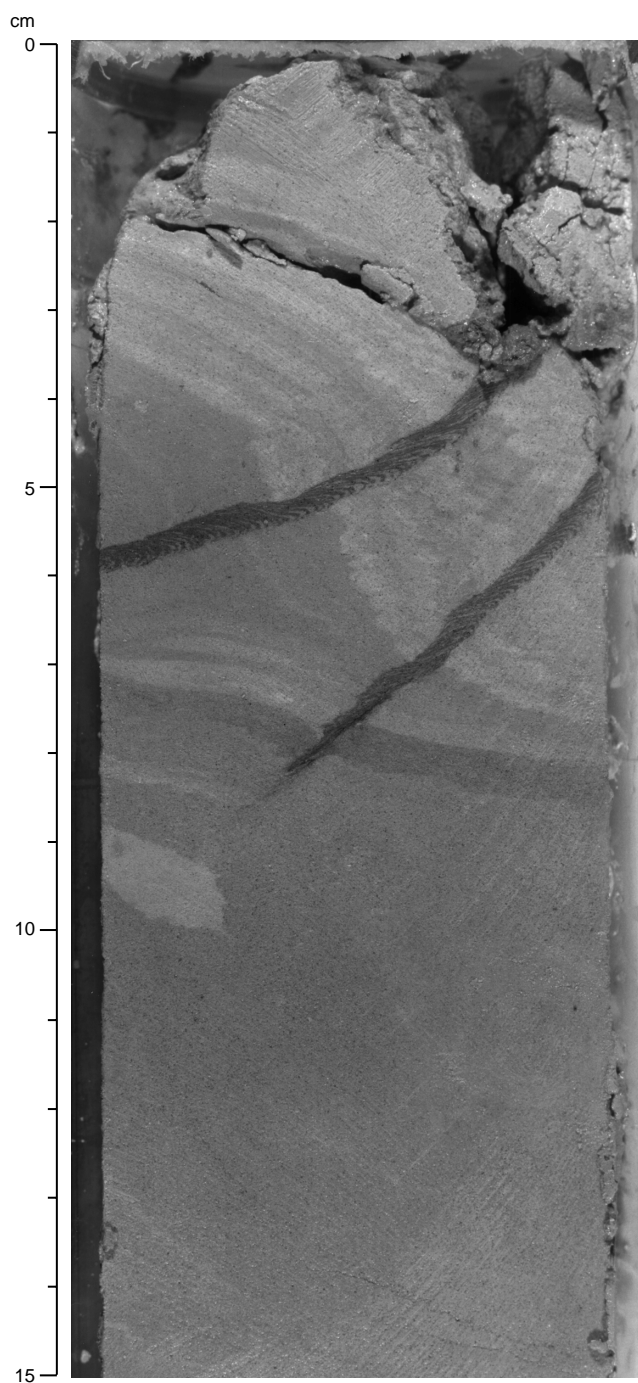
Figure 12. Interval 171B-1051A-49X-1, 0–15 cm. Convolute bedding cross-cut by undeformed *Zoophycos* burrows in lithologic Unit III.

at 5-cm intervals; where biscuiting was more severe, we were still generally able to get a reliable measurement at a spacing of <25 cm. We have thousands of color measurements through the section in each hole. Because the measurements were individually selected, we have minimized the compromise of data by disturbed intervals. The reliability of the measurements is demonstrated by matching color records from different holes at the same site (see "Core-Core Integration" section, this chapter).

Figure 3 shows the correlation between Holes 1050A and 1051A based on color, ash layers, and nannofossil and planktonic foramini-
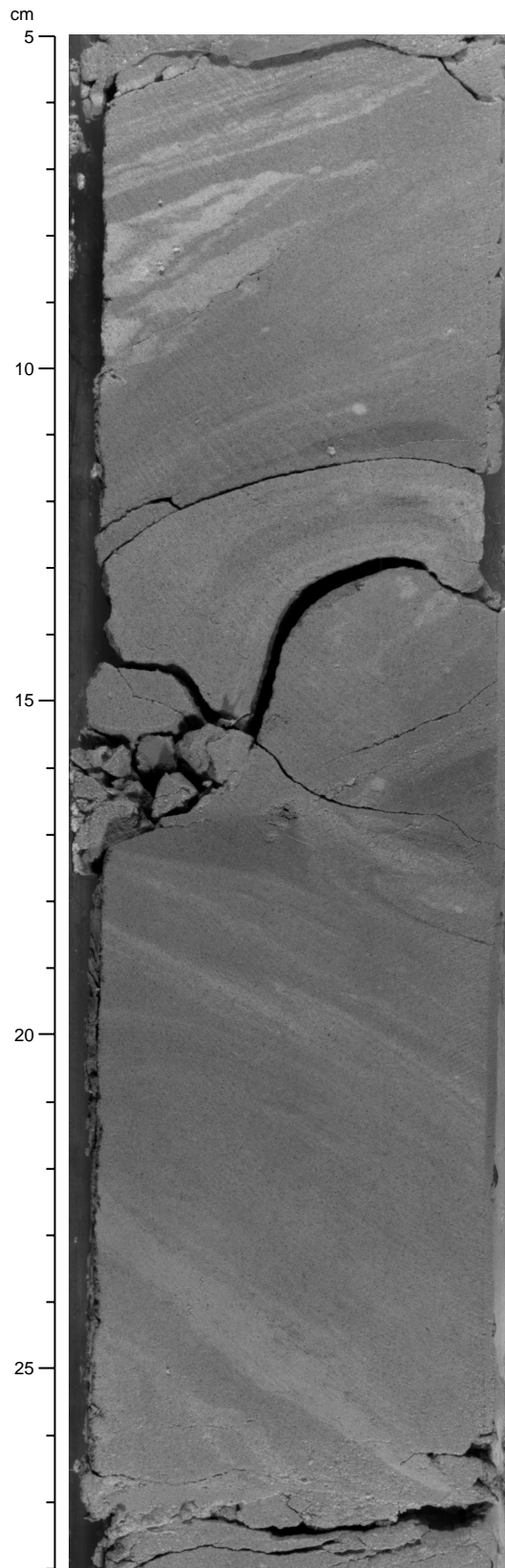
Figure 13. Interval 171B-1051A-49X-CC, 5-28 cm. Soft-sediment deformation postdated by a reverse microfault at 16–17 cm in lithologic Unit III.
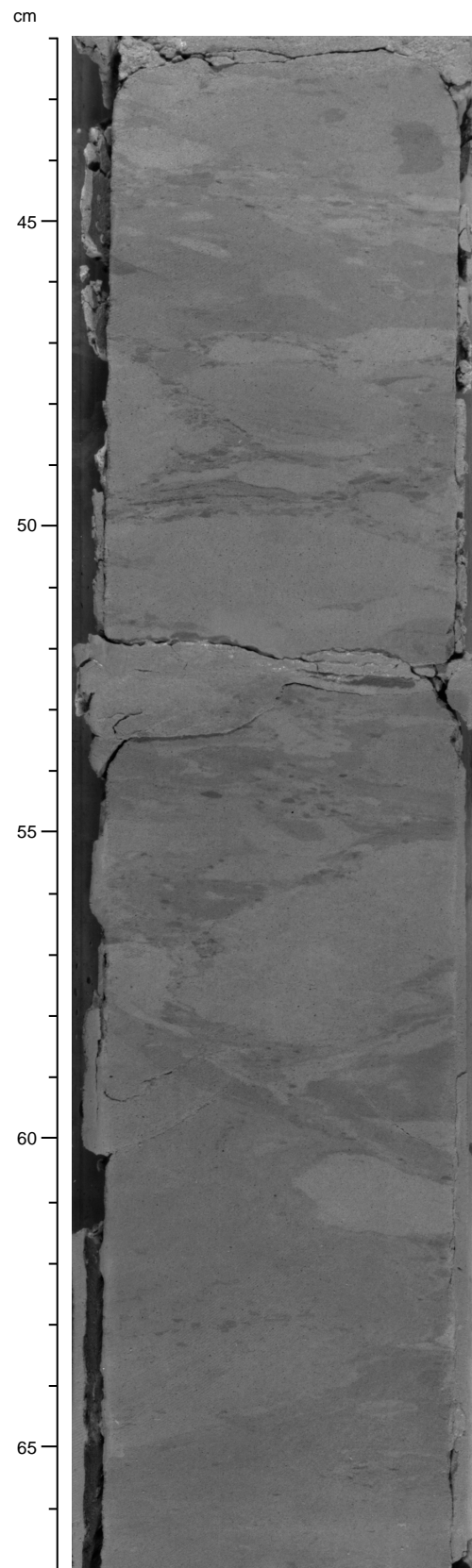
Figure 14. Interval 171B-1051B-60X-2, 42–67 cm. Intraformational mud clast layer in lithologic Unit III.
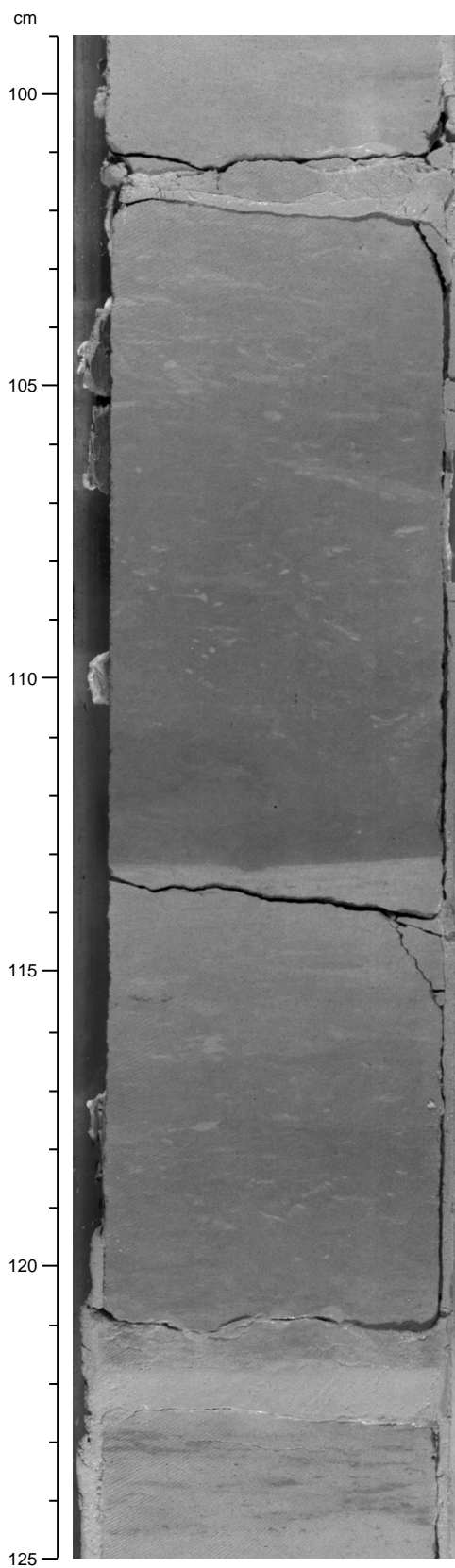
Figure 15. Interval 171B-1051B-60X-3, 99–125 cm. Light–dark color banding typical of lithologic Unit III.
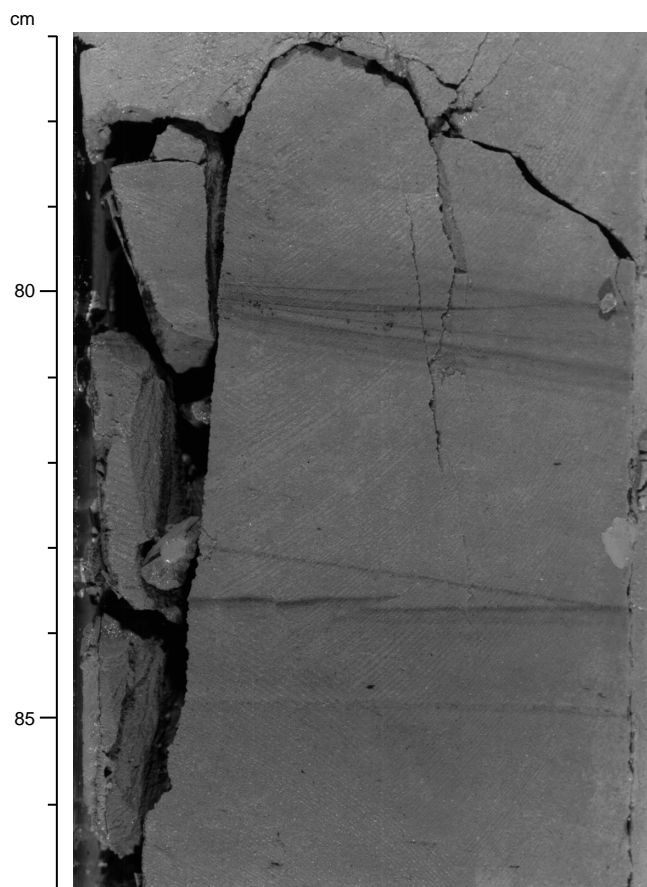
Figure 16. Interval 171B-1051A-62X-6, 77–87 cm. Inclined lamination, cross-lamination, and reverse microfaulting of laminae with variable glauconite content in lithologic Unit IV. Inclination and cross-bedding are probably caused by bottom-current activity.

fer datums (see "Biostratigraphy" section, this chapter). The most dramatic color change observed at both sites, the one from yellow to green in the upper portion of the section, is clearly time transgressive and cuts across both a prominent ash layer and several biostratigraphic boundaries. The composition of the sediment does not change across the contact, and despite pervasive burrow mottling, the contact is sharp and without piping. We attribute the shift to a diagenetic front imposed long after burial, but we have no constraints on whether it migrated down from the sediment/water interface or up through the sediment column. The subtler features observed in the rest of the sequence, on the other hand, largely parallel independent lines of correlation. Where lines of correlation cross, the disagreement can be attributed to the sampling resolution in micropaleontologic studies and/or intervals of poor preservation that have also led to inconsistencies among the biostratigraphic records based on different fossil groups. The color record also shows high-frequency variability (Fig. 4) on a length scale that is suggestive of Milankovich cyclicity. We hope these alternations will provide extremely high-resolution correlation among holes and sites. Finally, as the compositional and textural reasons for color variation become better known, the color data should provide a high-resolution proxy for changes in sediment supply and preservation that is important for understanding the paleoceanographic and deposition changes along the transect.

The common *Chondrites* and spreiten burrows, such as *Zoophycos* and *Teichichnus,* that are partly filled with pyritic fecal pellets
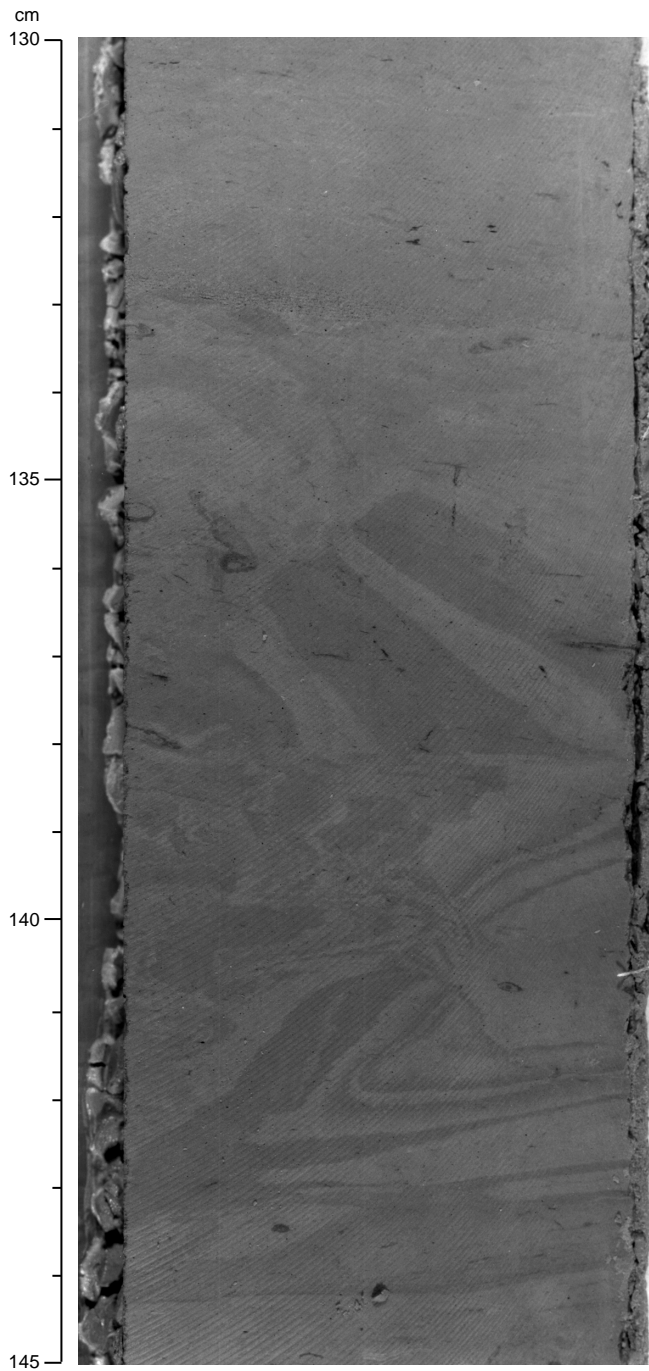
Figure 17. Interval 171B-1051A-65X-2, 130–145 cm. Convolute bedding in lithologic Unit IV. Burrows that cut through the deformational structures imply that the convolution is a result of nearly syndepositional, soft-sediment deformation.

(Fig. 20) suggest that the organic matter supply was not a limiting factor in the development of benthic communities. The present low concentrations of organic matter (0.1% total organic carbon [TOC] on average; see "Organic Geochemistry" section, this chapter) probably results from the breakdown of organic matter by the benthic organisms and inorganic oxidation. The provenance of the ash layers is discussed in the "Site 1050" chapter (this volume).
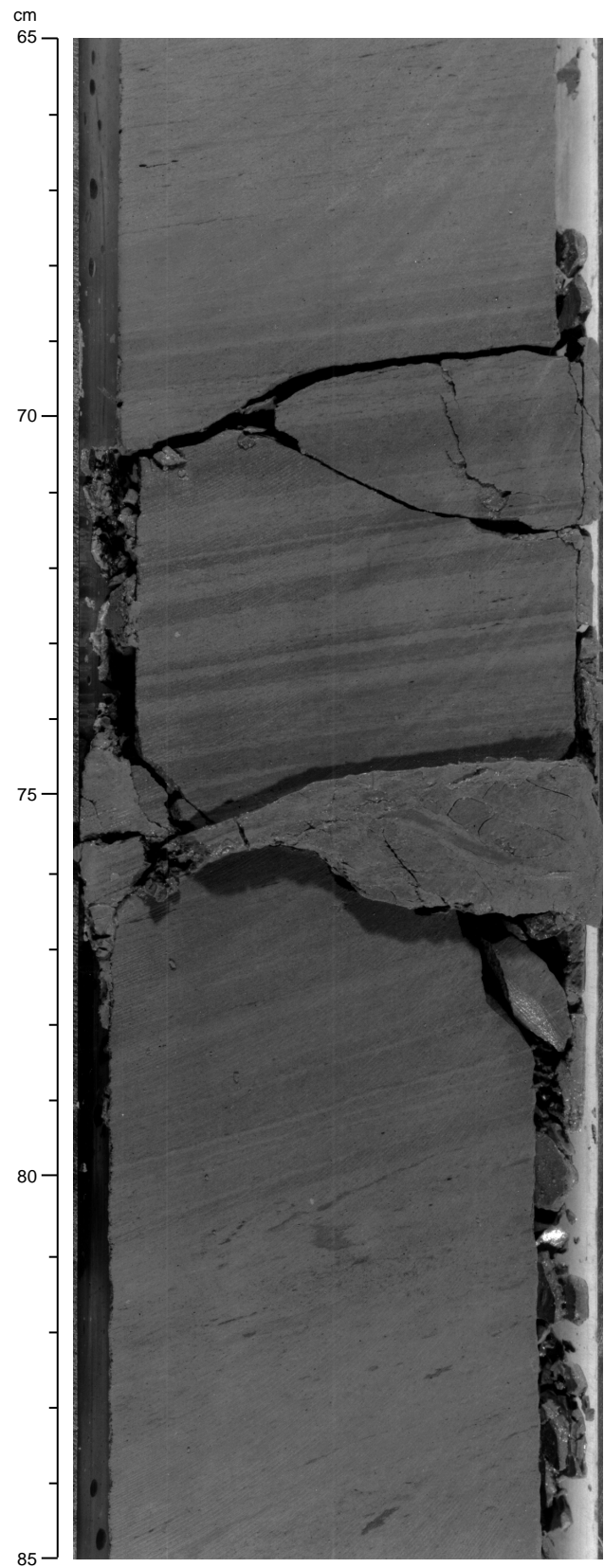
Figure 18. Interval 171B-1051A-65X-3, 65–85 cm. Laminated interval with alternating lighter siliceous nannofossil chalk and darker siliceous claystone, with nannofossils and carbonate grains in lithologic Unit IV.
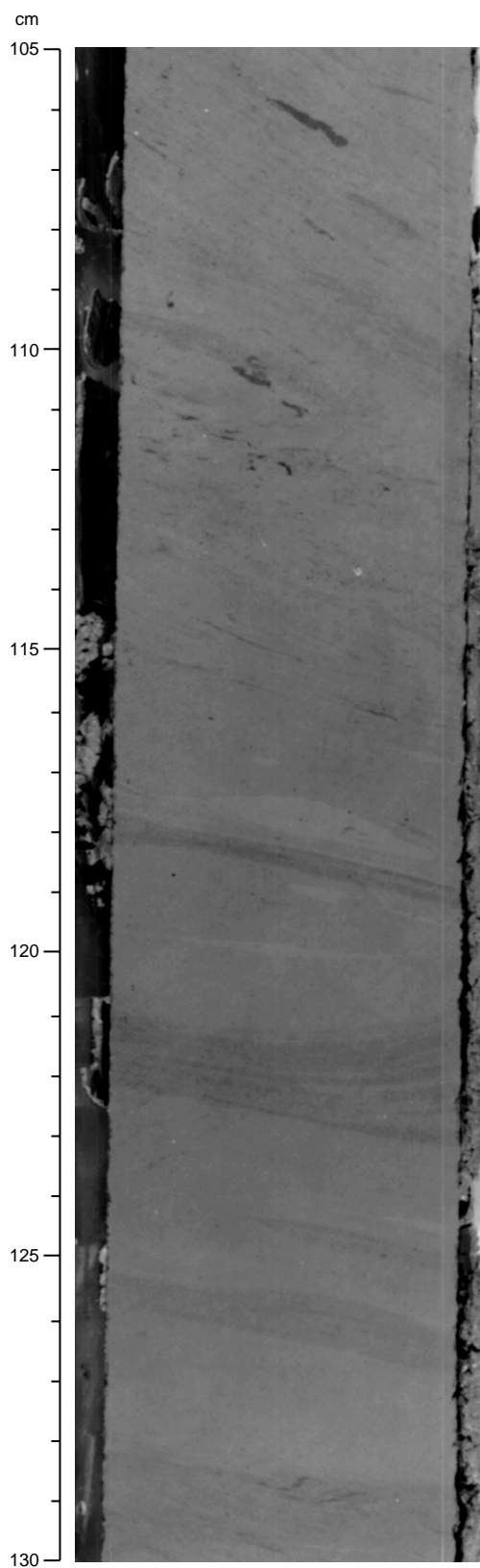
Figure 19. Interval 171B-1051A-65X-3, 105−130 cm. Flaser bedding in lighter siliceous nannofossil chalk and darker siliceous claystone, with nannofossils and carbonate grains in lithologic Unit IV. The flaser structure may have resulted from discontinuous deposition of different lithologic types because of bottom currents and later differential compaction.

Figure 20. Interval 171B-1051A-66X-2, 35−50 cm. *Zoophycos* burrows in lithologic Unit IV that are partly filled with pyritic fecal pellets in clayey radiolarite with sponge spicules and diatoms.

BIOSTRATIGRAPHY

Calcareous Nannofossils

Examination of calcareous nannofossil assemblages indicates that coring at Site 1051 recovered a sequence spanning the lowermost part of the upper Eocene to the upper part of the lower Paleocene (Fig. 21). Sample spacing is generally one per section (~1.5 m) in the cores from Hole 1051A. A list of chronostratigraphically significant biohorizons from this detailed examination is presented in Table 4. The
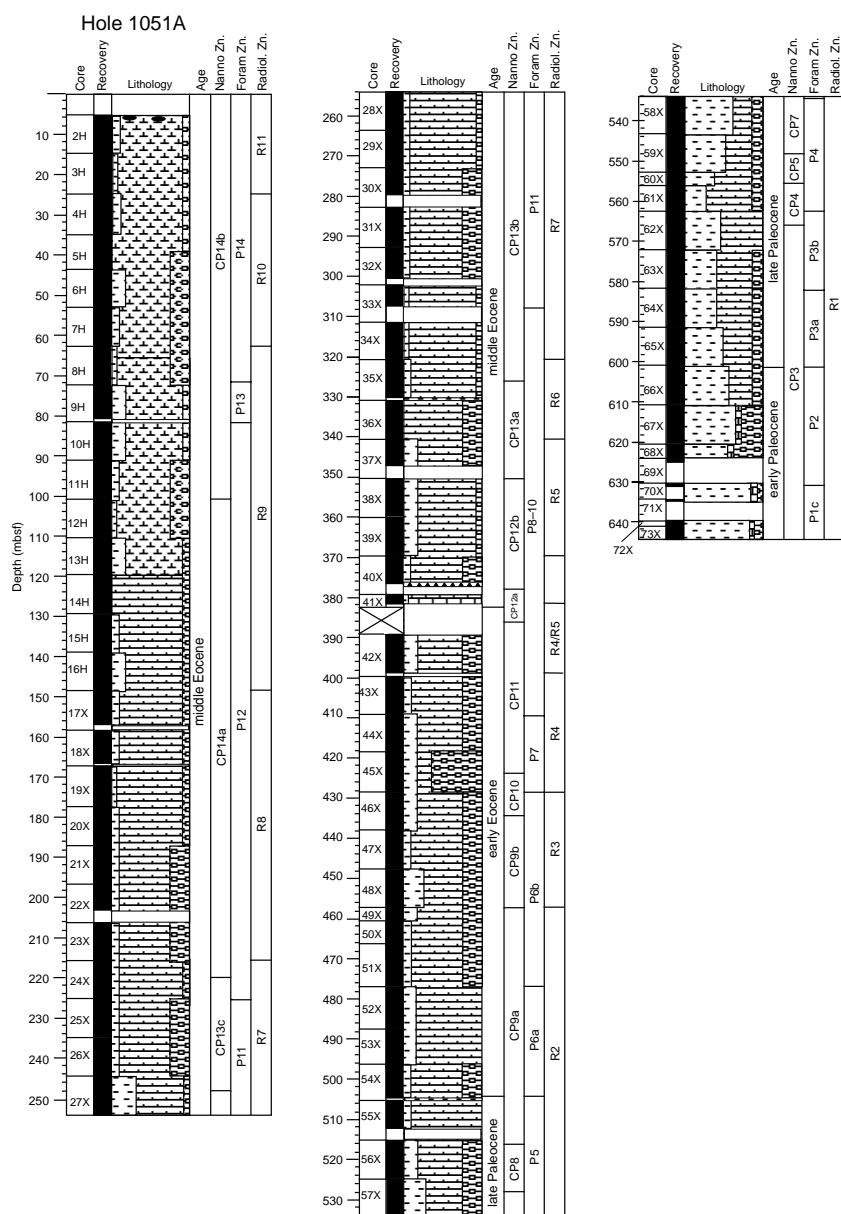
Figure 21. Biostratigraphic summary for Site 1051. See Figure 1, "Site 1049" chapter (this volume), for an explanation of the symbols used. Refer to the nannofossil and foraminifer datum tables (this chapter) for biostratigraphic data that reflect post-cruise additions and modifications to range data.

sequence from Hole 1051B was sampled generally from the core catchers to provide biostratigraphic correlation between the holes; however, a few select samples from within a given core were taken and are discussed below. Calcareous nannofossil preservation is good to very good in the upper and middle Eocene sequence, degenerates to moderate in the lower Eocene sequence, and becomes poor near the Paleocene/Eocene boundary. Preservation improves in the upper Paleocene sequence and is moderate throughout the lower Paleocene sequence.

The top few meters of the cored sequence in Hole 1051A were severely disturbed and yielded mixed assemblages. The first core in Hole 1051B was recovered with the sediment relatively intact. This core (171B-1051B-1H) contains *Chiasmolithus oamaruensis,* indicating that the base of the upper Eocene is present. The assemblage also includes rare specimens of the middle Eocene species *C. grandis,* suggesting that minor reworking was occurring at the seafloor during the earliest late Eocene.

Comparison with shipboard magnetostratigraphy shows that with the exception of the first occurrence (FO) of *Dictyococcites bisectus,*

most of the datums appear to correspond with previously published age dates. Although published correlations link it with Chronozone C17n.3n (Berggren et al., 1995), this datum makes its FO in C17r in Hole 1051A. This significantly earlier appearance causes this datum to appear below the line of correlation shown in Figure 22. This apparently earlier FO may be caused by the expanded nature of the section at Site 1051 and implies that the FO of *D. bisectus* may need to be recalibrated with respect to the time scale. The base of the middle Eocene (Core 171B-1051A-40X; 377 mbsf) was poorly recovered in Hole 1051A, whereas in Hole 1051B, this boundary is marked by a foraminifer packstone associated with a clay-rich interval containing a nannofossil assemblage from Subzone CP12a. The well-preserved nature of the nannofossil assemblage in association with common phillipsite in some of these samples indicates that the packstone was open to sufficient pore-water movement, which largely prevented opal-CT formation (and concomitant carbonate diagenesis). In other more clay-rich samples, well-developed opal-CT lepispheres in the nannofossil smear slides indicate silica remobilization and precipitation. As expected, carbonate diagenesis was advanced in these sedi-

Table 4. Calcareous nannofossil datums for Site 1051.

Datum	Species	Zone	Age (Ma)	Core, section, interval (cm)	Minimum depth (mbsf)	Maximum depth (mbsf)
				171B-1051A		
B	*D. bisectus*		38.0	8H-CC, 17-20	72.6	81.1
T	*C. solitus*	CP14b	40.4	12H-3, 67-68	103.0	104.5
B	*C. reticulatum*		42.0	17X-3, 47-48	151.8	153.4
B	*R. umbilica*	CP14a	42.7	20X-CC, 27-29	187.2	196.8
T	*N. fulgens*		43.1	25X-1, 64-65	225.5	226.1
T	*C. gigas*	CP13c	44.5	27X-CC, 36-38	244.6	254.5
B	*C. gigas*	CP13b	46.1	36X-4, 58-59	336.2	337.8
B	*N. fulgens*	CP13a	47.3	37X-CC, 13-16	347.1	355.6
B	*R. inflata*	CP12b	48.5	40X-CC, 38-40	377.2	379.8
B	*D. sublodoensis*	CP12a	49.7	41X-CC, 16-18	380.6	390.6
T	*T. orthostylus*		50.6	42X-1, 65-66	380.6	390.6
B	*T. crassus*	CP11	51.5	44X-CC, 42-44	419.0	428.6
B	*D. lodoensis*	CP10	52.9	45X-CC, 41-43	428.6	438.2
T	*T. contortus*	CP9b	53.6	50X-1, 68-69	460.5	460.8
B	*T. orthostylus*		53.6	48X-CC, 52-54	457.3	460.5
T	*T. bramlettei*		53.9	50X-5, 67-68	460.5	466.9
B	*T. contortus*		54.4	50X-CC, 47-49	467.4	470.5
B	*R. cuspis*	CP9a	55.2	55X-CC, 19-22	510.8	518.6
T	*F. tympaniformis*		55.3	56X-3, 65-66	510.9	518.6
B	*C. eodela*	CP8b	55.5	57X-4, 65-67	524.7	529.7
B	*D. multiradiatus*	CP8a	56.2	57X-4, 65-66	528.2	529.7
B	*D. nobilis*	CP7	56.9	58X-CC, 34-36	543.9	544.4
B	*H. riedelii*		57.3	58X-CC, 34-36	543.9	544.4
B	*D. mohleri*	CP6	57.5	58X-CC, 34-36	543.9	544.4
B	*H. kleinpellii*	CP5	58.4	60X-2, 68-69	555.5	556.2
B	*S. anarrhopus*		58.4	60X-2, 68-69	555.5	556.2
B	*F. tympaniformis*	CP4	59.7	61X-CC, 42-44	566.6	568.1
B	*C. consuetus*		59.7	61X-CC, 42-44	566.6	568.1
B	*F. ulii*		59.9	61X-CC, 42-44	569.5	571.1
B	*S. primus*		60.6	63X-CC, 34-36	588.8	590.2
B	*C. bidens*		60.7	64X-CC, 62-66	592.2	601.6

Notes: Bases of age datums are represented by B; tops of age datums are represented by T. These data reflect post-cruise modifications and are, thus, more up to date than data presented in the range charts and in the biostratigraphy and sedimentation rate figures (this chapter).

mentary rocks. Basal Subzone CP12a was not recorded at Sites 1049 and 1050.

The lower Eocene Cores 171B-1051A-41X through 55X (379.79–510.84 mbsf) contain siliceous claystones and chalks with generally poorly preserved nannofossil assemblages. Biostratigraphic datums are more difficult to determine with certainty because of this poor preservation, particularly near the base of the lower Eocene where identification of the *Rhomboaster-Tribrachiatus* lineage is hampered by overgrowth. Despite this apparent problem, there is no strong evidence for any disconformities in the lower Eocene.

The upper Paleocene record at Site 1051 (Cores 171B-1051A-56X through 64X) contains moderately preserved nannofossils in calcareous claystone. Nannofossil biostratigraphy indicates a disconformity between 543.9 and 544.4 mbsf where Zone CP6 is missing. This disconformity represents a hiatus of ~1 m.y. (Fig. 22). The early/late Paleocene boundary is marked by the FO of *Chiasmolithus bidens* in Sample 171B-1051A-64X-CC, 62–66 cm, and corresponds closely to the Zone P2/P3a boundary, which is delineated by diagnostic planktonic foraminifer species. Increasing quantities of clay in the lower upper Paleocene and lower Paleocene resulted in improved calcareous nannofossil preservation.

Planktonic Foraminifers

The 644-m sequence of dominantly siliceous nannofossil chalk recovered in Hole 1051A ranges from lower Paleocene planktonic foraminifer Zone P1b through upper–middle Eocene Zone P14. Planktonic foraminifers are abundant to common and mostly well preserved in the middle Eocene. Preservation is more variable in the lower Eocene. Samples with low foraminifer abundance are diluted by abundant siliceous microfossils (mostly radiolarians) or, in some intervals, by lithic fragments and chert. Preservation progressively worsens and foraminifer abundance diminishes in the Paleocene sequence as calcite infilling, shell recrystallization, and sediment
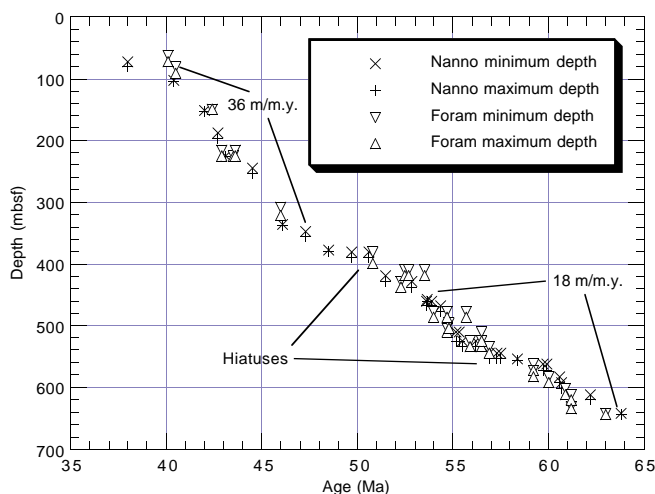
Figure 22. Sediment accumulation rate for Hole 1051A based on the planktonic foraminifer and calcareous nannoplankton datums listed in Tables 4 and 5, respectively.

lithification increase. Zonal assignments are summarized in Figure 21 and Table 5. A distribution chart for Hole 1051A is presented in Table 6.

A typical upper middle Eocene Zone P14 assemblage, characterized by *Turborotalia cerroazulensis, Morozovella spinulosa, Globigerina corpulenta, G. praeturritilina,* and *Catapsydrax dissimilis,* is present in the first seven cores of Hole 1051A. Zone P13 ranges from Samples 171B-1051A-8H-CC, 17–20 cm (72.59 mbsf), to 9H-CC (81.0 mbsf), based on the total range of *Orbulinoides beckmanni.* According to Berggren et al. (1995), this interval spans about 0.4 m.y. When *O. beckmanni* is absent, the LO of *Hantkenina dumblei* may be a useful proxy for the Zone P12/P13 boundary because the latter species only occurs with the former in the lowermost sample in Hole 1051B.

Zone P12 is an ~125-m interval extending from the FO of *O. beckmanni* (81 mbsf) to the LO of *Morozovella aragonensis* in Section 171B-1051A-24X-CC (225.4 mbsf). As observed at Site 1050, the LO of *M. aragonensis* is above the FO of *M. lehneri,* which is inconsistent with the relative order of biostratigraphic datums identified by Berggren et al. (1995). Relative to other species with assigned age datums (Table 5), it appears that the Berggren et al. (1995) age for the LO of *M. aragonensis* is too old. The only datum identified within Zone P12 is the FO of *Turborotalia pomeroli* in Section 171B-1051A-16H-CC (148.8 mbsf).

Recognition of the FO of *Turborotalia possagnoensis* in Section 171B-1051A-33X-CC (300.4 mbsf) determined placement of the base of Zone P11. As was observed at Site 1050, the distinctive FO of *H. dumblei* occurs in the upper part of this zone at the same level as the FO of *Morozovella lehneri. Globigerinatheka* index also occurs first at this level, although Berggren et al. (1995) suggest that this datum is younger than the FO of *M. lehneri* by about 0.6 m.y. The FOs of *M. spinulosa* and *Truncorotaloides topilensis* occur in the lower part of Zone P11, as does the FO of *Guembelitrioides higginsi,* which is higher than its FO in upper Zone P9–P10 at Site 1050.

Zones P8 through P10, which span from the lower to lower middle Eocene, could not be differentiated at Site 1051 because of the absence of the zonal markers for the base of Zones P10 (*Hantkenina nuttali*) and P9 (*Planorotalites palmerae*). Within the Zone P8–P10 interval are the FOs of *Morozovella caucasica, Acarinina bullbrooki,* and *Globigerinatheka subconglobata* in the lower part, and the FO of *G. mexicana* in the middle part.

The top of Zone P7 is placed at the LO of *Morozovella formosa,* which occurs between Sections 171B-1051A-42X-CC and 43X-CC.

Table 5. Planktonic foraminifer datums for Site 1051.

Datum	Species	Zone	Age (Ma)	Core, section, interval (cm)	Depth (mbsf)	Error depth (mbsf)
				171B-1051A-		
T	*G. beckmanni*	b P14	40.10	8H-CC, 17-20	72.59	62.90
B	*G. beckmanni*	b P13	40.50	9H-CC, 0-1	81.09	91.02
B	*T. pomeroli*		42.40	14H-CC, 25-27	129.81	138.97
T	*M. aragonensis*	b P12	43.60	24X-CC, 17-19	225.45	216.00
B	*G. index*		42.90	26X-CC, 46-48	244.63	254.47
B	*M. lehneri*		43.50	26X-CC, 46-48	244.63	254.47
B	*T. possagnoensis*	b P11	46.00	33X-CC, 13-16	307.74	321.71
T	*M. formosa*	t P7	50.80	43X-CC, 47-49	409.46	399.79
T	*M. marginodentata*		52.50	44X-CC, 42-44	418.99	409.48
T	*M. lensiformis*		52.70	44X-CC, 42-44	418.99	409.48
B	*M. aragonensis*	b P7	52.30	45X-CC, 38-40	428.58	430.47
T	*M. aequa*		53.60	46X-CC, 33-35	438.16	428.58
B	*M. formosa*	b P6b	54.00	51X-CC, 47-49	476.56	486.39
B	*M. lensiformis*	b P6b	54.00	51X-CC, 47-49	476.56	486.39
T	*M. acuta*		54.70	52X-CC, 47-49	486.43	476.58
B	*M. marginodentata*		54.80	53X-CC, 49-52	495.94	497.87
T	*M. velascoensis*	b P6a	54.70	54X-CC, 43-46	504.15	502.53
B	*M. subbotinae*		56.90	57X-CC, 48-50	524.72	528.17
T	*G. pseudomenardii*	b P5	55.90	57X-CC, 48-50	534.40	529.67
B	*A. subsphaerica*		59.20	61X-CC, 42-44	562.13	572.63
B	*G. pseudomenardii*	b P4	59.20	61X-CC, 42-44	562.13	572.63
B	*M. velascoensis*	b P3b	60.00	63X-CC, 34-36	582.30	592.15
B	*M. conicotruncata*	b P3a	60.90	65X-CC, 37-40	601.64	611.30
B	*M. praeangulata*		61.20	66X-CC, 42-45	611.30	620.09
B	*P. uncinata*	b P2	61.20	70X-CC, 41-42	631.20	634.78
B	*P. inconstans*	b P1c	63.00	72X-CC, 28-29	642.47	643.95

Notes: Bases of age and biozonal datums are represented by B and b; tops of age and biozonal datums are represented by T and t. Error depths refer to depth to next sample studied above or below a datum level. These data reflect post-cruise modifications and are, thus, more up to date than data presented in the range charts and in the biostratigraphy and sedimentation rate figures (this chapter).

The FO of *Acarinina pentacamerata* occurs in Section 171B-1051A-44X-CC (428.5 mbsf), one core below the FO of *M. formosa,* whereas Berggren et al. (1995) consider these two datums to be synchronous. The FO of *M. aragonensis* in Section 171B-1051A-45X-CC (428.5 mbsf) marks the base of Zone P7. However, this datum level also includes the LO of *M. marginodentata,* which, according to Berggren et al. (1995), should precede the FO of *M. aragonensis* by ~0.2 m.y.

The FOs of *Morozovella aequa, M. formosa,* and *M. lensiformis* were all identified in Section 171B-1051A-51X-CC (476.5 mbsf), providing the basis for recognizing the Zone P6b/P6a boundary. Although the LO of *M. aequa* occurs at the top of Zone P6b in Section 171B-1051A-46X-CC (438.16 mbsf), according to Berggren et al. (1995), this extinction should occur in the middle of this zone. Thus, either part of upper Zone P6b is missing at Site 1051, or the age of this datum should be revised. The Zone P6a/P5 boundary occurs between Samples 171B-1051A-54X-5, 83–86 cm, and 54X-CC (502.53–504.15 mbsf), based on the LO of *M. velascoensis.* The FOs of *Acarinina broedermanni* and *M. marginodentata* were identified within Zone P6a, which is consistent with the Berggren et al.'s (1995) biostratigraphic scheme.

Accurate placement of the Paleocene/Eocene boundary (i.e., Zone P6a/P5 boundary), which is based on the LO of *M. velascoensis,* was hampered by poor sample preservation including significant shell recrystallization and infilling of the foraminifer tests. *Morozovella acuta* and *M. occlusa* occur above the LO of *M. velascoensis,* which is higher than their range has been reported elsewhere (Berggren et al., 1995). Nonetheless, the FO of *M. marginodentata* in Section 171B-1051A-53X-CC and the LO of *M. velascoensis* in Section 171B-1051A-54X-CC clearly indicate that the Paleocene/Eocene boundary is within Core 171B-1051A-54X.

The Zone P4/P5 boundary, identified by the LO of *Globanomalina pseudomenardii,* is placed in Section 171B-1051A-57X-CC (534.38 mbsf). Although Berggren et al. (1995) suggest that the FO of *M. gracilis* should occur at the base of Zone P6a, this datum event was identified within the middle of Zone P5 at Site 1051. *Chiloguembelina wilcoxensis* also first occurs in the middle of this zone.

The FO of *Globanomalina pseudomenardii,* which defines the Zone P3/P4 boundary, occurs in Section 171B-1051A-61X-CC

(562.13 mbsf). All samples within Zone P4 are poorly preserved, rendering species identification difficult. The FO of *Acarinina subsphaerica* also occurs at this level, and the FOs of *Morozovella acuta* and *M. occlusa* occur in the middle of this zone.

The Subzone P3b/P3a boundary is placed in Section 171B-1051A-63X-CC (582.30 mbsf) based on the FO of *Morozovella velascoensis.* Sample preservation was too poor to distinguish between igorinids and other small taxa within this interval. The FO of *M. conicotruncata* in Section 171B-1051A-65X-CC (601.64 mbsf) enabled placement of the Subzone P3a/Zone P2 boundary between this level and Section 171B-1051A-66X-CC.

Zone P2 extends through an unusually long stratigraphic interval relative to the Berggren et al. (1995) time scale, ranging from Sections 171B-1051A-66X-CC through 70X-CC (611.30–631.20 mbsf). The base of this zone is defined on the FO of *Praemurica uncinata.* Subzone P1c is distinguished from Zone P2 by the absence of *P. uncinata* and the presence of *P. inconstans.* The lowermost sample recovered yields a typical Subzone P1c assemblage including *P. taurica, Eoglobigerina edita,* and *Globanomalina compressa.*

Benthic Foraminifers

The preservation of benthic foraminifers is generally good to moderate throughout the lower to middle Eocene interval cored in Hole 1051A, except for two lower Eocene samples (171B-1051A-54X-5, 83–86 cm, and 171B-1051A-55X-3, 26–29 cm) where preservation is poor (Table 7). Preservation is moderate to poor in the lower to upper Paleocene interval at Hole 1051A. Abundance of benthic foraminifers is low throughout Hole 1051A (see Table 7). The rare occurrences of benthic foraminifers in the middle Eocene are probably the result of high abundances of radiolarians diluting the benthic foraminifers, whereas the trace occurrence of benthic foraminifers in connection with the Paleocene/Eocene boundary (Cores 171B-1051A-54X through 56X) may be a response to the upper Paleocene benthic foraminifer extinction event. Benthic foraminifers are common in the lower Paleocene Sample 171B-1051A-66X-CC, 42–45 cm. Paleodepth estimates based on the almost ubiquitous occurrence of *Nuttallides truempyi* and *Aragonia* spp. indicate lower

Table 6. Distribution chart of planktonic foraminifers from Hole 1051A.

Core, section, interval column header prefix: 171B-1051A-

Age	Zone	Core, section, interval (cm)	Depth (mbsf)	Abundance	Preservation	Chiloguembelina midwayensis	Eoglobigerina edita	Eoglobigerina eobulloides	Globanomalina compressa	Parasubbotina pseudobulloides	Parasubbotina varianta	Praemurica taurica	Subbotina triloculinoides	Globoconusa daubjergensis	Praemurica inconstans	Eoglobigerina spiralis	Praemurica uncinata	Morozovella praeangulata	Globanomalina chapmani	Morozovella conicotruncata	Morozovella angulata	Morozovella velascoensis	Subbotina velascoensis	Globanomalina pseudomenardii	Acarinina subsphaerica	Subbotina hornibrooki	Morozovella acuta	Morozovella occlusa	Subbotina triangularis	Morozovella subbotinae	Acarinina primitiva
middle Eocene	P14	2H-CC, 27-29	15.25	C	M																										
middle Eocene	P14	3H-CC, 23-25	25.32	C	M																										
middle Eocene	P14	4H-CC, 24-26	34.54	C	M																										
middle Eocene	P14	5H-CC, 19-23	44.09	C	M																										
middle Eocene	P14	6H-CC, 21-24	53.62	C	M																										
middle Eocene	P14	7H-CC, 18-21	62.90	C	M																										
middle Eocene	P13	8H-CC, 17-20	72.59	C	M																										
middle Eocene	P13	9H-3, 65-67	75.95	A	VG																										
middle Eocene	P13	9H-CC, 0-1	81.09	C	M																										
middle Eocene	P12	10H-CC, 0-4	91.02	C	M																										
middle Eocene	P12	11H-CC, 0-3	100.03	A	G																									F	
middle Eocene	P12	12H-CC, 0-4	110.35	A	G																									F	
middle Eocene	P12	13H-CC, 12-14	119.93	C	G																										
middle Eocene	P12	14H-CC, 29-31	129.81	A	G																										
middle Eocene	P12	15H-CC, 14-16	138.97	A	G																									R	
middle Eocene	P12	16H-CC, 25-27	148.88	A	G																										
middle Eocene	P12	17X-CC, 16-19	156.82	C	G																										
middle Eocene	P12	18X-CC, 29-32	167.19	A	VG																										
middle Eocene	P12	19X-CC, 27-30	177.53	A	VG																										
middle Eocene	P12	20X-CC, 27-29	187.16	A	G																										
middle Eocene	P12	21X-CC, 32-34	196.80	A	G																										
middle Eocene	P12	22X-CC, 25-27	202.65	A	G																										
middle Eocene	P12	23X-CC, 36-38	215.98	A	G																										
middle Eocene	P12	24X-CC, 17-19	225.43	A	G																										
middle Eocene	P11	25X-CC, 32-34	235.25	A	G																										
middle Eocene	P11	26X-CC, 46-48	244.63	A	G																										
middle Eocene	P11	27X-CC, 36-38	254.47	A	G																										
middle Eocene	P11	28X-CC, 27-29	263.98	A	G																										
middle Eocene	P11	29X-CC, 22-24	273.42	A	G																										
middle Eocene	P11	30X-CC, 20-22	280.45	A	G																										
middle Eocene	P11	31X-CC, 37-39	292.80	A	G																										
middle Eocene	P11	32X-CC, 35-37	300.41	C	G																										
middle Eocene	P11	33X-CC, 13-16	307.74	R	P																										
middle Eocene	P10-P8	34X-CC, 62-64	321.71	C	M																										
middle Eocene	P10-P8	35X-CC, 33-35	330.50	F	M																										
middle Eocene	P10-P8	36X-CC, 34-36	340.89	C	M																										
middle Eocene	P10-P8	37X-CC, 13-16	347.06	F	M																										
early Eocene	P10-P8	38X-CC, 26-29	359.81	F	M																										
early Eocene	P10-P8	39X-CC, 35-38	369.72	F	M																										
middle Eocene	P10-P8	40X-CC, 38-40	377.18	R	P																										
early-middle Eocene	P10-P8	41X-CC, 16-18	380.58	F	M																										
early Eocene	P10-P8	42X-CC, 38-40	399.79	F	M																										
early Eocene	P7	43X-CC, 47-49	409.46	F	M																										
early Eocene	P7	44X-CC, 42-44	418.97	A	G																	R								R	R
early Eocene	P7	45X-CC, 41-43	428.58	A	G																	R		R						F	R
early Eocene	P6b	46X-CC, 33-35	438.16	F	M																									R	R
early Eocene	P6b	47X-CC, 52-54	447.76	R	M																									R	
early Eocene	P6b	48X-CC, 52-54	457.28	C	G																									R	R
early Eocene	P6b	49X-CC, 33-36	460.45	A	G																									R	
early Eocene	P6b	50X-CC, 47-49	467.39	A	G																		F							F	
early Eocene	P6b	51X-CC, 39-41	476.56	A	G																									F	R
early Eocene	P6a	52X-CC, 41-45	486.39	A	G																									F	R
early Eocene	P6a	53X-CC, 49-52	495.94	A	G																		R							F	R
early Eocene	P6a	54X-5, 83-86	502.53	A	M																		F							R	P
late Paleocene	P5	54X-CC, 43-46	504.15	F	M																					R	R			R	P
late Paleocene	P5	55X-4, 15-18	509.95	A	M																		F			F	R	R		A	
late Paleocene	P5	55X-CC, 19-22	510.84	C	M																		R			F	R	R		F	R
late Paleocene	P5	56X-CC, 52-54	524.72	F	P																		F	R		A	F		R	F	R
late Paleocene	P4	57X-CC, 48-50	534.38	F	P																	A			R	A	P		F	
late Paleocene	P4	58X-CC, 34-36	543.91	F	P																	F				A			F	
late Paleocene	P4	59X-CC, 42-44	553.12	C	P						R						P					A				A		R	F	
late Paleocene	P4	60X-CC, 34-36	556.16	C	P													F			A	A				A	R	F		R
late Paleocene	P4	61X-CC, 42-44	562.13	C	P							A	R					F			A	F				F	F		R	R
late Paleocene	P3a	62X-CC, 60-62	572.63	F	M							A	R					F			R	R				P	P			
late Paleocene	P3b	63X-CC, 34-36	582.30	R	P							R	P				R	P			P	P				P				
late Paleocene	P3a	64X-CC, 62-66	592.15	R	P							R	P					P			P									
late Paleocene	P3a	65X-CC, 37-40	601.64	R	P							P	P				R	P												
early Paleocene	P2	66X-CC, 42-45	611.30	R	P							R	R		R	P	R													
early Paleocene	P2	67X-CC, 60-62	620.09	F	M			R	F			R			F	P														
early Paleocene	P2	68X-CC, 47-49	624.83	F	M			R	R				R		R	P														
early Paleocene	P2	69X-CC, 42-45	625.29	R	M			R	R				P		R	P														
early Paleocene	P2	70X-CC, 41-42	631.20	F	M			R	R				P	R	F	P														
early Paleocene	P1c	71X-CC, 28-29	634.78	C	P	R	R	F	F	F	F		F	F	R	R														
early Paleocene	P1c	72X-CC, 20-22	642.47	C	P		F	F	R	F	F	F	F	R	P															
early Paleocene	P1c	73X-CC, 20-22	643.95	C	P	F	F	R	F	F	F	R	R	F																

Notes: Abundance: C = common; A = abundant; R = rare; F = few; P = present. Preservation: M = moderate; VG = very good; G = good; P = poor.

Table 6 (continued).

Age	Zone	Core, section, interval (cm)	Depth (mbsf)	Abundance	Preservation	Acarinina soldadoensis	Acarinina coalingensis	Chiloguembelina wilcoxensis	Morozovella gracilis	Subbotina patagonica	Acarinina angulosa	Acarinina quetra	Subbotina linaperta	Acarinina broedermanni	Morozovella marginodentata	Acarinina angulosa	Morozovella aequa	Morozovella formosa	Morozovella lensiformis	Pseudohastigerina micra	Acarinina cuneicamerata	Morozovella aragonensis	Acarinina pentacamerata	Globigerinatheka senni	Turborotalia lozanoi	Globigerinatheka subconglobata	Morozovella caucasica	Acarinina bullbrooki	Planorotalites pseudoscitula
		171B-1051A-																											
middle Eocene	P14	2H-CC, 27-29	15.25	C	M								F															R	
middle Eocene	P14	3H-CC, 23-25	25.32	C	M								F															R	
middle Eocene	P14	4H-CC, 24-26	34.54	C	M								F															R	
middle Eocene	P14	5H-CC, 19-23	44.09	C	M								F																
middle Eocene	P14	6H-CC, 21-24	53.62	C	M								F																
middle Eocene	P14	7H-CC, 18-21	62.90	C	M								F																
middle Eocene	P13	8H-CC, 17-20	72.59	C	M								F															R	
middle Eocene	P13	9H-3, 65-67	75.95	A	VG																							F	
middle Eocene	P13	9H-CC, 0-1	81.09	C	M								F															R	
middle Eocene	P12	10H-CC, 0-4	91.02	C	M																								
middle Eocene	P12	11H-CC, 0-3	100.03	A	G								F																
middle Eocene	P12	12H-CC, 0-4	110.35	A	G								F													F		F	
middle Eocene	P12	13H-CC, 12-14	119.93	C	G								F													F		F	
middle Eocene	P12	14H-CC, 29-31	129.81	A	G								F							F			P			F		F	
middle Eocene	P12	15H-CC, 14-16	138.97	A	G								F									R				F		R	
middle Eocene	P12	16H-CC, 25-27	148.88	A	G																	R				F		R	
middle Eocene	P12	17X-CC, 16-19	156.82	C	G								F													F		R	
middle Eocene	P12	18X-CC, 29-32	167.19	A	VG															F						R		F	
middle Eocene	P12	19X-CC, 27-30	177.53	A	VG								F							R								F	F
middle Eocene	P12	20X-CC, 27-29	187.16	A	G								F							F					R			F	F
middle Eocene	P12	21X-CC, 32-34	196.80	A	G								F							F								F	F
middle Eocene	P12	22X-CC, 25-27	202.65	A	G								F							F						R		F	F
middle Eocene	P12	23X-CC, 36-38	215.98	A	G								F							F						F		F	F
middle Eocene	P12	24X-CC, 17-19	225.43	A	G								F							F		P				F		F	F
middle Eocene	P11	25X-CC, 32-34	235.25	A	G								F							F						R		F	R
middle Eocene	P11	26X-CC, 46-48	244.63	A	G								F							F		R				F		F	F
middle Eocene	P11	27X-CC, 36-38	254.47	A	G								F							F		R				R		F	F
middle Eocene	P11	28X-CC, 27-29	263.98	A	G								F							F		R				R		F	F
middle Eocene	P11	29X-CC, 22-24	273.42	A	G								F							F		R		F		R		A	F
middle Eocene	P11	30X-CC, 20-22	280.45	A	G								F							F			P					F	F
middle Eocene	P11	31X-CC, 37-39	292.80	A	G								F	R						F								F	F
middle Eocene	P11	32X-CC, 35-37	300.41	C	G								F							R								F	F
middle Eocene	P11	33X-CC, 13-16	307.74	R	P								F															F	F
middle Eocene	P10-P8	34X-CC, 62-64	321.71	C	M								F								F							F	F
middle Eocene	P10-P8	35X-CC, 33-35	330.50	F	M																R					R		F	F
middle Eocene	P10-P8	36X-CC, 34-36	340.89	C	M																F							F	F
middle Eocene	P10-P8	37X-CC, 13-16	347.06	F	M															R	F							F	F
early Eocene	P10-P8	38X-CC, 26-29	359.81	F	M	A						P									F								
early Eocene	P10-P8	39X-CC, 35-38	369.72	F	M	F						A									F						P		
middle Eocene	P10-P8	40X-CC, 38-40	377.18	R	P		R														R							R	
early-middle Eocene	P10-P8	41X-CC, 16-18	380.58	F	M										F					R	R	R	A	R	F	R	R	F	R
early Eocene	P10-P8	42X-CC, 38-40	399.79	F	M								F								F	F	A			R	F		
early Eocene	P7	43X-CC, 47-49	409.46	F	M	F		R					F			F					R	R	F			R	R		
early Eocene	P7	44X-CC, 42-44	418.97	A	G	F		P		R			F			F		F	F		F	F	R			R	P		
early Eocene	P7	45X-CC, 41-43	428.58	A	G	F		R		R			F			F		A	R		R	R	P				R		
early Eocene	P6b	46X-CC, 33-35	438.16	A	M	F			P	F				F				R	R		R	R						
early Eocene	P6b	47X-CC, 52-54	447.76	R	M	F				F				R			F	R	R	R	F	R	R					
early Eocene	P6b	48X-CC, 52-54	457.28	C	G	F			P	F				F			R	F	R	R	R	R	R					
early Eocene	P6b	49X-CC, 33-36	460.45	A	G	F			P	F				F				F		R	R	R	R					
early Eocene	P6b	50X-CC, 47-49	467.39	A	G	F			P	F				F				F	R	R	R	F	R				R	
early Eocene	P6b	51X-CC, 39-41	476.56	A	G	F				R				F			R	F	F	F	R	R	P	F				
early Eocene	P6a	52X-CC, 41-45	486.39	A	G													F	F			P	R						
early Eocene	P6a	53X-CC, 49-52	495.94	A	G	F												R	F			P	R						
early Eocene	P6a	54X-5, 83-86	502.53	A	M	F				F			F																
late Paleocene	P5	54X-CC, 43-46	504.15	F	M	F				F								F											
late Paleocene	P5	55X-4, 15-18	509.95	A	M	F				F	R	R																	
late Paleocene	P5	55X-CC, 19-22	510.84	C	M	F		R	P	R		R																	
late Paleocene	P5	56X-CC, 52-54	524.72	F	P	R																							
late Paleocene	P4	57X-CC, 48-50	534.38	F	P																								
late Paleocene	P4	58X-CC, 34-36	543.91	F	P																								
late Paleocene	P4	59X-CC, 42-44	553.12	C	P																								
late Paleocene	P4	60X-CC, 34-36	556.16	C	P																								
late Paleocene	P4	61X-CC, 42-44	562.13	C	P																								
late Paleocene	P3a	62X-CC, 60-62	572.63	F	M																								
late Paleocene	P3b	63X-CC, 34-36	582.30	R	P																								
late Paleocene	P3a	64X-CC, 62-66	592.15	R	P																								
late Paleocene	P3a	65X-CC, 37-40	601.64	R	P																								
early Paleocene	P2	66X-CC, 42-45	611.30	R	P																								
early Paleocene	P2	67X-CC, 60-62	620.09	F	M																								
early Paleocene	P2	68X-CC, 47-49	624.83	F	M																								
early Paleocene	P2	69X-CC, 42-45	625.29	R	M																								
early Paleocene	P2	70X-CC, 41-42	631.20	F	M																								
early Paleocene	P1c	71X-CC, 28-29	634.78	C	P																								
early Paleocene	P1c	72X-CC, 20-22	642.47	C	P																								
early Paleocene	P1c	73X-CC, 20-22	643.95	C	P																								

Table 6 (continued).

Age	Zone	Core, section, interval (cm)	Depth (mbsf)	Abundance	Preservation	Subbotina inaequispira	Globigerinatheka mexicana	Subbotina cryptomphala	Acarinina spinuloinflata	Globigerinatheka kugleri	Subbotina eocaena	Truncorotaloides topilensis	Globigerina venezuelana	Turborotalia possagnoensis	Morozovella spinulosa	Subbotina hagni	Truncorotaloides rohri	Guembelitrioides higginsi	Chiloguembelina cubensis	Globigerinatheka index	Hantkenina dumblei	Morozovella lehneri	Subbotina frontosa	Acarinina densa	Catapsydrax dissimilis	Subbotina praeturritilina	Globigerina corpulenta	Turborotalia pomeroli	Subbotiona venezuelana	Orbulinoides beckmanni	Turborotalia cerroazulensis
		171B-1051A-																													
middle Eocene	P14	2H-CC, 27-29	15.25	C	M	R									P		R								A	P					R
middle Eocene	P14	3H-CC, 23-25	25.32	C	M	R							R												F	F	F				R
middle Eocene	P14	4H-CC, 24-26	34.54	C	M	R							F												F	F					R
middle Eocene	P14	5H-CC, 19-23	44.09	C	M	F							R		R										F	F					F
middle Eocene	P14	6H-CC, 21-24	53.62	C	M	R							R								P					R	F				R
middle Eocene	P14	7H-CC, 18-21	62.90	C	M	R						P	F								F					F	F				R
middle Eocene	P13	8H-CC, 17-20	72.59	C	M	R						P	F		P						P					F	F		R	R	R
middle Eocene	P13	9H-3, 65-67	75.95	A	VG	A								R							F					F			F	R	R
middle Eocene	P13	9H-CC, 0-1	81.09	C	M	F							R		R						F					R				R	
middle Eocene	P12	10H-CC, 0-4	91.02	C	M	F						F	R								F						F				
middle Eocene	P12	11H-CC, 0-3	100.03	A	G	A						A	R		R						F	F		F		R		R		
middle Eocene	P12	12H-CC, 0-4	110.35	A	G	F							R		R		R				R			R			R		
middle Eocene	P12	13H-CC, 12-14	119.93	C	G	F								F	R	R	F							F		F	R	F	R	
middle Eocene	P12	14H-CC, 29-31	129.81	A	G						F	R	F	R	R	R			R	R	R	P		F	F		R	F	
middle Eocene	P12	15H-CC, 14-16	138.97	A	G										R	F		R		F	R			F	R				
middle Eocene	P12	16H-CC, 25-27	148.88	A	G	F	A											R		F	R	R			R				
middle Eocene	P12	17X-CC, 16-19	156.82	C	G	F	R													A	P								
middle Eocene	P12	18X-CC, 29-32	167.19	A	VG	F	F											A			F	F							
middle Eocene	P12	19X-CC, 27-30	177.53	A	VG	F	R					R	R					F	R	F	F	F	R	F	R				
middle Eocene	P12	20X-CC, 27-29	187.16	A	G	R	F					R					F	F	F	R	F	F	F	R				
middle Eocene	P12	21X-CC, 32-34	196.80	A	G													A			R	F							
middle Eocene	P12	22X-CC, 25-27	202.65	A	G	F	F					R			R	R	R	R	F	R	P	F	R	R	R	F			
middle Eocene	P12	23X-CC, 36-38	215.98	A	G	F	A					R	R					F	R	R	F	R	R	R				
middle Eocene	P12	24X-CC, 17-19	225.43	A	G	R	R					F	R		F		F		F	F	F	R	R				
middle Eocene	P11	25X-CC, 32-34	235.25	A	G	F	F						R		A	R	A	R	F	R	R				
middle Eocene	P11	26X-CC, 46-48	244.63	A	G		F					F	F	F	A	A	F	F	R	R	P	R				
middle Eocene	P11	27X-CC, 36-38	254.47	A	G	F	R					F	R	F	R		R										
middle Eocene	P11	28X-CC, 27-29	263.98	A	G	R						R	F	F	R	R										
middle Eocene	P11	29X-CC, 22-24	273.42	A	G	R	R					R	R	F	R	F										
middle Eocene	P11	30X-CC, 20-22	280.45	A	G	R	R					R	R	R	F	F										
middle Eocene	P11	31X-CC, 37-39	292.80	A	G	R						R	F	F	F											
middle Eocene	P11	32X-CC, 35-37	300.41	C	G	F	R				F	P	P	P	P	R	F	R								
middle Eocene	P11	33X-CC, 13-16	307.74	R	P	F					P	P	P	R	R		F	F	R							
middle Eocene	P10-P8	34X-CC, 62-64	321.71	C	M	F	F				P	R	R				F	R								
middle Eocene	P10-P8	35X-CC, 33-35	330.50	F	M	R	R	P	P		R	R	R	R											
middle Eocene	P10-P8	36X-CC, 34-36	340.89	C	M						R	R	R	R											
middle Eocene	P10-P8	37X-CC, 13-16	347.06	F	M						R	R	F	R											
early Eocene	P10-P8	38X-CC, 26-29	359.81	F	M						P	P													
early Eocene	P10-P8	39X-CC, 35-38	369.72	F	M	F	P				P	P													
middle Eocene	P10-P8	40X-CC, 38-40	377.18	R	P																				
early-middle Eocene	P10-P8	41X-CC, 16-18	380.58	F	M	R																			
early Eocene	P10-P8	42X-CC, 38-40	399.79	F	M																				
early Eocene	P7	43X-CC, 47-49	409.46	F	M																				
early Eocene	P7	44X-CC, 42-44	418.97	A	G																				
early Eocene	P7	45X-CC, 41-43	428.58	A	G																				
early Eocene	P6b	46X-CC, 33-35	438.16	F	M																				
early Eocene	P6b	47X-CC, 52-54	447.76	R	M																				
early Eocene	P6b	48X-CC, 52-54	457.28	C	G																				
early Eocene	P6b	49X-CC, 33-36	460.45	A	G																				
early Eocene	P6b	50X-CC, 47-49	467.39	A	G																				
early Eocene	P6b	51X-CC, 39-41	476.56	A	G																				
early Eocene	P6a	52X-CC, 41-45	486.39	A	G																				
early Eocene	P6a	53X-CC, 49-52	495.94	A	G																				
early Eocene	P6a	54X-5, 83-86	502.53	A	M																				
late Paleocene	P5	54X-CC, 43-46	504.15	F	M																				
late Paleocene	P5	55X-4, 15-18	509.95	A	M																				
late Paleocene	P5	55X-CC, 19-22	510.84	C	M																				
late Paleocene	P5	56X-CC, 52-54	524.72	F	P																				
late Paleocene	P4	57X-CC, 48-50	534.38	F	P																				
late Paleocene	P4	58X-CC, 34-36	543.91	F	P																				
late Paleocene	P4	59X-CC, 42-44	553.12	C	P																				
late Paleocene	P4	60X-CC, 34-36	556.16	C	P																				
late Paleocene	P4	61X-CC, 42-44	562.13	C	P																				
late Paleocene	P3a	62X-CC, 60-62	572.63	F	M																				
late Paleocene	P3b	63X-CC, 34-36	582.30	R	P																				
late Paleocene	P3a	64X-CC, 62-66	592.15	R	P																				
late Paleocene	P3a	65X-CC, 37-40	601.64	R	P																				
early Paleocene	P2	66X-CC, 42-45	611.30	R	P																				
early Paleocene	P2	67X-CC, 60-62	620.09	F	M																				
early Paleocene	P2	68X-CC, 47-49	624.83	F	M																				
early Paleocene	P2	69X-CC, 42-45	625.29	R	M																				
early Paleocene	P2	70X-CC, 41-42	631.20	F	M																				
early Paleocene	P1c	71X-CC, 28-29	634.78	C	P																				
early Paleocene	P1c	72X-CC, 20-22	642.47	C	P																				
early Paleocene	P1c	73X-CC, 20-22	643.95	C	P																				

bathyal depths (1000–2000 m) during late Paleocene–middle Eocene times at Site 1051.

The lower to middle Eocene fauna (between Samples 171B-1051A-5H-CC, 19–23 cm, and 50X-CC, 47–49 cm) is characterized by typical post-Paleocene/Eocene benthic extinction taxa including *Aragonia semireticulata, Bulimina* cf. *semicostata, B. macilenta, B. semicostata, B. thanetensis, B. tuxpamensis, Buliminella grata, Cibicidoides grimsdalei, C. praemundulus, C. subspiratus, Karreriella subglabra, Osangularia mexicana, Pullenia eocaenica,* and *Uvigerina rippensis,* along with *Globocassidulina subglobosa* and *Quadrimorphina profunda.* An additional component of the Eocene fauna is represented by several taxa through the early Paleocene into the middle Eocene (i.e., pleurostomellids, *Bulimina trinitatensis, Buliminella beaumonti, Nodogenerina* spp., *Nonion* spp., *Oridorsalis* spp., *Tritaxia* spp., and common *Nuttallides truempyi*).

One of the uppermost Paleocene samples (171B-1051A-55X-CC, 19–22 cm) contains a few benthic foraminifers representing a mixed assemblage of both pre- and post-Paleocene/Eocene benthic extinction taxa (i.e., *Aragonia velascoensis, Osangularia velascoensis;* and *A. semireticulata, O. mexicana,* respectively), indicating that this sample is located near (below) the Paleocene/Eocene boundary. The next three (upward) samples of latest Paleocene to earliest Eocene age (Samples 171B-1051A-55X-4, 15–18 cm, through 54X-CC, 43–46 cm; see Table 7) have only traces of benthic foraminifers without any typical pre- or post-Paleocene/Eocene benthic extinction marker species among them. The faunas in these samples are represented by a few moderately preserved, minute buliminids and lagenids, *Nonion* spp., *Oridorsalis* spp., and *Pullenia* spp., indicating that the establishment of a typical post-Paleocene/Eocene benthic extinction benthic foraminifer fauna emerged rather slowly over a considerable length of time. This interval of at least 10 m may thus represent an expanded and thereby unique interval of environmental disturbance affecting the benthic foraminifer community at the Blake Nose. It may provide an excellent opportunity to study environmentally stressed benthic foraminifer faunas, the nature of the upper Paleocene deep-sea benthic foraminifer extinction event, and the structure of benthic foraminifer recolonization and faunal development linked to the improvement of environmental conditions during the early Eocene. For example, shipboard examination of samples from within this interval revealed an elongate buliminid taxon (referred to as *Bulimina* sp. [elongate]) that has its FO in the late Paleocene (Sample 171B-1051A-55X-CC, 19–22 cm) and ranged through all the samples of the critical interval (Table 7) to disappear in the early Eocene (Sample 171B-1051A-50X-CC, 47–49 cm). During its relatively short stratigraphic range, *Bulimina* sp. (elongate) shows rapid morphological evolution. In the late Paleocene, the taxon is represented by rather small, stout tests with blunt initial ends that change to much larger, elongated forms with pointing initial ends in the early Eocene. If this evolutionary lineage can be verified by subsequent data, it may provide a useful biostratigraphic marker for the Paleocene/Eocene boundary interval.

The LO of *Gavelinella beccariiformis* in Sample 171B-1051A-56X-CC, 52–54 cm, marks the upper limit of the benthic foraminifer fauna typical of the late Paleocene in Hole 1051A. As at Site 1050 (see "Site 1050" chapter, this volume), *G. beccariiformis* disappears somewhat earlier than *Aragonia velascoensis* and *Osangularia velascoensis,* suggesting that the benthic foraminifer extinction was not necessarily an instantaneous event at the Blake Nose.

The pre-extinction fauna in Hole 1050A occurs in Samples 171B-1051A-73X-CC, 20–22 cm, to 56X-CC, 52–54 cm (Table 7), and is characterized by a number of taxa that were victimized by the Paleocene/Eocene benthic extinction (e.g., Tjalsma and Lohmann, 1983; Van Morkhoven et al., 1986), represented by *Aragonia velascoensis, Bolivinoides delicatulus, Bulimina spinea* (= *midwayensis*), *B. velascoensis, Cibicidoides dayi, C. hyphalus, Coryphostoma midwayensis, Gavelinella beccariiformis, Osangularia velascoensis, Parala-*

Table 7. Hole 1051A samples examined for benthic foraminifers.

Age	Core, section, interval (cm)	Depth (mbsf)	Abundance	Preservation
	171B-1051A-			
middle Eocene	5H-CC, 19-23	44.09	Few	Moderate
middle Eocene	10H-CC, 0-4	91.02	Common	Moderate
middle Eocene	15H-CC, 14-16	138.97	Rare	Good
middle Eocene	20X-CC, 27-29	187.16	Rare	Good
middle Eocene	25X-CC, 32-34	235.25	Rare	Good
middle Eocene	30X-CC, 20-22	280.45	Rare	Good
middle Eocene	35X-CC, 33-35	330.50	Few	Moderate
early-middle Eocene	41X-CC, 16-18	380.58	Few	Moderate
early Eocene	45X-CC, 41-43	428.58	Rare	Good
early Eocene	50X-CC, 47-49	467.39	Rare	Good
early Eocene	54X-5, 83-86	502.53	Trace	Poor
early Eocene	54X-CC, 43-46	504.15	Trace	Moderate
early Eocene	55X-3, 26-29	508.56	Trace	Poor
late Paleocene	55X-4, 15-18	509.95	Trace	Moderate
late Paleocene	55X-CC, 19-22	510.84	Few	Moderate
late Paleocene	56X-CC, 52-54	524.72	Rare	Poor
late Paleocene	60X-CC, 34-36	556.16	Few	Poor
early Paleocene	66X-CC, 42-45	611.30	Common	Poor
early Paleocene	70X-CC, 41-42	631.20	Few	Moderate
early Paleocene	73X-CC, 20-22	643.95	Few	Poor

bamina hillebrandti, Pullenia coryelli, Pyrmidina rudita, and *Spiroplectammina* cf. *jarvisi.*

The ratio of *G. beccariiformis* to *N. truempyi* at Site 1051 is similar to that at Sites 1049 and 1050 (see "Site 1049" and "Site 1050" chapters, this volume). This may indicate that the benthic foraminifer faunas at Site 1051 were influenced by low-oxygen, warm, saline, deep waters compatible to the deeper parts of the Blake Nose during Maastrichtian and Paleogene times (see "Site 1049" and "Site 1050" chapters, this volume).

Radiolarians

Radiolarian recovery was remarkable in Hole 1051A, as shown by well-preserved faunas in most of the core-catcher samples. Their ages span the late middle Eocene to the early Paleocene. Most of the core-catcher samples from Hole 1051A were processed and examined, but none was analyzed from Hole 1051B because of time constraints. The faunas from the upper half of the hole were all well preserved. However, a few core catchers downhole, especially from Sections 171B-1051A-60X-CC through 72X-CC, displayed reduced faunal preservation and abundance because of higher clay input and radiolarian test dissolution. Also, rare downhole contamination and reworking of older sediments produced broken forms that were easily distinguishable from the in situ fauna. The zonal scheme for low-latitude radiolarian faunas (Riedel and Sanfilippo, 1978) was used for zonal assignments, and the numbers R1–R11 (see "Explanatory Notes" chapter, this volume) were used in the biostratigraphic correlation, shown in Figure 21. Occurrence, abundance, and preservation of the radiolarian taxa are shown in Table 8.

All but the very top of the middle Eocene is represented by well-preserved radiolarian faunas. The uppermost core-catcher samples 171B-1051A-2H-CC and 3H-CC contain radiolarians assignable to the upper middle Eocene *Podocyrtis goetheana* Zone (Zone R11; Fig. 21). The base of this zone is defined by the FO of *P. goetheana* and is synchronous with the FO of *Lithocyclia aristotelis.* The evolutionary transition of *Thyrsocyrtis tricantha* to *T. tetracantha* also occurs near the base of Zone R11. Samples 171B-1051A-4H-CC through 7H-CC contain faunas assignable to the *P. chalara* Zone (Zone R10), the base of which is defined by the evolutionary transition from *P. mitra* to *P. chalara.* The lower limit of the zone is synchronous with the extinction of the key marker *Phormocyrtis striata striata.* An inflated, undescribed morphotype similar to *P. s. striata* appears in the lower part of Zone R10 and ranges into the overlying *P. chalara* Zone. *P. trachodes* also makes its final appearance in the

upper part of the zone. Core-catcher Samples 171B-1051A-8H-CC through 14H-CC and 16H-CC contain a well-preserved fauna characteristic of the *P. mitra* Zone (Zone R9). The base of Zone R9 is marked by the evolutionary transition of *P. sinuosa* to *P. mitra* and its top by the last appearance of *P. mitra.* Another specific event within this zone is the LO of *Eusyringium lagena.*

Core-catcher Samples 171B-1051A-17X-CC, 18X-CC, 20X-CC, 22X-CC, and 23X-CC contain radiolarians assignable to the middle Eocene *Podocyrtis ampla* Zone (Zone R8). The base of this zone is defined by the FO of *P. ampla* (evolutionary transition of *P. phyxis* to *P. ampl*a); *P. trachodes* makes it FO and *P. dorus* its LO near the upper part of the zone. Unfortunately, *P. ampla* occurs sporadically in these core catchers. Samples 171B-1051A-24X-CC, 26X-CC, 28X-CC, 30X-CC, 32X-CC, and 34X-CC contain a fauna assignable to the *Thyrsocyrtis triacantha* Zone (Zone R7), the base of which is defined by the first appearance of *Eusyringium lagena.* Although generally rare throughout Zone R7, *E. lagena* does increase in abundance in the overlying *P. ampla* Zone. *E. fistuligerum,* which is characterized by an extended postabdominal tube, evolved from *E. lagena* and first appears in Section 171B-1051A-24X-CC.

Sections 171B-1051A-35X-CC and 36X-CC contain radiolarians assignable to the *Dictyopora mongolfieri* Zone (Zone R6), the base of which is defined by the FO of *D. mongolfieri. Theocotyle conica* also makes its first appearance near the base of the zone. *D. mongolfieri,* like *E. lagena,* exhibits tremendous variation in morphology throughout its range, and several early morphotypes were observed in Section 171B-1051A-36X-CC. The distinct taxa *Lamptonium fabaeforme fabaeforme* has its LO in the top part of the zone. Samples 171B-1051A-37X-CC through 39X-CC contain radiolarians indicative of the *T. cryptocephala* Zone (Zone R5). The base of this zone is defined by the evolutionary transition of *T. nigriniae* to *T. cryptocephala. Theocotyle venezuelensis* is unique in making its first appearance near the base of Zone R5 because most taxa within Zone R5 have their origin in the early Eocene and become extinct in the overlying *D. mongolfieri* and *Thyrsocyrtis triacantha* Zones. The first Site 1051A core catcher with poor radiolarian preservation is 171B-1051A-37X-CC, and Sample 171B-1051A-40X-CC is completely barren of radiolarians.

The radiolarian faunas from 171B-1051A-41X-CC through 45X-CC are assignable to the *Phormocyrtis striata striata* Zone (Zone R4). The lower limit of this zone is determined by the first appearances of *P. s. striata* as well as *Lychnocanoma bellum, Thyrsocyrtis hirsuta,* and *T. rhizodon.* Both the distinct markers *Buryella clinata* and *Spongatractus balbis* make their last appearance in the top of the zone in Section 171B-1051A-41X-CC. Several forms of the species *Pterocodon ampla* are found in Section 45X-CC and are probably the result of reworking. The morphotypic evolution of *P. striata exquisita* to *P. s. striata* begins in Section 171B-1051A-47X-CC in the underlying *B. clinata* Zone and continues into 45X-C. Unfortunately, however, part of the transition is missing, as 46X-CC only contained rare, poorly preserved radiolarians.

Samples 171B-1051A-46X-CC through 48X-CC were assigned to the *Buryella clinata* Zone (Zone R3). The base of this zone is marked by the FO of *B. clinata* as well as *Spongatractis babis* and *Thecotyle nigriniae.* Other marker taxa that make their final appearances in the upper part of the zone are *Bekoma bitardensis, Buryella tetradica,* and *Pterodon ampla.*

Samples 171B-1051A-49X-CC through 57X-CC are assigned to the *Bekoma bitardensis* Zone (Zone R2), which ranges across the Paleocene/Eocene boundary (Fig. 21). Preservation and abundance of the radiolarian fauna near the boundary in Section 171B-1051A-46X-CC are moderate, although the radiolarian tests are recrystallized. The base of the zone is characterized by the first appearance of *B. bidartensis.* The taxa *Lamptonium f. chaunothorax* and *Pterocodon ampla* make their first appearance just above the base of the zone. The species *Pterodon? anteclinata* is restricted to this zone, and

other forms, such as *Stylosphaera coranatus coranatus* and *S. goruna,* range downward into the Paleocene. The species *L. pennatum* was found to straddle the *B. bidartensis/B. campechensis* zonal boundary at both Sites 1050 and 1051.

The remainder of the samples from Hole 1051A (Samples 171B-1051A-58X-CC through 73X-CC) are assigned to the Paleocene *Bekoma campechensis* Zone (Zone R1). This zone is defined by the first appearance of *B. campechensis* and contains the common form *Buryella tetradica,* which ranges down into the unzoned Paleocene. Another *Buryella* species, *B. pentadica,* although generally rare, is restricted to this zone.

Many of the Paleocene taxa shown in Table 6 are not a part of the low-latitude zonal scheme of Riedel and Sanfilippo (1978). However, both Blome (1992) and Nishimura (1992) have shown that many of these taxa can be biostratigraphically useful in the Paleocene part of the *Buryella bidartensis* Zone and all through the *B. campechensis* Zone. Specific examples include *Cromyomma riedeli, Stylosphaera goruna,* and *Stylotrochus alveatus.*

Sediment Accumulation Rates

Ages and sub-bottom depths for calcareous nannofossil and planktonic foraminifer datums used to calculate sediment accumulation rates are listed in Tables 4 and 5 and are plotted in Figure 22. The 620-m sequence cored in Hole 1051A ranges in age from 38 to 64 Ma and has an average accumulation rate of 27 m/m.y. Sedimentation rates for the Eocene were ~36 m/m.y., and the Paleocene averaged ~18 m/m.y. Accumulation rates for this site were greater than those in nearby Hole 1050A, which averaged 20 m/m.y. Increased biosiliceous productivity may be the cause for such rapid rates of sediment accumulation. It is worth noting, however, that despite increased clay input, sedimentation rates decreased in the Paleocene relative to the Eocene in Hole 1051A.

Two hiatuses, each ~2 m.y. long, were observed, one within the Eocene at 380 mbsf and one within the Paleocene at 543 mbsf. These disconformities correspond in age to hiatuses reported at Site 1050A.

PALEOMAGNETISM

Laboratory Procedures and Interpretations

Portions from nearly all cores yielded useful but noisy magnetostratigraphic data using the shipboard pass-through magnetometer, and the interpretations were augmented by the post-cruise thermal demagnetization of 195 minicores. Polarity intervals were reproduced for Holes 1051A and 1051B, and the composite polarity pattern correlates with Chrons C28n through C16n of the Paleocene through upper Eocene.

Measurements were made using the pass-through cryogenic magnetometer on the archive half of all core sections >40 cm long from both holes. Each section was measured at 5-cm intervals at natural remanent magnetization (NRM) and then at a 20 mT alternating-field (AF) demagnetization step. The tensor tool was used to obtain the orientation of APC cores in both holes (Cores 171B-1051A-4H through 8H and 171B-1051B-4H through 15H). Discrete samples taken (approximately four oriented cylinders or plastic cubes per core) to enhance the magnetostratigraphic reliability were analyzed post cruise using progressive thermal and AF demagnetization. Thermal demagnetization results of 195 discrete samples from Hole 1051A were completed at the paleomagnetics laboratories at the University of Oxford and the University of Michigan. These analyses and associated polarity interpretations are included in this *Initial Results* volume (see Tables 9 [ASCII format], 10 [PDF format] on CD-ROM, backpocket, this volume). Progressive thermal demagnetization was generally at 30°C increments from ~140° through 360°C, with continuation to higher thermal steps for the more stable samples. A thermal

Table 8. Radiolarian abundance and preservation at Hole 1051A.

Age	Zone	Core, section, interval (cm)	Depth (mbsf)	Abundance	Preservation	Bathropyramis woodringi	Buryella pentadica	Buryella tetradica	Cromyomma riedeli	Phormocyrtis striata praexquisita	Spongurus (?) regularis group	Stylosphaera coronatus coronatus	Thyrsocyrtis (?) annikae	Entapium regulare	Periphaena decora	Xiphosphaera circularis	Phormocyrtis striata exquisita	Bekoma campechensis	Spongurus quadratus	Stylotrochus alveatus	Stylosphaera goruna	Astrosphaerin sp. E	Astrosphaerin sp. F	Lamptonium pennatum	Lithomespilus mendosa	Bekoma bidartensis	Lamptonium fabaeforme chaunothorax	Pterocodon ampla	Pterocodon? anteclinata	Theocotylissa alpha	Lamptonium fabaeforme fabaeforme	Calocycloma castum	Spongatractus balbis	Theocotyle nigriniae	Buryella clinata	Lithocyclia ocellus group	Periphaena decora	Calocyclas hispida	Podocyrtis (Podocyrtis) papalis
		171B-1051A-																																						
middle Eocene	P. goetheana	2H-CC, 27-29	15.25	F	M																																		R	C
middle Eocene	P. goetheana	3H-CC, 23-25	25.32	A	VG																																C		R	C
middle Eocene	Podocyrtis chalara	4H-CC, 24-26	34.54	C	VG																																		F	C
middle Eocene	Podocyrtis chalara	5H-CC, 19-23	44.09	A	VG																																	C	F	C
middle Eocene	Podocyrtis chalara	6H-CC, 21-24	53.62	F	M																																			R
middle Eocene	Podocyrtis chalara	7H-CC, 18-21	62.9	A	VG																																F	C	F	C
middle Eocene	Podocyrtis mitra	8H-CC, 17-20	72.59	C	G																																		F	C
middle Eocene	Podocyrtis mitra	9H-CC, 0-1	81.09	C	G																																C	C		C
middle Eocene	Podocyrtis mitra	10H-CC, 0-4	91.02	A	VG																																		F	C
middle Eocene	Podocyrtis mitra	11H-CC, 0-3	100.03	C	VG																																F		F	C
middle Eocene	Podocyrtis mitra	12H-CC, 0-4	110.35	A	VG																																F		F	F
middle Eocene	Podocyrtis mitra	13H-CC, 12-14	119.93	A	VG																																C		F	F
middle Eocene	Podocyrtis mitra	14H-CC, 29-31	129.81	A	VG																																		F	F
middle Eocene	Podocyrtis mitra	16H-CC, 25-27	148.88	A	VG																																		F	F
middle Eocene	Podocyrtis ampla	17X-CC, 16-19	156.82	A	VG																																F		F	C
middle Eocene	Podocyrtis ampla	18X-CC, 29-32	167.19	C	G																																		F	F
middle Eocene	Podocyrtis ampla	20X-CC, 27-29	187.16	F	M																																			F
middle Eocene	Podocyrtis ampla	22X-CC, 25-27	202.65	C	G																																C	F	F	C
middle Eocene	Podocyrtis ampla	23X-CC, 36-38	215.98	A	VG																																C		F	C
middle Eocene	T. triacantha	24X-CC, 17-19	225.43	C	M																																	C	F	F
middle Eocene	T. triacantha	26X-CC, 46-48	244.63	C	G																																C	C		C
middle Eocene	T. triacantha	28X-CC, 27-29	263.98	C	VG																																C	C		C
middle Eocene	T. triacantha	30X-CC, 20-22	280.45	C	G																																C	C	F	C
middle Eocene	T. triacantha	32X-CC, 35-37	300.41	C	VG							C																									C	C	C	C
middle Eocene	T. triacantha	34X-CC, 62-64	321.71	C	VG							C																										C	F	C
middle Eocene	D. mongolfieri	35X-CC, 33-35	330.5	C	G																						R				F								F	R
middle Eocene	D. mongolfieri	36X-CC, 34-36	340.89	A	VG																						F				F								F	
middle Eocene	T. cryptocephala	37X-CC, 13-16	347.06	F	P						F					C											R				F								R	
middle Eocene	T. cryptocephala	38X-CC, 26-29	359.81	C	G						C					A											R				R								F	
middle Eocene	T. cryptocephala	39X-CC, 35-38	369.72	C	G						C					A											R				C									C
Barren	Unknown	40X-CC, 38-40	377.18																																			
early Eocene	T. cryptocephala-P. striata striata	41X-CC, 16-18	380.58	A	G						A					A											R				F	F	F	F		C		F	C
early Eocene	P. striata striata	42X-CC, 38-40	399.79	C	VG						C					C										R	R				F	C	F	R		C	C	R	C
early Eocene	P. striata striata	43X-CC, 47-49	409.46	C	VG						C					A											R				F	C	C	R		C		R	C
early Eocene	P. striata striata	44X-CC, 42-44	418.97	C	G						A					C											F				F	R	R	F					C
early Eocene	P. striata striata	45X-CC, 41-43	428.58	C	G						C					C										R			R		R	R	F	C		R		C	F
early Eocene	B. clinata	46X-CC, 33-35	438.16	F	P					F	F					R											R				F	F		F	R	F	F			R	F
early Eocene	B. clinata	47X-CC, 52-54	447.76	C	G					F	C					C											R				F	F	R	F	R		F		R	F
early Eocene	B. clinata	48X-CC, 52-54	457.28	C	M					F	C					C										F	F				F	R	R	F	R		F	C		
early Eocene-late Paleocene	B. bidartensis	49X-CC, 33-36	460.45	C	M					F	C					C	C									R	F	C				R	R							
early Eocene-late Paleocene	B. bidartensis	50X-CC, 47-49	467.39	C	G						C					C	F									R	R	F				R	R							
early Eocene-late Paleocene	B. bidartensis	52X-CC, 41-45	486.39	C	M						C				C	F	A												F	F		F								
early Eocene-late Paleocene	B. bidartensis	54X-CC, 43-46	504.15	F	M					C	C		R			C	A									R	F	F	R	R										
Paleocene	B. bidartensis	56X-CC, 52-54	524.72	C	G					C	C		R		C	C	F	C	R							R									F				
Paleocene	B. bidartensis	57X-CC, 48-50	534.38	C	G					C	A				C	C	F	C	C		F				C		F	F	F										
Paleocene	B. campechensis	58X-CC, 34-36	543.91	C	M		F	C			C				C	C	F	C			F						F	C	F	F									
Paleogene	B. campechensis	60X-CC, 34-36	556.16	C	G		R	R			C				C	C	F	C	C		F						C	F	F	F									
Paleocene	B. campechensis	62X-CC, 60-62	572.63	F	M		R	R			C				C	C	R		R	R					R		R	F											
Paleocene	B. campechensis	64X-CC, 62-66	592.15	R	P			R			R	F				R		R			R					R		R	R											
Paleocene	B. campechensis	66X-CC, 42-45	611.3	F	P		R	R			R	F				F			R	R					R	R		R	R	R										
Paleocene	B. campechensis	68X-CC, 47-49	624.83	F	P						F	F				C									R	R		R	R	R										
Paleocene	B. campechensis	70X-CC, 11-14	630.9	C	P	R	R	F			C	C				F	F				R					R														
Paleocene	B. campechensis	72X-CC, 20-22	642.47	C	P	R	R	F		F	C	C				F	F				F					F														
Paleocene	B. campechensis	73X-CC, 20-22	643.95	C	M	R	F	C	F	C	C	C	C	F																											

Notes: Abundance: C = common; A = abundant; R = rare; F = few; P = present. Preservation: M = moderate; VG = very good; G = good; P = poor.

Table 8 (continued).

Age	Zone	Core, section, interval (cm)	Depth (mbsf)	Abundance	Preservation	Phormocyrtis striata striata	Thyrsocyrtis (Thyrsocyrtis) hirsuta	Thyrsocyrtis (Thyrsocyrtis) rhizodon	Lamptonium fabaeforme fabaeforme	Theocotylissa ficus	Thyrsocyrtis (Thyrsocyrtis) tarsipes	Thyrsocyrtis (Pentalacorys) tensa	Podocyrtis (Lampterium) sinuosa	Podocyrtis (Podocyrtoges) diamesa	Theocotyle cryptocephala	Theocotyle venezuelensis	Thyrsocyrtis (Thyrsocyrtis) robusta	Dictyoprora mongolfieri	Theocotyle conica	Eusyringium lagena	Thyrsocyrtis (Pentalacorys) triacantha	Spongatractus pachystylus	Eusyringium fistuligerum	Podocyrtis (Podocyrtoges) phyxis	Lychnocanoma bellum	Podocyrtis (Podocyrtoges) ampla	Podocyrtis (Lampterium) trachodes	Podocyrtis (Podocyrtoges) dorus	Podocyrtis (Lampterium) mitra	Sethochytr triconiscus	Thyrsocyrtis (Pentalacorys) lochites	Podocyrtis (Lampterium) fasciolata	Podocyrtis (Lampterium) chalara	Tristylospyris triceros	Cryptocarpium ornatum	Lithocyclia aristotelis group	Thyrsocyrtis (Pentalacorys) tetracantha	Dictyoprora pirum	Lophocyrtis (Lophocyrtis) jacchia
		171B-1051A-																																						
middle Eocene	P. goetheana	2H-CC, 27-29	15.25	F	M			F		F F								C			R		F								R		C R R			R	R	F	R R
middle Eocene	P. goetheana	3H-CC, 23-25	25.32	A	VG			F		F R								C			C		F								R	F	C R				R		
middle Eocene	Podocyrtis chalara	4H-CC, 24-26	34.54	C	VG			F										C			F		F								R	R	F F						
middle Eocene	Podocyrtis chalara	5H-CC, 19-23	44.09	A	VG			F										C			F		F	R F							R	R	C						
middle Eocene	Podocyrtis chalara	6H-CC, 21-24	53.62	F	M			F										A			F		F	R			F				R	R	C						
middle Eocene	Podocyrtis chalara	7H-CC, 18-21	62.9	A	VG			F		C								C			F		F		R	F	F		F		R		R						
middle Eocene	Podocyrtis mitra	8H-CC, 17-20	72.59	C	G	R	R	C		C								A			F		C			F	F		F	R	F								
middle Eocene	Podocyrtis mitra	9H-CC, 0-1	81.09	C	G	R	R	C		C								A			F		F			R F	R		F		F								
middle Eocene	Podocyrtis mitra	10H-CC, 0-4	91.02	C	VG	R	F	C		F	R R							A			R		C			R R	F R		F		R								
middle Eocene	Podocyrtis mitra	11H-CC, 0-3	100.03	C	VG	C	C	F		F								C			F		F			F R	R		F	F									
middle Eocene	Podocyrtis mitra	12H-CC, 0-4	110.35	A	VG	C	C	F		F								C		T	R		F			F			F R	R	R								
middle Eocene	Podocyrtis mitra	13H-CC, 12-14	119.93	A	VG	C	C			F								C		T R	C	F	F			F			F F	R	F			R					
middle Eocene	Podocyrtis mitra	14H-CC, 29-31	129.81	A	VG	C	C			F								C	R R		F	R	F	R		F			R R	R R	R			F					
middle Eocene	Podocyrtis mitra	16H-CC, 25-27	148.88	A	VG	C	C			R								C	R R		F	F	F	R					F		R			R					
middle Eocene	Podocyrtis ampla	17X-CC, 16-19	156.82	A	VG	C	C			F			F					C		T	F	F	F			F	F			C									
middle Eocene	Podocyrtis ampla	18X-CC, 29-32	167.19	C	G	C	F			F										T	F		C				F		F										
middle Eocene	Podocyrtis ampla	20X-CC, 27-29	187.16	F	M	F	F			F							F	C			R		C				F		R										
middle Eocene	Podocyrtis ampla	22X-CC, 25-27	202.65	C	G	C											C	C			R		R			R R	R R		F R										
middle Eocene	Podocyrtis ampla	23X-CC, 36-38	215.98	A	VG	C				F			R			R	A	A			R		F		R	R R	R R		R										
middle Eocene	T. triacantha	24X-CC, 17-19	225.43	F	M	F	R		F								C	A			R		R			F	R		F										
middle Eocene	T. triacantha	26X-CC, 46-48	244.63	C	G	C			F				F F			F R	C	A			R		R			F	F		F										
middle Eocene	T. triacantha	28X-CC, 27-29	263.98	C	VG	C	F	F		F F			F				C	A			R		F	R															
middle Eocene	T. triacantha	30X-CC, 20-22	280.45	C	G	C	A	C		F							C	A			R		F																
middle Eocene	T. triacantha	32X-CC, 35-37	300.41	C	VG	C	R	C									A	A			R		F																
middle Eocene	T. triacantha	34X-CC, 62-64	321.71	C	VG	C	F					C F				R F	A	A	R R		F		F																
middle Eocene	D. mongolfieri	35X-CC, 33-35	330.5	C	G	C	R	F			R R	C R	F		R	R R	A	A	R																				
middle Eocene	D. mongolfieri	36X-CC, 34-36	340.89	C	VG	C	R R				R R	F F	F		F	R R	A	C	R																				
middle Eocene	T. cryptocephala	37X-CC, 13-16	347.06	F	P	C	R	F				F F		R R	R R	R R	C																						
middle Eocene	T. cryptocephala	38X-CC, 26-29	359.81	C	G	C	R					F F		F R R	R R	F R																							
middle Eocene	T. cryptocephala	39X-CC, 35-38	369.72	C	G	C						R	T	F R	R																								
Barren	Unknown	40X-CC, 38-40	377.18																																			
early Eocene	T. cryptocephala-P. striata striata	41X-CC, 16-18	380.58	A	G	C	C			F	R R	R																											
early Eocene	P. striata striata	42X-CC, 38-40	399.79	C	VG	C	C			R	R R																												
early Eocene	P. striata striata	43X-CC, 47-49	409.46	C	VG	C	C	R	R A																														
early Eocene	P. striata striata	44X-CC, 42-44	418.97	C	G	C	F																																
early Eocene	P. striata striata	45X-CC, 41-43	428.58	C	G	C	F	R																															
early Eocene	B. clinata	46X-CC, 33-35	438.16	F	P																																		
early Eocene	B. clinata	47X-CC, 52-54	447.76	C	G																																		
early Eocene	B. clinata	48X-CC, 52-54	457.28	C	M																																		
early Eocene-late Paleocene	B. bidartensis	49X-CC, 33-36	460.45	C	M																																		
early Eocene-late Paleocene	B. bidartensis	50X-CC, 47-49	467.39	C	G																																		
early Eocene-late Paleocene	B. bidartensis	52X-CC, 41-45	486.39	C	M																																		
early Eocene-late Paleocene	B. bidartensis	54X-CC, 43-46	504.15	F	M																																		
Paleocene	B. bidartensis	56X-CC, 52-54	524.72	C	G																																		
Paleocene	B. bidartensis	57X-CC, 48-50	534.38	C	G																																		
Paleocene	B. campechensis	58X-CC, 34-36	543.91	C	M																																		
Paleogene	B. campechensis	60X-CC, 34-36	556.16	C	G																																		
Paleocene	B. campechensis	62X-CC, 60-62	572.63	C	M																																		
Paleocene	B. campechensis	64X-CC, 62-66	592.15	R	P																																		
Paleocene	B. campechensis	66X-CC, 42-45	611.3	F	P																																		
Paleocene	B. campechensis	68X-CC, 47-49	624.83	F	P																																		
Paleocene	B. campechensis	70X-CC, 11-14	630.9	C	P																																		
Paleocene	B. campechensis	72X-CC, 20-22	642.47	F	P																																		
Paleocene	B. campechensis	73X-CC, 20-22	643.95	C	M																																		

demagnetization step of 200°C was generally adequate to remove overprints, although most sediments lost nearly all of their magnetization or became magnetically unstable at thermal steps exceeding 330°C.

The bioturbated firm oozes and chalks of Site 1051 display paleomagnetic properties similar to the coeval sediments of Site 1050. Most of these sediments do not exhibit a significant drilling-induced overprint (characterized as steeply downward, radially inward magnetizations); however, the magnetic directions after AF demagnetization commonly exhibit variable (and quasi-random) inclinations and declinations.

There are three possible factors contributing to this magnetic behavior. First, most of these nannofossil oozes and chalks, especially those with light green color, have weak magnetizations, and the magnetic carriers are probably diluted by biogenetic components or are partially removed during diagenetic reactions. Second, the light yellow nannofossil oozes forming the upper 40 m at this site may be discolored from long-term exposure to the overlying oxidizing bottom waters, in which case the prevalent "normal-polarity" inclinations may represent a late-stage chemical remanent magnetic carrier (goethite) that required removal by thermal demagnetization. Third, most XCB cores were rendered into alternations of 5- to 10-cm-thick drilling biscuits with equal thicknesses of homogenized slurry. Thus, a new magnetization is imparted to this "drilling sediment" as it becomes firmer.

Recognition of polarity zones in the shipboard measurements was based mainly on the clustering of positive inclinations (normal polarity) and negative inclinations (reversed polarity) after the 20-mT demagnetization step. The 20-mT data were filtered before being plotted; the few measurements with inclinations >80° were assumed to be dominated by a steep-downward drilling overprint, intervals of anomalously high intensity were eliminated (these are usually associated with fragments broken off the drill bit or rust particles within the drilling slurry), and data from the uppermost 20 cm of the disturbed top of each core were removed. We also omitted all samples with magnetizations $<2 \times 10^{-2}$ mA/m after 20-mT AF demagnetization, presuming that these would contain an unacceptably high component of noise. However, in retrospect, it is probable that any sample with magnetization greater than 1×10^{-2} mA/m would be useful for magnetic polarity, and we may have inadvertently filtered out some incompletely demagnetized reversed-polarity intervals. A three-point moving mean was applied to the inclination record to smooth artifacts before plotting (Figs. 23, 24).

We grouped the stratigraphic array of inclination data from the shipboard pass-through magnetometer into polarity clusters with two simplifying assumptions: (1) stratigraphic intervals displaying a preponderance of negative inclinations represent incomplete demagnetization of reversed-polarity zones and (2) intervals that display only rare negative inclinations are normal-polarity zones. Between these two end-members lies a vague "indeterminate" category with possible biases of normal or reversed polarity. An additional consideration was our section-by-section tabulation of the demagnetization behaviors of intervals and significant coherent blocks distinguished from slurry-rich zones. In a few cases, the observations on the individual blocks indicate an original magnetization that is opposite from that carried by the enclosing drilling slurry. The resulting identification of polarity zones is indicated in Figures 23 and 24. For Hole 1051A, an improved polarity zonation was provided by the extensive array of minicores (Fig. 23A, B).

Biomagnetostratigraphy

Composite Polarity Zones and Chron Assignments

The majority of the independent polarity zone interpretations in the two holes can be correlated after a slight upward adjustment to the mbsf depths in Hole 1051B relative to Hole 1051A (Fig. 25). A ver-

tical offset of 2–5 m between these two holes is also indicated by marker layers of ash beds and the sharp upward transition from greenish to light yellow sediments in lithologic Unit I. A composite polarity column was constructed by merging the common aspects of the polarity patterns between the two holes, with due consideration in each interval for which hole displayed a more reliable polarity signature. Therefore, the minicore-enhanced polarity interpretations of Hole 1051A were given the greatest weight (Fig. 25).

Assignments of polarity chrons to these polarity intervals rely upon the shipboard micropaleontology datums (especially nannofossil zones) and the chronostratigraphy of Berggren et al. (1995).

Eocene

The uppermost meters of Site 1051 are assigned a Priabonian age (late Eocene) according to the presence of nannofossil Zone CP15. Therefore, the uppermost normal-polarity interval and underlying reversed-polarity zone in Hole 1051B are correlated with Chrons C16n and C16r (Fig. 25).

The main features of the polarity pattern between 10 and 380 mbsf provide an undistorted image of the middle Eocene Chrons C17n through C21n including the brief reversed-polarity Subchron C17n.1r, located within Chron C17n, at about 30 mbsf. Resolution of this polarity structure required thermal demagnetization of discrete minicores (e.g., compare interpretations of Hole 1051A from minicores and shipboard interpretations of Hole 1051B from AF demagnetization with the long-core magnetometer). The expanded thicknesses of the polarity Zones C19r–C20n indicate that accumulation rates in the upper portion of the Lutetian stage (lower middle Eocene) were relatively rapid compared with the overlying Bartonian (Chrons C17n–C18n)or lower Lutetian (Chrons C20r–C21n).

The boundary between the Ypresian and Lutetian stages (contact between lower Eocene and middle Eocene) is a biostratigraphic hiatus at all sites drilled during Leg 171B. In contrast to Sites 1049 and 1050 where this hiatus juxtaposes upper Chron C21n over lower Chron C22n, Hole 1051B indicates the presence of a narrow reversed-polarity zone above this hiatus, which we tentatively correlate with the uppermost portion of Chron C21r. Therefore, Site 1051 appears to have the most complete section of the Lutetian stage of the array of Leg 171B sites.

The Ypresian (early Eocene) polarity succession appears to be a complete record of Chrons C22n through C24r (Fig. 25). Assignment of polarity chrons is consistent with the general biostratigraphic zonation. Resolution of the polarity structure of this interval required post-cruise thermal demagnetization of minicores, although the major polarity zones were partially evident in the shipboard long-core measurements of the biscuit-rich core recovery. However, weak or unstable magnetizations of the lower Ypresian sediments obscured the delineation of polarity details near Chron C24n (~430–475 mbsf).

Paleocene

In contrast to the continuous Eocene stratigraphy and biomagnetochronology at Site 1051, the Paleocene portion is distorted by both sedimentary discontinuities and problems in interpreting the polarity structure.

Chron C25n, the youngest normal-polarity chron of the Paleocene, is tentatively assigned to a narrow, poorly documented, normal-polarity interval at about 520–525 mbsf, based upon its coincidence with the boundary between nannofossil Zones CP7 and CP8 (Fig. 25). This polarity Zone C25n is best represented in Hole 1051B. The absence of nannofossil Zone CP6 indicates that the lower portion of reversed-polarity Chron C25r is truncated.

Biostratigraphy of Hole 1051A indicates that the Selandian stage (early late Paleocene) is condensed, with an implied shortening of the major reversed-polarity Chron C26r. However, there is a discrepancy
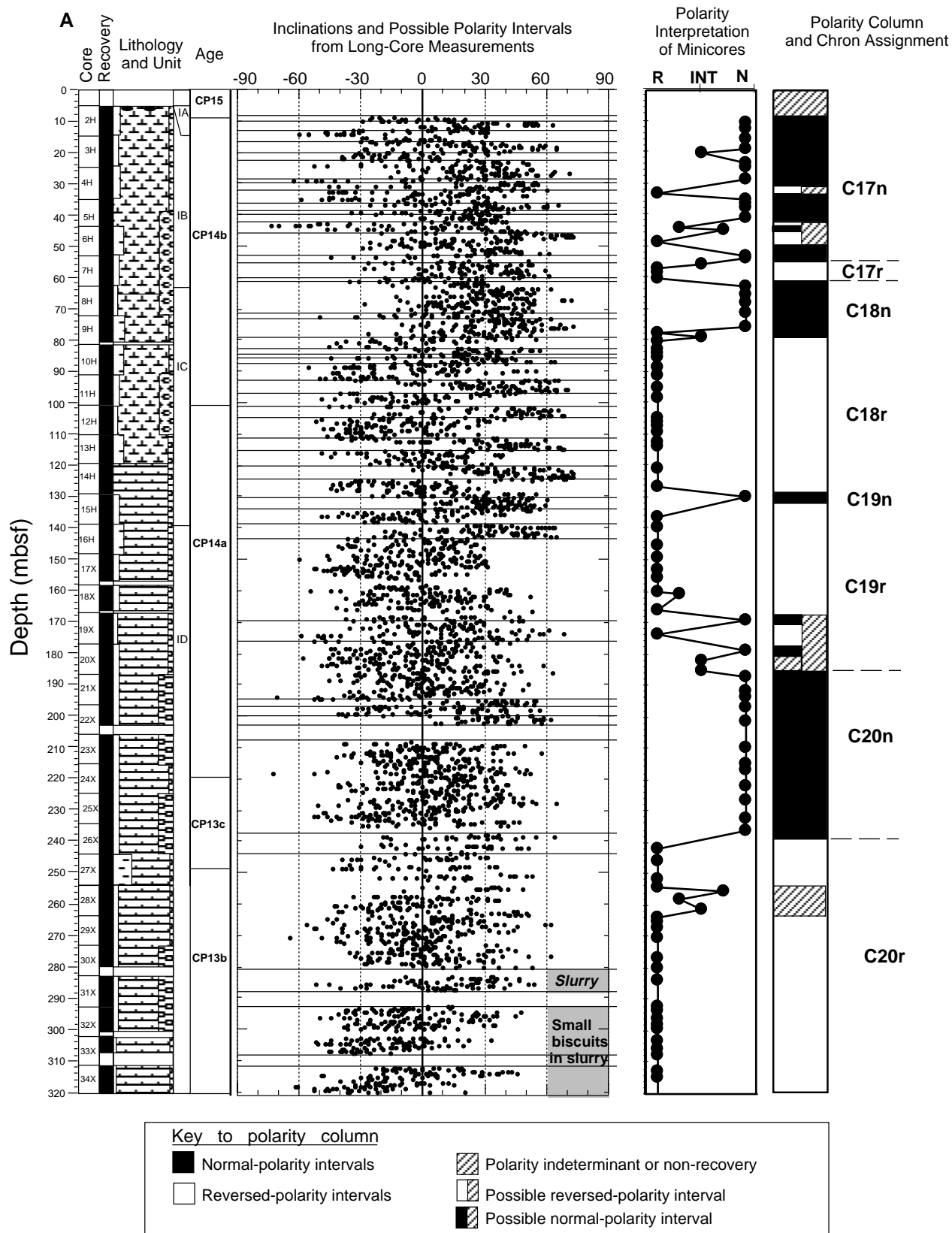
Figure 23. **A.** Magnetostratigraphy of the upper half of Hole 1051A. Magnetic inclinations from long-core measurements are after AF demagnetization at 20 mT and were filtered using a three-point moving average. Measurements from the uppermost 20 cm of each core and those having anomalously high or low magnetic intensities were removed. Horizontal lines delineate clusters of predominantly positive, negative, or equally mixed magnetic inclinations that were used for a preliminary shipboard polarity column. Polarity of discrete minicores are from interpretation of progressive thermal demagnetization and are assigned relative degrees of certainty. These polarity interpretations from discrete samples are given priority in the compilation of the summary polarity column. Polarity chron assignments are based upon the polarity zone pattern and nannofossil biostratigraphy.

Figure 23 (continued). **B.** Magnetostratigraphy of the lower half of Hole 1051A. Magnetic inclinations from long-core measurements are after AF demagnetization at 20 mT and were filtered using a three-point moving average. Measurements from the uppermost 20 cm of each core and those having anomalously high or low magnetic intensities were removed. Horizontal lines delineate clusters of predominantly positive, negative, or equally mixed magnetic inclinations that were used for a preliminary shipboard polarity column. Polarity of discrete minicores are from interpretation of progressive thermal demagnetization and are assigned relative degrees of certainty. These polarity interpretations from discrete samples are given priority in the compilation of the summary polarity column. Polarity chron assignments are based upon the polarity zone pattern and nannofossil biostratigraphy.

Figure 24. **A.** Magnetostratigraphy of the upper part of Hole 1051B. Magnetic inclinations from long-core measurements are after AF demagnetization at 20 mT and were filtered using a three-point moving average. Measurements from the uppermost 20 cm of each core and those having anomalously high or low magnetic intensities were removed. Horizontal lines delineate clusters of predominantly positive, negative, or equally mixed magnetic inclinations that were used for a preliminary shipboard polarity column. Polarity chron assignments are based upon the polarity zone pattern and nannofossil biostratigraphy.
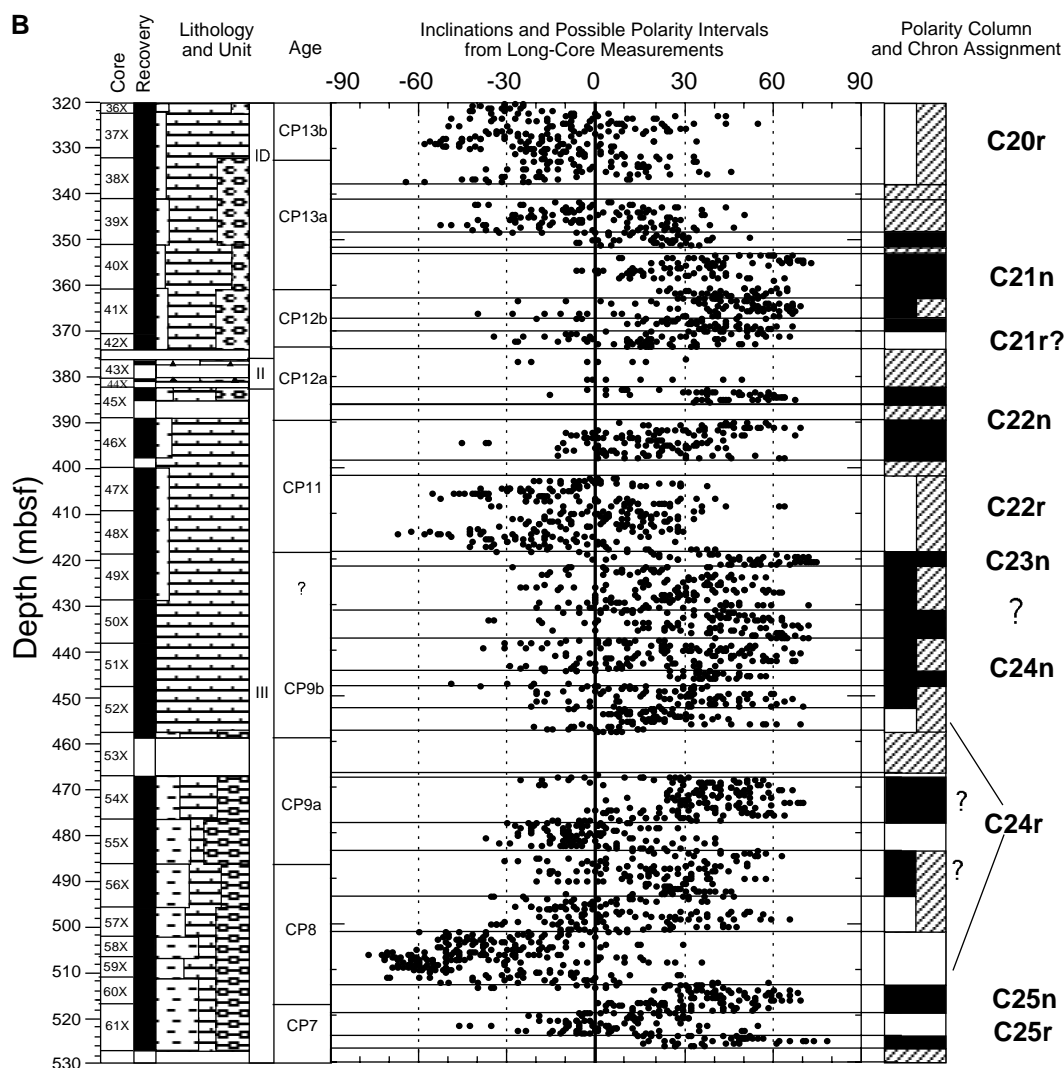
Figure 24 (continued). **B.** Magnetostratigraphy of the lower part of Hole 1051B. Magnetic inclinations from long-core measurements are after AF demagnetization at 20 mT and were filtered using a three-point moving average. Measurements from the uppermost 20 cm of each core and those having anomalously high or low magnetic intensities were removed. Horizontal lines delineate clusters of predominantly positive, negative, or equally mixed magnetic inclinations that were used for a preliminary shipboard polarity column. Polarity chron assignments are based upon the polarity zone pattern and nannofossil biostratigraphy.

between the apparent normal polarity associated with nannofossil Zone CP4 in this hole and the predicted reversed polarity of this zone in the biomagnetochronology of Berggren et al. (1995), which suggests that there is a problem either with the biostratigraphic assignments or the polarity interpretations (Fig. 25).

The polarity zonation of the Danian (lower Paleocene) could not be reliably correlated with the magnetic polarity time scale. The entire lower 80 m of Hole 1051A was assigned to nannofossil Zone CP3, but the predominance of normal polarity in the lower 50 m requires a correlation to Chron C28n. This polarity correlation suggests that nannofossil CP2 should be present, and this reinterpretation is considered possible under the available biostratigraphic datums in this hole. In any case, the accumulation rates in the lower Danian are considerably greater than those in the overlying upper Danian through Selandian, reflecting the influx of terrigenous clastics.

It should be possible to correlate the cyclostratigraphy from downhole logs and color analyses to several of the individual polarity zones within the upper Paleocene through middle Eocene. Such a composite stratigraphy, once calibrated to Milankovitch orbital peri-

ods, will enable us to make direct estimates of the duration of these polarity chrons and associated oceanic spreading rates.

CORE-CORE INTEGRATION

At Site 1051, magnetic susceptibility and GRAPE density data from the multisensor track (MST) and output from the Minolta color scanner were available for core-core integration (Tables 11, 12 on CD-ROM, back pocket, this volume). The section cored is quite thick, but only a fraction was double cored with the APC. A lack of overlap between some core intervals from Holes 1051A and 1051B prevented the construction of a complete composite depth scale. In addition, some intervals do not appear to preserve any suitably detailed stratigraphy for high-resolution correlation; this was caused partially by severe biscuiting of the core in some intervals. Unfortunately, the magnetic susceptibility values are low over most of the section, and the record is confused by spikes that may represent downhole contamination (drill-pipe rust). Severe biscuiting and frac-
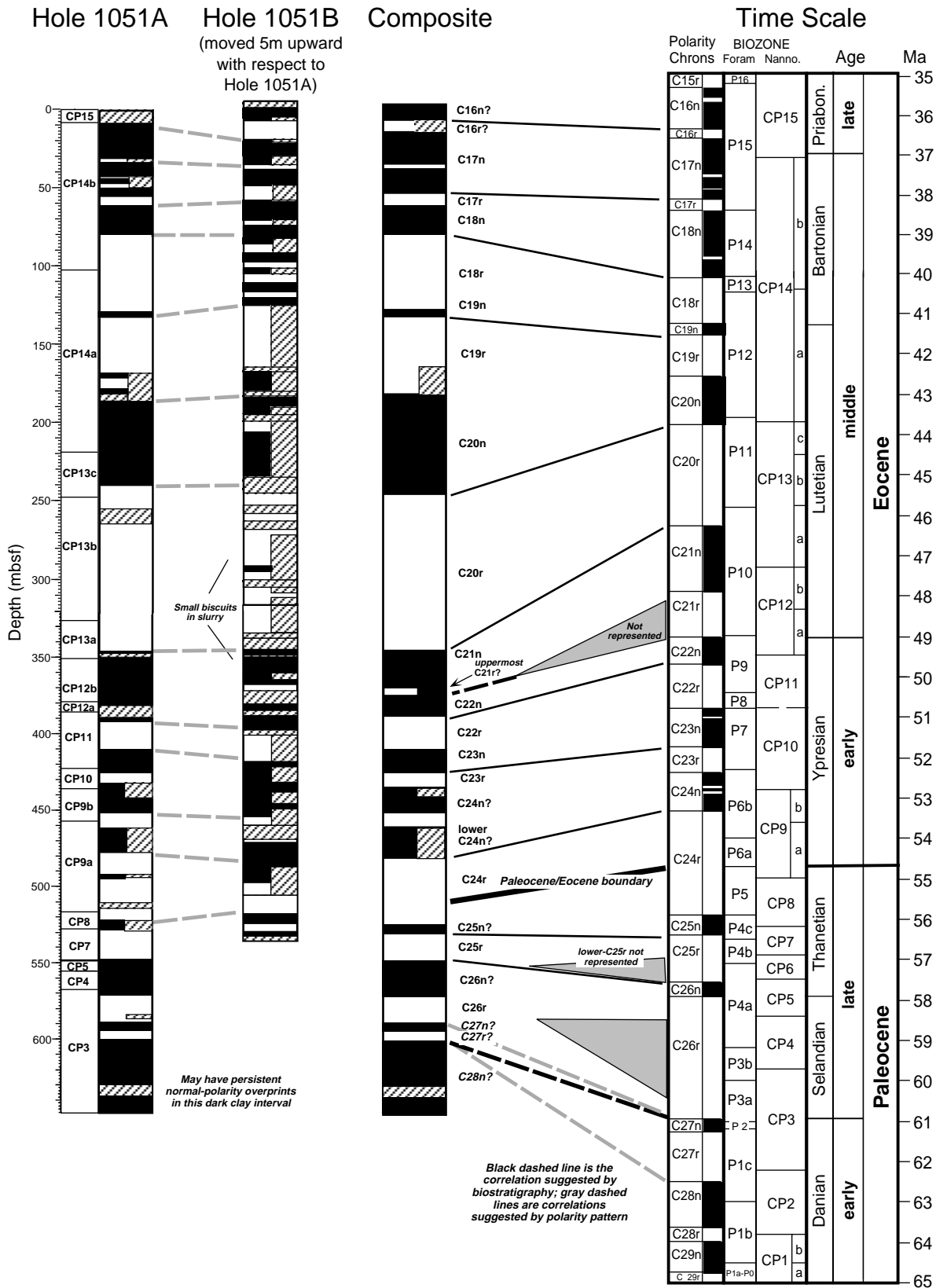
Figure 25. Comparison of polarity interpretations from the two holes at Site 1051 with Paleogene chronostratigraphy. Polarity chron assignments are based upon the polarity zone pattern and nannofossil biostratigraphy.

turing, which affect both the lightness (because of surface roughness) and color (because of the varying addition of water and slurry from other intervals), contributed a great deal of noise to the color data. Despite these difficulties, a few intervals were spliced to generate records that are probably continuous over several cores.

Table 13 lists the depth offsets applied to successive cores to produce the composite depth scale. The depth on the composite depth scale of any sample from a particular core is obtained by adding the offset for that core to the depth of the sample on the mbsf scale. Note that there are several places where there is no evidence on which to base the depth of a core; for convenience, the depth offset applied to such a core is the same as that for the core immediately above it. Table 14 lists the tie points for constructing a splice at Site 1051. The chief purpose of this table is to provide some guidance to scientists who want to sample parts of the site at high resolution, and for this reason, the table is annotated to indicate which ties are reasonably reliable and which are not. Between Cores 171B-1051A-29X and 48X, no splice is presented, as it is hard to document good core-to-core correlations that significantly improve the record that can be sampled in a single hole. It is quite possible that high-resolution stable isotope records and/or refined biostratigraphy will lead to substantial changes in some of the ties presented. The reliability of Table 13 is not sufficient to justify using the high-resolution shipboard MST and color data directly for time-series analysis; consequently, the data for Site 1051 are not listed vs. mcd in the CD-ROM tables, as was done on previous drilling legs for composite sections developed in Pliocene–Pleistocene sequences.

Figures 26A and 26B show records of magnetic susceptibility and three color parameters for the interval from 220 to 240 mcd in Holes 1051A and 1051B, respectively. Over this interval magnetic susceptibility is low and the records in the two holes do not resemble each other. The best records are given by the L*a*b codes L and a, both of which display regular cyclicity with a wavelength of about 1.5 m. In this particular interval, core recovery was high, and the record from a single hole would be quite reliable; however, the records are by no means identical, and there is some distortion. Elsewhere, especially in intervals of lower recovery using the XCB, a single cycle may be stretched up to double its original length. On other occasions, the bit may have been temporarily clogged, in which case some material is omitted from the recovered interval, and a cycle may be shortened.

Figures 27A and 27B show the same data sets for Holes 1051A and 1051B, respectively, in a Paleocene interval (540–560 mcd). The sediment is much more lithified and was recovered in long unbroken pieces; the recovery is slightly lower, but the records from the two holes match extremely well despite the fact that the cyclicity has a predominant wavelength only of about 30 cm. In this interval both magnetic susceptibility and L*a*b lightness show excellent, correlatable signals, whereas the two color codes reproduce rather poorly between the holes. Figure 28 shows the splice constructed from these data and its extension upward. Coring at Hole 1051B terminated at about 527 mbsf (527 mcd), so the composite section cannot be extended deeper. In this interval the predominant cyclicity is probably related to climatic precession (the precession of the Earth's rotational axis with respect to the elliptical orbit), with a period of about 21 k.y. This spliced record is long enough that it will probably prove possible to generate a useful section of a relative astronomical time scale.

ORGANIC GEOCHEMISTRY

Gas Analyses

In Hole 1051A, gas chromatographic analysis of the headspace samples detected methane (C_1), with traces of ethane (C_2) and propane (C_3) hydrocarbon gases (Table 15). Both the C_1/C_2 and $C_1/(C_2 +$ C_3) ratios below 261 mbsf were in the potentially hazardous range of <100 (Table 15; Fig. 29). No action was taken because the total gas content remained below 0.1 vol% C_1. Because no hazardous levels of gas were detected in Hole 1051A, gases were not monitored in Hole 1051B.

Six gas zones were recognized in Hole 1051A (Fig. 29). The surface gas zone, which averages 5 ppm C_1, shows a generally increasing gas content from 2 to 10 ppm C_1 over the interval of about 0–250 mbsf. Near 250 mbsf, a clay bed may form a seal that has trapped C_{2+} gases and has an increased quantity of gas below it. This clay bed forms the upper boundary of the middle gas zone. The middle gas zone, which averages 19 ppm C_1 and ranges from 11 to 32 ppm C_1, shows a minor peak in gas content just below the clay bed near 250 mbsf. Below the middle gas zone an increase in gas content occurs just below a chert bed at about 390 mbsf. This chert bed may form another seal that has trapped an increased quantity of gas below it. The chert bed marks the top of the deep I gas zone. The deep I zone, which averages 45 ppm C_1 and ranges from 14 to 79 ppm C_1, occurs from 390 to 480 mbsf. At 480 mbsf, the beginning of the deep II gas zone is marked by the onset of increasing clay content and a sharply reduced gas content in the lower portion of lithologic Unit III. The deep II gas zone, which averages 4 ppm C_1 and ranges from 2 to 12 ppm C_1, extends from 480 to 560 mbsf. A major portion of the deep II gas zone contains only C_1, with no C_{2+} gases. Below deep II the gas zone is characterized by increased gas content and the reappearance of C_{2+} gases. The deep III gas zone, which averages 102 ppm C_1 and ranges from 32 to 290 ppm C_1, extends from 560 to 615 mbsf. The deep III gas zone shows a sharp peak of 222 ppm C_1 at 596 mbsf. The peak in gas content seems to be marked by a decrease in density, shown by downhole logging data, as well as by an increase in the proportion of nannofossil chalk. A claystone bed is at the top of lithologic Subunit IVB and marks the top of the deep IV gas zone that continues to the total depth of Hole 1051A at 645 mbsf. The deep IV gas zone is markedly lower in gas content, which decreases to an average of 44 ppm C_1 and ranges from 25 to 69 ppm C_1.

Elemental Analyses

Three samples were taken from each core for carbonate-carbon and CHNS analyses. The carbonate analyses show major changes that were subsequently used to define changes in the lithologic units as well as cyclic variation of carbonate content within Unit I (Fig. 30). The cyclic variations within this unit are discussed in the "Lithostratigraphy" section (this chapter). Lithologic Units I and II average 78 wt% $CaCO_3$ and range from 63 to 91 wt% $CaCO_3$. The transition to Unit III is marked by an abrupt decrease in $CaCO_3$ content at 390 mbsf (Fig. 30). In Unit III, the $CaCO_3$ content averages 52 wt% with a range from 37 to 72 wt%. The transition to Unit IV is marked by another abrupt decrease in $CaCO_3$ content at 534 mbsf. Below 534 mbsf, the $CaCO_3$ content averages 41 wt%, with a range of 15 to 62 wt%.

TOC content of all lithologic units is low, averaging 0.06 wt%. All lithologic units contain little kerogen, as shown by a TOC analysis averaging 0.06 wt% and ranging from below the detection limit to 0.7 wt% TOC (Table 16; Figs. 30, 31).

The nitrogen and sulfur contents of these rocks are low (Table 16; Fig. 31). Sulfur was detected in only two of 207 samples, and of these analyses, the one reported as 1.71 wt% may be spurious. Nitrogen is also low, averaging 0.01 wt% and ranging from 0 to 0.13 wt%. Elevated nitrogen values occur in the claystone-bearing portions of lithologic Units III and IV (Fig. 32). The C/N ratio of the organic matter in Units III and IV is generally <15, which is typical of marine kerogen (Rashid, 1985). The claystone in Hole 1051A probably has an elevated nitrogen content in the marine organic matter because of de-

Table 13. Offsets applied to the depths (mbsf) of individual cores at Site 1051 to generate a composite section and a composite depth scale (mcd).

Core	Offset (m)	Constrained by tie to adjacent hole		Core	Offset (m)	Constrained by tie to adjacent hole
171B-1051A-				68X	28.60	No
2H	0.38	Yes		69X	28.60	No
3H	3.50	Yes		70X	28.60	No
4H	3.95	Yes		71X	4.84	No
5H	6.35	Yes		72X	25.60	No
6H	7.25	Yes		73X	25.60	No
7H	8.40	Yes				
8H	10.36	Yes		171B-1051B-		
9H	10.36	No		2H	0.00	No
10H	10.36	No		3H	−0.05	Yes
11H	10.36	No		4H	0.30	Yes
12H	10.93	Yes		5H	2.90	Yes
13H	10.18	Yes		6H	4.75	Yes
14H	9.68	Yes		7H	3.05	Yes
15H	10.28	Yes		8H	5.25	Yes
16H	11.65	Yes		9H	8.75	Yes
17X	11.91	Yes		10H	5.51	Yes
18X	9.54	Yes		11H	8.75	No
19X	10.88	Yes		12H	8.61	Yes
20X	12.94	Yes		13H	10.33	Yes
21X	14.11	Yes		14H	11.43	Yes
22X	14.36	Yes		15H	11.98	Yes
23X	13.65	Yes		16X	12.11	Yes
24X	13.65	No		17X	12.52	Yes
25X	14.81	Yes		18X	12.46	Yes
26X	15.95	Yes		19X	14.05	Yes
27X	15.95	No		20X	12.12	Yes
28X	16.49	Yes		21X	11.30	Yes
29X	17.55	Yes		22X	12.52	Yes
30X	19.07	Yes		23X	12.80	Yes
31X	17.42	Yes		24X	12.80	No
32X	19.48	Yes		25X	12.80	No
33X	19.43	No		26X	15.89	Yes
34X	19.43	No		27X	16.71	Yes
35X	19.47	Yes		28X	15.17	Yes
36X	18.69	Yes		29X	16.64	Yes
37X	18.09	Yes		30X	16.53	Yes
38X	18.09	No		31X	16.52	Yes
39X	18.09	No		32X	15.30	Yes
40X	18.09	No		33X	16.75	Yes
41X	18.09	No		35X	15.72	Yes
42X	17.92	Yes		36X	18.43	Yes
43X	17.79	Yes		37X	19.27	Yes
44X	17.87	Yes		38X	20.27	Yes
45X	19.51	Yes		39X	19.40	Yes
46X	20.13	Yes		40X	19.40	No
47X	20.32	Yes		41X	20.15	Yes
48X	20.32	No		42X	20.87	Yes
49X	21.18	Yes		43X	21.10	Yes
50X	21.18	No		44X	24.67	No
51X	21.80	Yes		45X	21.10	No
52X	21.80	No		46X	17.22	Yes
53X	22.03	Yes		47X	15.72	Yes
54X	22.18	Yes		48X	18.39	Yes
55X	25.68	Yes		49X	17.16	Yes
56X	25.68	No		50X	17.44	Yes
57X	26.82	Yes		51X	18.93	Yes
58X	28.60	No		52X	21.76	Yes
59X	28.60	No		53X	24.37	Yes
60X	28.60	No		54X	19.06	Yes
61X	28.60	No		55X	23.08	Yes
62X	28.60	No		56X	23.08	No
63X	28.60	No		57X	23.26	Yes
64X	28.60	No		58X	23.26	No
65X	28.60	No		59X	26.54	Yes
66X	28.60	No		60X	26.54	No
67X	28.60	No		61X	30.56	Yes

creased opportunities for alteration in these relatively impermeable strata. Enhanced preservation and a marine origin may also be indicated by the relatively high hydrogen content of these samples, which averages 0.36 wt% and ranges from 0.09 to 0.96 wt% (Table 16). However, the measured hydrogen content is high for the TOC levels measured, and perhaps H from inorganic sources has biased the analyses.

Samples with TOC content >0.32 wt% contain little nitrogen (Fig. 31). Low-nitrogen samples may be caused a terrestrial source for the organic matter or by the biodegradation of marine organic matter. The presence of at least some terrestrial organic matter that most likely has a low nitrogen content is shown by a 4-cm piece of fossil charcoal recovered from Sample 171B-1051A-39X-CC, 0–2 cm.

INORGANIC GEOCHEMISTRY

Analytical Results

Interstitial waters were taken from 26 core samples in Hole 1051A (Table 17). In general, pore-water salinities in this hole are within a narrow range (35.5–36.0). However, a slightly higher salinity (37) was recorded at 548.05 mbsf (Fig. 33A).

Table 14. Splice table for Site 1051.

Hole, core, section, interval (cm)	Depth (mbsf)	Depth (mcd)	Whether tied	Hole, core, section, interval (cm)	Depth (mbsf)	Depth (mcd)
171B-						
1051B-1H			All			
1051B-2H			All; append			
1051B-3H-1, 0.00-0.00	13.80	13.75	Start	171B-		
1051B-3H-6, 130.00-130.10	22.60	22.55	Tie to	1051A-3H-3, 75.00-75.10	19.05	22.55
1051A-3H-4, 135.00-135.10	21.15	24.65	Tie to	1051B-4H-1, 55.00-55.10	24.35	24.65
1051B-4H-7, 35.00-35.10	33.15	33.45	Tie to	1051A-4H-4, 20.00-20.10	29.50	33.45
1051A-4H-6, 40.00-40.10	32.70	36.65	Tie to	1051B-5H-1, 45.00-45.10	33.75	36.65
1051B-5H-7, 70.00-70.10	43.00	45.90	Tie to	1051A-5H-4, 75.00-75.10	39.55	45.90
1051A-5H-6, 45.00-45.10	42.25	48.60	Tie to	1051B-6H-1, 105.00-105.10	43.85	48.60
1051B-6H-CC, 10.00-10.10	52.42	57.17	Tie to	1051B-7H-2, 28.50-28.60	54.12	57.17
1051B-7H-CC, 5.00-5.10	62.24	65.29	Tie to	1051A-7H-3, 58.50-58.60	56.89	65.29
1051A-7H-5, 15.00-15.10	59.45	67.85	Tie to	1051B-8H-1, 80.00-80.10	62.60	67.85
1051B-8H-7, 40.00-40.10	71.20	76.45	Tie to	1051A-8H-3, 150.00-150.00	66.09	76.45
1051A-8H-8, 15.00-15.10	71.74	82.10	Tie to	1051B-9H-2, 55.00-55.10	73.35	82.10
1051B-9H-CC, 5.00-5.10	81.15	89.90	Tie to	1051A-9H-5, 123.50-123.60	79.54	89.90
1051A-9H-6, 76.00-76.10	80.56	90.92	Tie to	1051B-10H-4, 9.00-9.10	85.41	90.92
1051B-10H-CC, 10.00-10.10	90.63	96.14	Append	1051B-11H-1, 0.00-0.00	87.30	96.05
1051B-11H-5, 125.00-125.10	94.55	103.30	Tie to	1051A-11H-2, 13.50-13.60	92.94	103.30
1051A-11H-4, 30.00-30.10	96.10	106.46	Tie to	1051B-12H-1, 105.00-105.10	97.85	106.46
1051B-12H-7, 5.00-5.10	105.85	114.46	Tie to	1051A-12H-2, 123.00-123.10	103.53	114.46
1051A-12H-4, 115.00-115.10	106.45	117.38	Tie	1051B-13H-1, 75.00-75.10	107.05	117.38
1051B-13H-6, 85.00-85.10	114.65	124.98	Tie	1051A-13H-3, 150.00-150.00	114.80	124.98
1051A-13H-6, 85.00-85.10	118.65	128.83	Tie	1051B-14H-2, 10.00-10.10	117.40	128.83
1051B-14H-7, 45.00-45.10	125.25	136.68	Tie	1051A-14H-5, 120.00-120.10	127.00	136.68
1051A-14H-6, 55.00-55.10	127.85	137.53	Tie	1051B-15H-1, 25.00-25.10	125.55	137.53
1051B-15H-CC, 5.00-5.10	134.50	146.48	Tie	1051A-15H-5, 90.00-90.10	136.20	146.48
1051A-15H-6, 130.00-130.10	138.10	148.38	Tie	1051B-16X-1, 147.00-147.00	136.27	148.38
1051B-16X-CC, 9.00-9.10	143.89	156.00	Tie	1051B-17X-1, 17.50-17.60	143.48	156.00
1051B-17X-CC, 10.00-10.10	152.82	165.34	Append	1051B-18X-1, 0.00-0.00	152.90	165.36
1051B-18X-CC, 23.00-23.10	162.62	175.08	Append	1051B-19X-1, 0.00-0.00	162.50	176.55
1051B-19X-3, 119.00-119.10	166.69	180.74	Tie	1051A-19X-2, 41.50-41.60	169.86	180.74
1051A-19X-4, 138.00-138.10	173.68	184.56	Tie	1051B-20X-1, 33.50-33.60	172.44	184.56
1051B-20X-7, 35.00-35.10	181.45	193.57	Tie	1051B-21X-1, 54.50-54.60	182.27	193.57
1051B-21X-6, 75.00-75.10	189.95	201.25	Tie	1051A-21X-1, 12.50-12.60	187.14	201.25
1051A-21X-3, 25.00-25.10	190.25	204.36	Tie	1051B-22X-1, 63.50-63.60	191.84	204.36
1051B-22X-6, 147.00-147.10	200.17	212.69	Tie	1051A-22X-2, 23.00-23.10	198.33	212.69
1051A-22X-3, 58.00-58.10	200.18	214.54	Tie	1051B-23X-1, 92.00-92.10	201.74	214.54
1051B-23X-5, 128.00-128.10	208.08	220.88	Tie	23X-1, 103.00-103.10	207.23	220.88
1051A-23X-3, 90.00-90.10	210.10	223.75	Tie	1051B-24X-1, 44.50-44.60	210.95	223.75
1051B-24X-CC, 20.00-20.10	220.13	232.93	Append	1051B-25X-1, 0.00-0.00	220.10	232.90
1051B-25X-7, 18.00-18.10	229.28	242.08	Tie	1051A-25X-2, 36.00-36.10	227.27	242.08
1051A-25X-4, 140.00-140.10	231.30	246.11	Tie	1051B-26X-1, 49.00-49.10	230.22	246.11
1051B-26X-7, 20.00-20.10	238.90	254.79	Tie	1051A-26X-3, 84.00-84.10	238.84	254.79
1051A-26X-CC, 33.00-33.10	244.50	260.45	Append	1051A-27X-1, 0.00-0.00	244.60	260.55
1051A-27X-3, 102.00-102.10	248.62	264.57	Tie	1051B-28X-1, 39.00-39.10	249.40	264.57
1051B-28X-7, 26.00-26.10	258.26	273.43	Tie	1051A-28X-2, 124.00-124.10	256.94	273.43
1051A-28X-4, 25.00-25.10	258.95	275.44	Tie	1051B-29X-1, 20.00-20.10	258.80	275.44
1051B-29X-7, 25.00-25.10	267.85	284.49	Tie	1051A-29X-3, 12.50-12.60	266.94	284.49
1051A-29X-CC, 15.00-15.10	273.35	290.90				
1051A-48X-7, 27.00-27.00	456.27	476.59	Tie	1051B-52X-5, 123.00-123.00	454.83	476.59
1051B-52X-7, 23.00-23.00	456.83	478.59	Tie	1051A-49X-1, 31.00-31.00	457.41	478.59
1051A-49X-3, 47.00-47.00	460.07	481.25	Append	1051A-50X-1, 0.00-0.00	460.20	481.38
1051A-50X-4, 55.00-55.00	465.25	486.43	Tie	1051B-54X-1, 47.00-47.00	467.37	486.43
1051B-54X-4, 23.00-23.00	471.63	490.69	Tie	1051A-51X-2, 59.00-59.00	468.89	490.69
1051A-51X-8, 35.00-35.00	476.52	498.32	Append	1051A-52X-1, 0.00-0.00	476.50	498.30
1051A-52X-2, 147.00-147.00	479.47	501.27	Tie	1051B-55X-2, 19.00-19.00	478.19	501.27
1051B-55X-7, 31.00-31.00	485.81	508.89	Append	1051B-56X-1, 0.00-0.00	486.10	509.18
1051B-56X-7, 59.00-59.00	495.19	518.27	Tie	1051A-54X-1, 39.00-39.00	496.09	518.27
1051A-54X-2, 19.00-19.00	497.39	519.57	Tie	1051B-57X-1, 60.01-60.01	496.31	519.57
1051B-57X-5, 55.00-55.00	502.25	525.51	Append	1051B-58X-1, 0.00-0.00	502.30	525.56
1051B-58X-5, 35.00-35.00	508.43	531.69	Tie	1051A-55X-1, 71.00-71.00	506.01	531.69
1051A-55X-2, 147.00-147.00	508.27	533.95	Tie	1051B-59X-1, 111.00-111.00	507.41	533.95
1051B-59X-4, 39.00-39.00	510.96	537.50	Tie	1051B-60X-1, 5.50-5.50	510.96	537.50
1051B-60X-3, 75.00-75.00	514.65	541.19	Tie	1051A-56X-1, 60.00-60.00	515.51	541.19
1051A-56X-6, 51.00-51.00	522.91	548.59	Tie	1052B-61X-1, 112.00-112.00	518.03	548.59
1051B-61X-6, 131.00-131.00	525.71	556.27	Tie	1051A-57X-4, 44.02-44.02	529.45	556.27
1051A-57X-7, 35.00-35.00	533.85	560.67	End			

Notes: Where choice was available, this splice uses material from Hole 1051B, because some routine shipboard sampling was done in Hole 1051A that may affect the availability of material for high-resolution sampling at regular depth intervals. Between 171B-1051A-29X and 171B-1051B-47X, the generation of a spliced record is not at present justified. In an ideal situation, the bottom of each segment is tied to the same depth (mcd) in another hole; if the composite section does not permit this, the next deeper core is appended. In this situation, it is possible that the interval missing is greater than indicated, especially if the top of the appended core is disturbed by coring.

Pore-water chloride shows a wider range (558–594 mM) than sodium concentrations (479–492 mM), but both show an overall increase with depth from near seawater concentrations (Cl^-, ~560 mM; Na^+, ~480 mM) in the upper 150 m of the section, to slightly higher values (Cl^-, ~590 mM; Na^+, ~490 mM) in the lower 250 m of the hole (Fig. 33B).

Alkalinity shows a steady increase from ~3 mM at the top of the section to ~6.5 mM at 375 mbsf (Fig. 33C). This steady increase is followed by an overall decrease to values of ~3–5 mM in the lower 200 m of the hole. The pH of pore waters in Hole 1051A shows a slight overall decrease (7.67 to ~7.3) with depth from the top of the section to ~375 mbsf (Fig. 33C). This decrease is followed by an abrupt increase to 7.81 at 403.9 mbsf and a subsequent general decrease to lower pH values (7.74–7.25) in the lower 200 m of the hole.

Pore-water calcium concentrations in Hole 1051A are always higher than standard seawater (10.55 mM), and they increase steadily
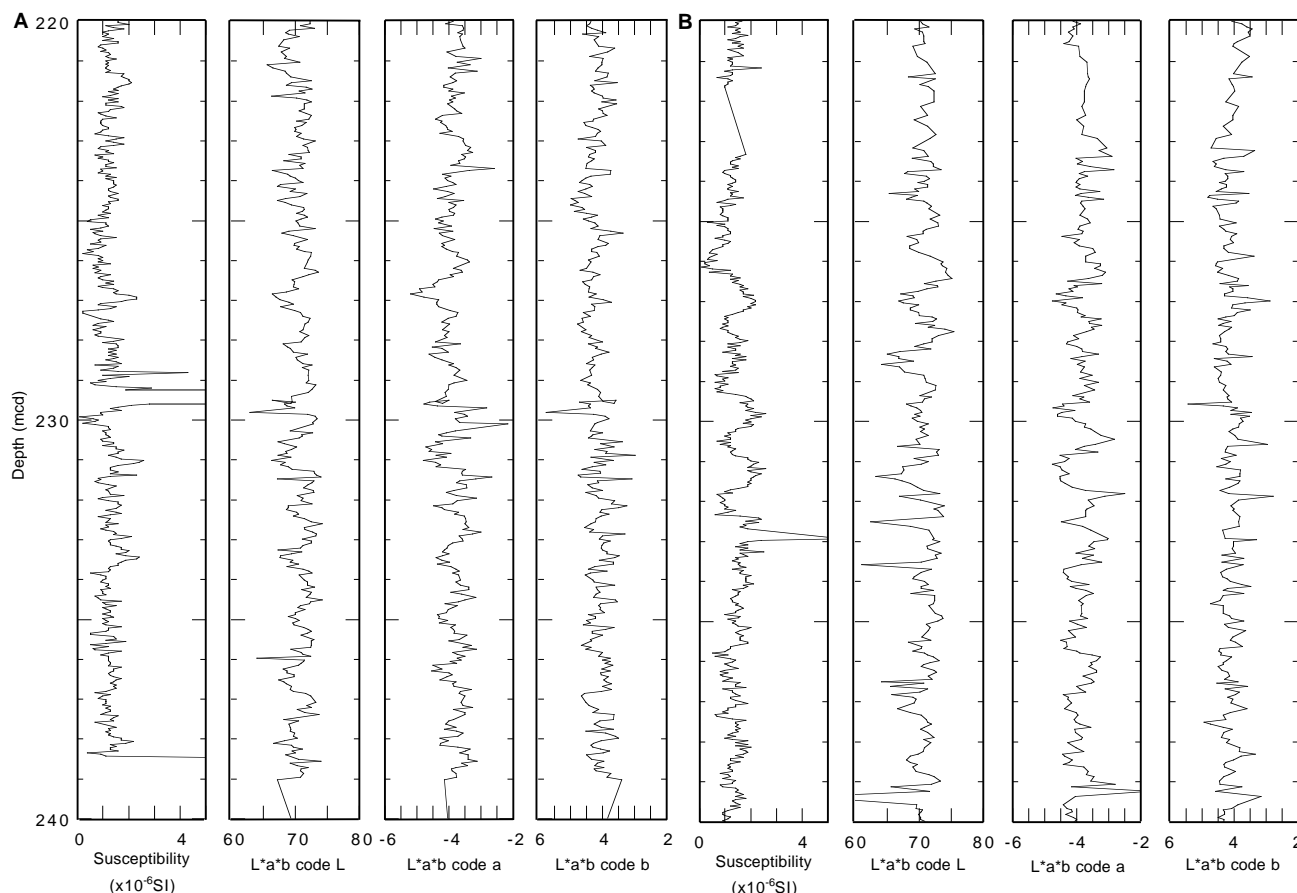
Figure 26. Magnetic susceptibility data and L*a*b codes L (lightness), a, and b from 220 to 240 mcd in (**A**) Hole 1051A and (**B**) Hole 1051B. The magnetic susceptibility and color data are available on CD-ROM (back pocket, this volume). Conversion of data to mcd requires the use of Table 11.

from a minimum of 10.63 mM in the shallowest sample (10.25 mbsf) to 22.18 mM at ~375 mbsf (Fig. 33A). This steady increase is followed by an abrupt increase to 29.65 mM at 403.9 mbsf and a subsequent overall increase to values >31.5 mM in the lower 200 m of the hole. Pore-water magnesium concentrations in Hole 1051A mirror changes in calcium concentrations. Magnesium concentrations are always lower than standard seawater (54 mM) and decrease steadily from a maximum of 53.76 mM in the shallowest sample (10.25 mbsf) to 46.11 mM at ~375 mbsf (Fig. 33A). This steady decrease is followed by an abrupt decrease to 41.12 mM at 403.9 mbsf and a subsequent overall decrease to values <40 mM in the lower 200 m of the hole.

Pore-water potassium concentrations in the upper 300 m of Hole 1051A are significantly higher than standard seawater (10.44 mM; Fig. 33D) and show a general decrease with depth from 12.3 mM in the shallowest sample (10.25 mbsf) to about 10.4 mM at ~375 mbsf. This general decrease is followed by an abrupt decrease to 8.31 mM at 403.9 mbsf and a subsequent steady decrease to 6.59 mM at the bottom of the hole.

Pore-water rubidium concentrations in the upper 400 m of Hole 1051A are significantly higher than standard sea water (1.4 μM) and show an overall increase with depth from ~1.9 μM at the top of the section to a maximum of 2.23 μM at 172.2 mbsf (Fig. 33E). Below this maximum there is a general decrease to 0.97 μM at the base of the hole, except for a sharp decrease from 1.88 to 1.53 μM between ~375 and 404 mbsf.

Pore-water strontium concentrations in Hole 1051A increase sharply with depth from near seawater values (91 μM) at the top of

the section to 370 μM at ~285 mbsf, and then increase less sharply to 409 μM at ~375 mbsf (Fig. 33F). These increases are followed by a remarkable step to a much higher concentration (665 μM) at 403.9 mbsf and a further sharp increase to 914 μM at the bottom of the hole. In general, calculated Sr^{2+}/Ca^{2+} (μM/mM) values show a similar pattern to the Sr^{2+} concentration depth profile, except for two intervals (Fig. 33G, F, respectively). First, Sr^{2+}/Ca^{2+} values decrease over the interval with the relatively gradual increase in Sr^{2+} concentrations (~285−375 mbsf). Second, Sr^{2+}/Ca^{2+} values show two steplike increases to higher values with depth (Fig. 33G). The first of these steps in Sr^{2+}/Ca^{2+} occurs between 374.10 and 403.9 mbsf and coincides with the step to higher strontium concentrations. The second occurs between 490.5 and 522.25 mbsf and coincides with a minor decrease in pore-water Ca^{2+} concentrations (Fig. 33A).

Pore-water lithium concentrations in Hole 1051A increase relatively gradually with depth from near seawater values (~30 μM) at the top of the section to ~38 μM at 48.25 mbsf, and then increase more sharply to 202 μM at ~375 mbsf (Fig. 33F). These increases are followed by an abrupt shift to a much higher concentration (446 μM) at 403.9 mbsf and a further gradual increase to 613 μM at the bottom of the hole.

Dissolved silica concentrations of the interstitial-water samples taken from Hole 1051A show a significant increase with depth to values of ~1050 μM between about 285 and 400 mbsf (Fig. 33H). Below this depth, silica concentrations decrease sharply to 608 μM at 622.05 mbsf.

Pore-water sulfate concentrations in Hole 1051A are relatively high (maximum value = 29.9 mM) in the upper 30 m of the section
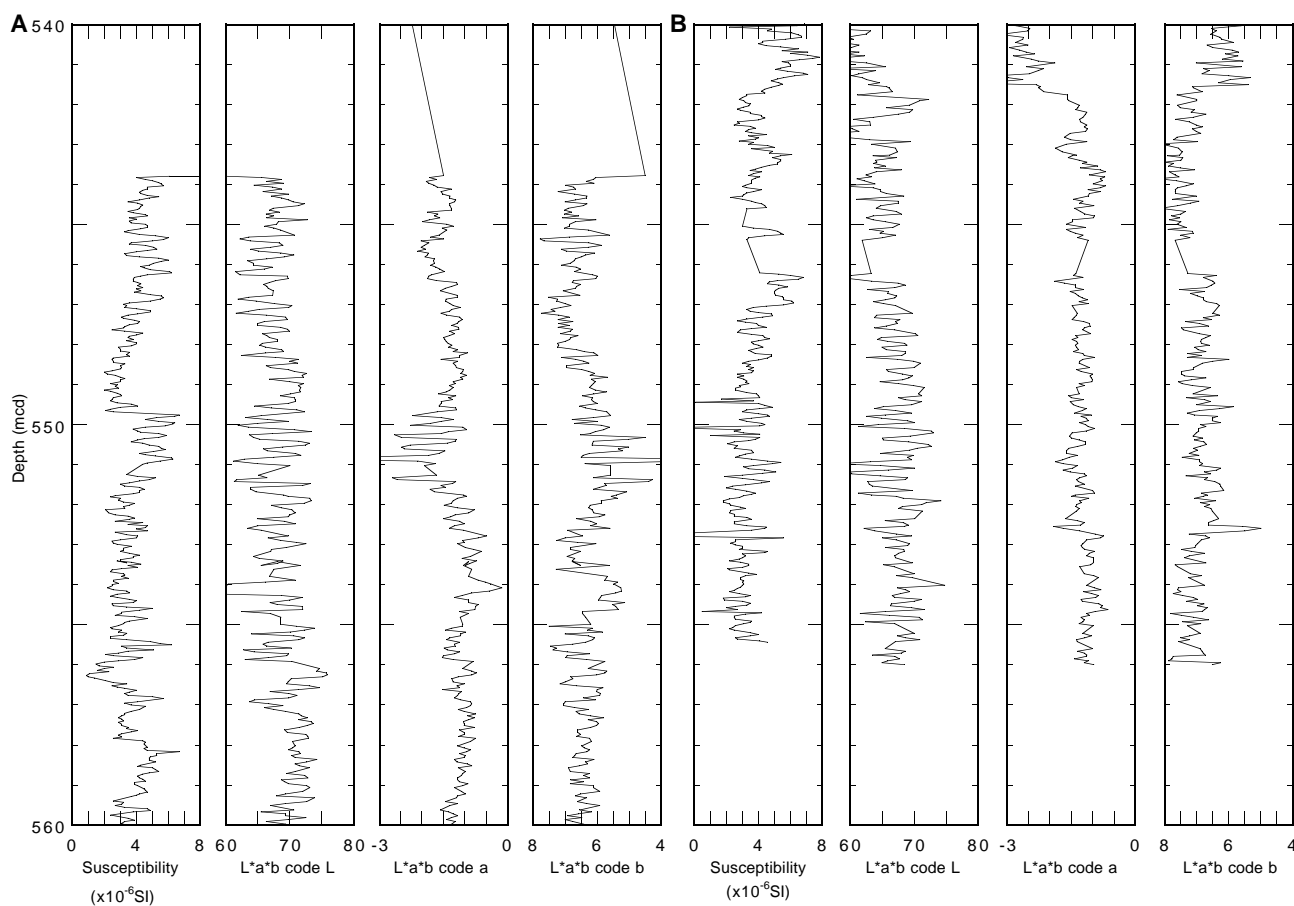
Figure 27. Magnetic susceptibility data and L*a*b codes L (lightness), a, and b from 540 to 560 mcd in (**A**) Hole 1051A and (**B**) Hole 1051B. The magnetic susceptibility and color data are available on CD-ROM (back pocket, this volume). Conversion of data to mcd requires the use of Table 11.

and thereafter show a consistent decrease with depth to 16 mM at 567.25 mbsf (Fig. 33I). Pore-water ammonium concentrations range from 8.7 to 480 µM and show an overall increase with depth (Fig. 33I). Superimposed on this general increase is a steplike increase in ammonium concentrations from 236 µM at ~375 mbsf to 336 µM at 403.9 mbsf.

Pore-water boron concentrations in Hole 1051A range between 226 and 598 µM and show a general decrease with depth (Fig. 33J).

Discussion

The overall pore-water calcium and magnesium concentration depth gradients in Hole 1051A are even smaller than those in Holes 1049A and 1050A (see Figs. 33A, 25A in "Site 1049" chapter [this volume] and Fig. 42 in "Site 1050" chapter [this volume]). Such gentle gradients are consistent with the extreme distance (>5 km; see "Introduction" chapter, this volume) to basement and suggest that pore-water concentrations of these cations in the Blake Nose sediments are controlled by seawater interaction with volcaniclastic sediments (such as the volcanic ashes found throughout the section) and/or dolomitization in the underlying Jurassic and Cretaceous carbonate platform. The sodium, potassium, and rubidium depth profiles in Hole 1051A are consistent with significant alteration of the volcaniclastic sediments within the section and possible reverse weathering reactions within the clays in the lower 200 m of the hole (see "Lithostratigraphy" section, this chapter). Dissolved silica concentrations in Hole 1051A indicate a significant alteration of siliceous sediments within the section. Two potential sources for dissolved silica in pore

waters within this hole are biogenic opal and volcaniclastic sediments. The excellent preservation of radiolarians within the hole (especially around ash layers; see "Lithostratigraphy" section, this chapter) may indicate that the volcaniclastic sediments are the more important of these two silica sources at this site.

The overall increase in Sr^{2+} concentrations and calculated Sr^{2+}/Ca^{2+} values with depth within Hole 1051A are consistent with the recrystallization of biogenic calcite in the sediment column and alteration of volcaniclastic materials.

Pore-water sulfate and ammonium concentrations in Hole 1051A show significant depth-related changes that are consistent with minor oxidation of organic matter within Hole 1051A (see "Organic Geochemistry" section, this chapter).

Perhaps the most remarkable feature of the pore-water chemistry in Hole 1051A is the extreme level of lithium concentrations recorded (~20 times that of seawater at the bottom of the hole). Extreme distance from basement (as previously mentioned) and the shape of the pore-water lithium depth profile indicate that the source of Li^+ for these fluids is most likely within the sedimentary column at Site 1051. The correlation between the Li^+ and Ca^{2+} depth profiles in Hole 1051A suggests that Li^+ originates from the volcaniclastic sediments within the section.

The second remarkable feature of the pore-water chemistry in Hole 1051A is the sudden change in alkalinity, pH, Ca^{2+}, Mg^{2+}, K^+, Rb^{2+}, Sr^{2+}, Li^+, sulfate, and ammonium observed between 374.1 and 403.9 mbsf. These sudden changes are consistent with the compartmentalization of the pore-water system at this site by a relatively impermeable layer at this depth. Such an interpretation is consistent
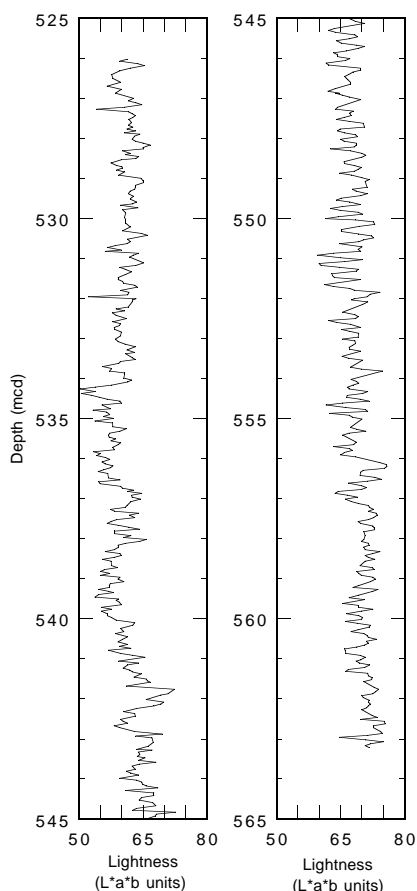
Figure 28. Spliced L*a*b color (lightness) record for Site 1051 from 525 to 565 mcd.

with the recovery of a clay and porcellanite unit that forms a major unconformity at Site 1051 and produces a prominent seismic reflector across the Blake Nose (lithologic Unit II; see "Lithostratigraphy" section, this chapter). Low concentrations of Mg^{2+}, K^+, and Rb^{2+} and high concentrations of Ca^{2+}, Li^+, Sr^{2+}, and silica in the Hole 1051A pore-water fluids may be at least partially attributable to the alteration of volcaniclastic sediments within the section. However, discrete volcaniclastic ash layers are most abundant above the clay and porcellanite unit (see "Lithostratigraphy" section, this chapter). Therefore, the differences between the concentrations of these pore-water chemical constituents above and below the clay and porcellanite unit suggest that the disseminated volcaniclastic sediments in this hole are volumetrically more significant and/or are more readily altered than the discrete ash layers. This conclusion is consistent with the consistent occurrence of mica and biotite grains within smear slides from lithologic Units III through V (see "Lithostratigraphy" section, this chapter).

PHYSICAL PROPERTIES

Physical properties at Site 1051 were measured on both whole-round sections and discrete samples from split-core sections. Whole-round measurements included the determination of GRAPE bulk density, magnetic susceptibility, compressional P-wave velocity, natural gamma radiation, and measurements of thermal conductivity. Index properties, compressional P-wave velocity, shear strength, and resistivity were measured on discrete samples from split-core sections at a typical frequency of three measurements per core.

MST Measurements

The GRAPE and MST P-wave velocity data were filtered to remove anomalous values that are artifacts of section-end and void or crack effects. The data sets were filtered to remove values outside the 10% error band of a reference curve, which was calculated from a 10-point running mean of the data. This filtering of the data set significantly improves visual presentation and aids data interpretation.

GRAPE bulk density was measured on all cores from Hole 1051A and on APC cores from Hole 1051B (Fig. 34; Tables 18, 19 on CD-ROM, back pocket, this volume). These data, along with magnetic susceptibility and color reflectance, were used to form a Site 1051 composite stratigraphic section (see "Core-Core Integration" section, this chapter).

GRAPE bulk density shows a gradual increase in magnitude from ~1.5 to 1.7 g/cm^3 between 0 and 150 mbsf, which corresponds to the nannofossil ooze of lithologic Subunits IB and IC. The contact between lithologic Subunits IB and IC cannot be distinguished using GRAPE data because this contact is defined by a color change. Between 150 and 375 mbsf, which corresponds to the nannofossil chalk of lithologic Subunit ID, GRAPE bulk density shows minor fluctuations about an approximate average of 1.7 g/cm^3. At the transition from lithologic Subunit ID to lithologic Unit II at 375 mbsf, GRAPE bulk density decreases from 1.7 to 1.6 g/cm^3. GRAPE bulk density increases from 1.6 to 2.0 g/cm^3 in the interval 375–570 mbsf, which corresponds to the siliceous nannofossil chalk of lithologic Unit III. Between 570 mbsf and total depth, which corresponds to the clayey nannofossil chalk of lithologic Unit IV, GRAPE bulk density fluctuates between 1.4 and 1.9 g/cm^3. The magnitude of the fluctuations in GRAPE bulk density is greater below 375 mbsf, compared with fluctuations above this depth.

MST measurements of magnetic susceptibility from both holes at Site 1051 are shown in Figure 35 (also see Tables 20, 21 on CD-ROM, back pocket, this volume). Above 375 mbsf, magnetic susceptibility fluctuations cannot be distinguished from background levels, except for a number of magnetic susceptibility "spikes," some of which correlate with ash layers (see "Lithostratigraphy" section, this chapter). Below 375 mbsf, magnetic susceptibility can be measured above background levels. Magnetic susceptibility values increase from background levels to 9×10^{-5} SI across the interval from 375 mbsf to total depth and show significant fluctuations.

MST P-wave velocity data from Hole 1051A APC cores are shown in Figure 36 (also see Table 22 on CD-ROM, back pocket, this volume). Despite the apparent scatter in this data set, which may be the result of cracking of the sediment or poor liner/sediment contact, it can be observed that P-wave velocity increases slightly with depth, from ~1.45 to 1.48 km/s across the depth range 0–140 mbsf. MST P-wave velocity data were not collected below this depth.

Natural gamma-radiation counts measured on the MST for Hole 1051A are shown in Figure 37 (also see Tables 23, 24 on CD ROM, back pocket, this volume). Natural gamma-radiation counts fluctuate slightly around background levels of 6 counts per second (cps) in the upper 375 m of the sediment column. Below 375 mbsf, the counts fluctuate between 7 and 11 cps. The highest number of counts occurs in the interval between 450 mbsf and total depth, which corresponds to the higher clay contents of lithologic Units III and IV.

Index Properties

Index properties were determined in Hole 1051A (Table 25; Fig. 38). Index properties data indicate that progressive sediment compaction and fluid expulsion with depth are the major factors contributing

Table 15. Headspace gas composition in Hole 1051A.

Depth (mbsf)	Gas zone	C_1 (ppm)	C_2 (ppm)	$C_2=$ (ppm)	C_3 (ppm)	$C_3=$ (ppm)	Total gas (ppm)	C_1/C_2	$C_1/(C_2+C_3)$
10.3	Surface	1.94					1.94		
19.8	Surface	1.95					1.95		
29.3	Surface	1.93					1.93		
38.8	Surface	1.9					1.90		
48.3	Surface	1.92					1.92		
57.8	Surface	1.91					1.91		
66.1	Surface	2.02					2.02		
76.8	Surface	2.54					2.54		
86.3	Surface	2.75					2.75		
95.8	Surface	4.13					4.13		
105.3	Surface	3.55					3.55		
114.8	Surface	6.37					6.37		
124.3	Surface	4.92					4.92		
133.8	Surface	5.88					5.88		
143.3	Surface	3.94					3.94		
152.8	Surface	6.31					6.31		
162.7	Surface	7.79					7.79		
172.3	Surface	3.72					3.72		
181.9	Surface	6.26					6.26		
191.5	Surface	6.19					6.19		
201.1	Surface	7.9					7.90		
210.7	Surface	8.17					8.17		
220.3	Surface	7.67					7.67		
229.9	Surface	9.79					9.79		
239.5	Middle	18.66					18.66		
249.1	Middle	15.89					15.89		
258.7	Middle	20.92					20.92		
268.3	Middle	33.07	0.70	0.20			33.97	47.2	36.74
276.4	Middle	11.01					11.01		
287.5	Middle	21.9					21.90		
295.6	Middle	22.96					22.96		
305.2	Middle	22.58					22.58		
316.3	Middle	16.65					16.65		
326.0	Middle	27	0.64				27.64	42.2	42.19
335.6	Middle	14.03					14.03		
345.2	Middle	22.96	0.49				23.45	46.9	46.86
354.9	Middle	14.13					14.13		
364.6	Middle	11.34					11.34		
374.2	Middle	11.59	0.18				11.77	64.4	64.39
394.4	Deep I	58.4	1.27	0.18			59.85	46.0	40.28
404.0	Deep I	44.27	1.09				45.36	40.6	40.61
413.6	Deep I	20.35					20.35		
423.2	Deep I	59.59	1.33				60.92	44.8	44.80
432.8	Deep I	71.72	1.59				73.31	45.1	45.11
442.4	Deep I	44.28	0.98				45.26	45.2	45.18
452.0	Deep I	78.84	2.80	0.50	0.3		82.44	28.2	21.90
458.6	Deep I	14.18	1.11	0.30			15.59	12.8	10.06
463.2	Deep I	20.89	1.09				21.98	19.2	19.17
471.3	Deep I	36.87	4.04	1.79	0.68	1.5	44.88	9.1	4.60
481.0	Deep II	12.15	1.11	0.39			13.65	10.9	8.10
490.6	Deep II	8.03	0.47				8.50	17.1	17.09
500.2	Deep II	2.75					2.75		
506.8	Deep II	3.71					3.71		
517.9	Deep II	3.2					3.20		
529.0	Deep II	3.1					3.10		
538.6	Deep II	2.8					2.80		
548.2	Deep II	2.73					2.73		
554.8	Deep II	2.48					2.48		
559.4	Deep II	1.9					1.90		
567.4	Deep III	30.49	1.57				32.06	19.4	19.42
577.0	Deep III	47.3	1.26		1.03		49.59	37.5	20.66
586.6	Deep III	89	2.54	0.30	1.6		93.44	35.0	20.05
596.3	Deep III	222.2	23.80	15.20	13.7	14.8	289.70	9.3	3.29
607.5	Deep III	122.9	5.70	3.60	3.5	2.5	138.20	21.6	8.03
615.6	Deep IV	60.9	3.00	1.70			65.60	20.3	12.96
622.2	Deep IV	25.3	2.00	0.60	0.3	0.2	28.40	12.7	8.16
624.3	Deep IV	38.3	3.10	0.80	0.6		42.80	12.4	8.51
630.4	Deep IV	36.3	2.70	0.40			39.40	13.4	11.71
641.5	Deep IV	68.8	4.70	0.70	0.4		74.60	14.6	11.86
643.1	Deep IV	38.4	2.80	1.20	1.2	1.1	44.70	13.7	6.10

Notes: In all cases, the injected sample size was 5 cm^3. Concentration of gas is in parts per million by volume. Total gas is the sum of C_1 to C_3 hydrocarbons for plotting purposes. Where no values are reported, concentrations are below detection limits.

to the physical nature of the sediments. Bulk and dry density values show a steady increase with depth in the upper 375 m, from average values of 1.55 to 1.85 g/cm^3 and 0.9 to 1.3 g/cm^3, respectively, whereas grain density values fluctuate between 2.55 and 2.67 g/cm^3. Below a coring gap between 382 and 389 mbsf, bulk, dry, and grain density values show a decrease in magnitude; this is followed by a steady increase to near maximum values of bulk and dry densities at 460 mbsf.

The reduction in magnitude of bulk, dry, and grain densities at 390 mbsf corresponds to the uppermost part of lithologic Unit II. The maximum bulk and dry density values occur between 450 and 555 mbsf, whereas grain density values in this interval are distinctly lower than values from above 375 mbsf. This distinctive change in grain density with depth observed at 375 mbsf corresponds to the contact between lithologic Units II and III. This change reflects an increase
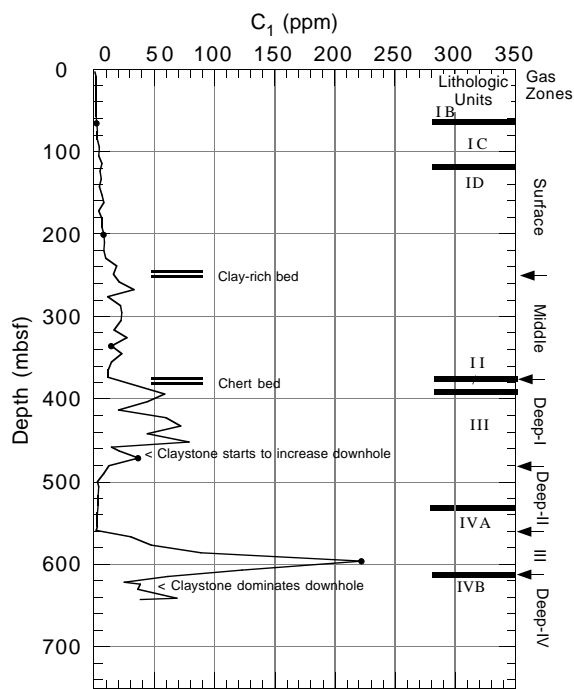
Figure 29. Methane (C_1) content vs. depth in Hole 1051A. Lithologic units are described in the "Lithostratigraphy" section (this chapter).

in the relative amount of clay minerals in lithologic Unit III compared with lithologic Unit II (see "Lithostratigraphy" section, this chapter) and a decrease in the relative amount of carbonate (see "Organic Geochemistry" section, this chapter). At 570 mbsf, bulk and dry density values decrease from 2.0 to 1.75 g/cm³ and 1.6 to 1.2 g/cm³, respectively, which corresponds to the contact between lithologic Units III and IV. The index properties data do not display distinct changes at the ooze to chalk transition at 120 mbsf, as seen at Site 1050.

Sediment porosity, water content, and void ratio (Fig. 38) show complementary inverse trends with depth to the trends observed for bulk, dry, and grain densities. In the upper 375 m of Hole 1051A, porosity, water content, void ratio, and also bulk and dry density data define five intervals where measured values are either higher or lower than the general trend. These excursion values correlate with ash layers (see "Lithostratigraphy" section, this chapter) and represent intervals of increased porosity and decreased bulk and dry densities. It is possible that the ash layers were initially of a higher porosity and lower density than the nannofossil ooze, and that intervals of secondary porosity were formed in the carbonate surrounding the ashes as a result of preferential fluid flow through these intervals. Localized minima of percentage carbonate within these intervals provide additional support for this hypothesis (see "Organic Geochemistry" section, this chapter).

Discrete bulk density measurements show good agreement with the GRAPE bulk density estimates for Hole 1051A (Fig. 39). Between the seafloor and 140 mbsf, which was drilled with the APC, the GRAPE bulk density closely matches the values obtained by discrete measurements. Between 140 and 375 mbsf, cored with the XCB, the average GRAPE bulk density slightly underestimates the values obtained by discrete measurements. Below 390 mbsf, the GRAPE bulk density values are significantly lower than the discrete bulk density values, although depth trends are still reproduced in both data sets. GRAPE bulk densities are most likely underestimates of true values because of the occurrence of void spaces, tension cracks created by sediment unloading or reduced core diameter, and the presence of slurry between drilling biscuits, which is common in the XCB cores.
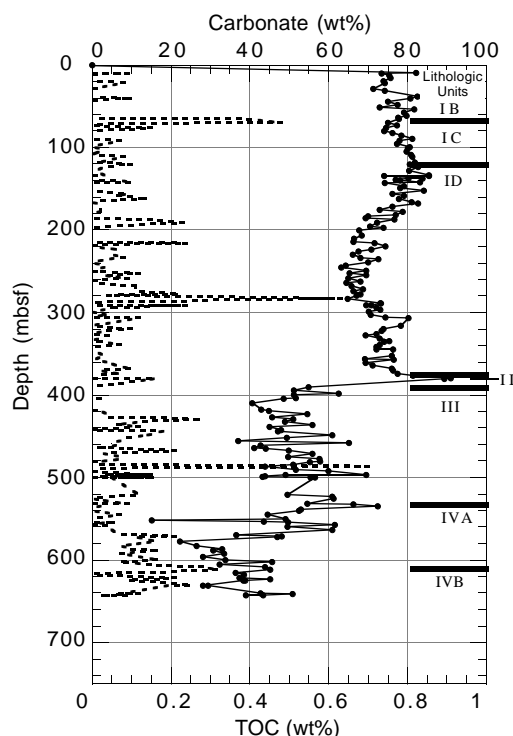
Figure 30. TOC and CaCO₃ contents vs. depth in Hole 1051A. Except for the four values above 0.3 wt%, TOC values are considered below the detection limit of the difference method. Lithologic units are described in the "Lithostratigraphy" section (this chapter).

Figure 39 shows that GRAPE bulk density may be of value even in sections where drilling techniques may result in an incompletely filled core liner.

P-wave Velocity

Discrete measurements of *P*-wave velocity were obtained on split-core sections by using the Hamilton Frame velocimeter (Table 26; Fig. 40). Comparison of discrete measurements of *P*-wave velocity with those from the MST *P*-wave logger (PWL) shows that the MST PWL significantly underestimates true *P*-wave velocity.

P-wave velocity shows a general increase in magnitude with depth. The contact between lithologic Subunits IB and IC cannot be recognized using velocity data because these units are defined by color changes. Between 0 and 140 mbsf, *P*-wave velocity increases in magnitude from 1.55 to 1.6 km/s. There is a sharp increase in *P*-wave velocity from 1.6 to 1.7 km/s between 140 and 160 mbsf that could be explained by the ooze to chalk transition, which occurs at ~120 mbsf (see "Lithostratigraphy" section, this chapter). Between 160 and 390 mbsf, which comprises lithologic Subunit ID and Unit II, *P*-wave velocity shows a general increase from 1.7 to 1.8 km/s. At 390 mbsf, *P*-wave velocity increases in magnitude, and this change corresponds to the contact between lithologic Units II and III. *P*-wave velocity increases from 1.8 to 2.2 km/s across the interval 390–570 mbsf, which corresponds to lithologic Unit III. Within lithologic Subunit IVA, between 570 and 610 mbsf, *P*-wave velocity drops to an average value of 1.9 km/s. Between 610 mbsf and total depth, which is

Table 16. Hole 1051A total inorganic carbon, carbonate, total carbon, total organic carbon, nitrogen, sulfur, and hydrogen analyses.

Core, section, interval (cm)	Midpoint (mbsf)	TIC (wt%)	CaCO$_3$ (wt%)	TC (wt%)	TOC (wt%)	N (wt%)	S (wt%)	H (wt%)
171B-1051A-								
2H-3, 78-79	9.59	9.87	82.21	9.84	0.00		0.05	0.16
2H-3, 133-139	10.16	8.81	73.40	8.90	0.09		0.00	0.26
2H-5, 78-79	12.59	9.05	75.40	8.94	0.00		0.03	0.25
3H-1, 77-78	16.08	9.09	75.68	9.05	0.00			0.28
3H-3, 135-139	19.67	8.86	73.82	8.87	0.01			0.26
3H-5, 78-79	22.09	8.91	74.25	8.99	0.08			0.26
4H-3, 135-140	29.18	8.56	71.31	8.53	0.00			0.31
4H-5, 78-79	31.59	8.92	74.32	8.84	0.00			0.27
5H-3, 133-139	38.66	9.91	82.55	9.85	0.00			0.16
5H-5, 79-80	41.10	9.68	80.67	9.78	0.10			0.18
6H-1, 78-79	44.59	9.00	74.99	8.82	0.00			0.23
6H-3, 135-139	48.17	9.29	77.42	9.24	0.00			0.22
6H-6, 78-79	52.09	8.76	72.96	8.69	0.00			0.25
7H-1, 72-73	54.03	9.80	81.67	9.71	0.00			0.17
7H-3, 134-139	57.67	9.50	79.11	9.45	0.00			0.22
7H-6, 77-78	61.58	9.57	79.74	9.51	0.00			0.17
8H-2, 78-79	63.88	9.33	77.69	9.25	0.00			0.21
8H-3, 134-139	65.96	9.33	77.76	9.71	0.38			0.21
8H-6, 77-78	69.87	9.01	75.03	9.49	0.48			0.25
9H-1, 78-79	73.09	9.29	77.37	9.24	0.00			0.21
9H-3, 135-140	76.68	8.94	74.48	9.09	0.15			0.23
9H-6, 78-79	80.59	8.88	73.97	8.86	0.00			0.23
10H-1, 73-74	82.54	9.14	76.12	9.10	0.00			0.21
10H-3, 134-139	86.17	9.42	78.46	9.44	0.00			0.19
10H-6, 68-69	89.99	9.75	81.21	9.64	0.00			0.18
11H-1, 77-78	92.08	9.35	77.88	9.42	0.07			0.20
11H-3, 135-139	95.67	9.29	77.38	9.32	0.03			0.20
11H-6, 77-78	99.58	9.67	80.52	9.61	0.00			0.20
12H-1, 77-78	101.58	9.61	80.05	9.63	0.02			0.18
12H-3, 134-139	105.17	9.57	79.76	9.59	0.02	0.01		0.22
12H-6, 77-78	109.08	9.71	80.89	9.64	0.00			0.18
13H-1, 77-78	111.08	9.74	81.12	9.82	0.08			0.17
13H-6, 77-78	118.58	9.82	81.82	9.83	0.01			0.17
14H-1, 78-79	120.59	9.67	80.53	9.77	0.10			0.19
14H-3, 135-140	124.18	9.92	82.67	9.95	0.03			0.18
14H-6, 78-79	128.09	9.66	80.46	9.67	0.01			0.18
15H-3, 135-140	133.68	10.25	85.41	10.28	0.03			0.14
15H-4, 97-98	134.78	10.26	85.42	10.25	0.00			0.12
15H-4, 103-104	134.84	8.89	74.04	8.88	0.00			0.26
15H-6, 77-78	137.58	10.06	83.82	10.01	0.00			0.15
15H-6, 98-99	137.79	9.63	80.24	9.57	0.00			0.20
16H-1, 78-79	139.59	9.23	76.90	9.21	0.00			0.23
16H-1, 133-135	140.14	9.37	78.09	9.44	0.07	0.01		0.24
16H-3, 78-79	142.59	9.98	83.10	10.08	0.10			0.15
16H-3, 120-125	143.03	8.92	74.32	8.91	0.00			0.24
16H-6, 78-79	147.09	9.50	79.16	9.33	0.00			0.21
17X-1, 77-78	149.08	9.37	78.07	9.25	0.00			0.21
17X-3, 142-145	152.74	10.10	84.11	10.04	0.00			0.16
17X-6, 59-60	156.40	9.14	76.14	9.23	0.09			0.23
18X-1, 78-79	158.99	9.50	79.11	9.56	0.06			0.19
18X-3, 117-119	162.38	9.34	77.81	9.48	0.14			0.20
18X-6, 80-82	166.51	9.73	81.02	9.73	0.00			0.17
19X-1, 62-63	168.43	9.93	82.69	9.94	0.01			0.17
19X-3, 127-130	172.09	9.15	76.25	9.17	0.02			0.23
19X-6, 12-13	175.43	8.75	72.86	8.77	0.02			0.27
20X-1, 73-74	178.14	9.46	78.79	9.48	0.02			0.21
20X-3, 135-138	181.77	9.23	76.89	9.13	0.00			0.22
20X-5, 20-23	183.62	8.41	70.06	8.26	0.00	0.01		0.33
20X-6, 79-80	185.70	8.32	69.34	8.29	0.00			0.28
21X-1, 81-82	187.82	9.20	76.65	9.31	0.11			0.22
21X-3, 133-136	191.35	8.69	72.37	8.92	0.23			0.28
21X-6, 101-102	195.52	8.47	70.52	8.50	0.03			0.30
22X-1, 84-85	197.45	8.88	73.94	8.88	0.00			0.26
22X-3, 105-108	200.67	8.13	67.72	8.07	0.00			0.34
23X-1, 82-83	207.03	8.20	68.33	7.97	0.00			0.34
23X-3, 137-139	210.58	7.98	66.51	8.13	0.00			0.33
23X-6, 73-74	214.44	7.96	66.29	7.92	0.00			0.35
24X-1, 78-79	216.59	8.59	71.55	8.83	0.24			0.26
24X-3, 135-139	220.17	8.94	74.44	8.94	0.00			0.30
24X-6, 77-78	224.08	8.49	70.75	8.55	0.06			0.30
25X-1, 77-78	226.18	8.10	67.51	8.16	0.06			0.32
25X-3, 130-134	229.72	7.94	66.16	7.99	0.05	0.01		0.33
25X-6, 73-74	233.64	8.16	67.99	8.24	0.08			0.35
26X-1, 83-84	235.84	8.72	72.60	8.76	0.04			0.26
26X-3, 133-136	239.35	8.41	70.08	8.37	0.00			0.33
26X-6, 78-79	243.29	7.73	64.36	7.76	0.03			0.39
27X-1, 82-83	245.43	7.59	63.24	7.62	0.03			0.38
27X-3, 136-139	248.98	8.35	69.54	8.30	0.00			0.32
27X-6, 77-78	252.88	7.84	65.28	7.96	0.12			0.36
28X-1, 79-80	255.00	8.35	69.52	8.38	0.03			0.31
28X-3, 133-136	258.55	7.80	64.98	7.89	0.09			0.35
28X-6, 75-76	262.46	8.17	68.02	8.16	0.00			0.29
29X-1, 69-70	264.50	7.75	64.56	7.71	0.00			0.30
29X-3, 137-140	268.19	7.90	65.80	8.01	0.11	0.01		0.37
29X-6, 78-79	272.09	8.25	68.74	8.36	0.11			0.26
30X-1, 75-76	274.16	7.97	66.36	8.08	0.11			0.32
30X-3, 137-140	277.79	8.17	68.04	8.39	0.22			0.31

Table 16 (continued).

Core, section, interval (cm)	Midpoint (mbsf)	TIC (wt%)	CaCO₃ (wt%)	TC (wt%)	TOC (wt%)	N (wt%)	S (wt%)	H (wt%)
30X-5, 47-48	279.88	8.05	67.02	8.09	0.04			0.33
31X-1, 79-80	283.80	7.78	64.79	8.41	0.63			0.30
31X-4, 136-138	288.87	8.78	73.11	8.78	0.00			0.29
31X-4, 141-143	288.92	8.79	73.24	8.77	0.00			0.28
31X-6, 76-77	291.27	8.50	70.83	8.41	0.00			0.31
31X-6, 79-80	291.30	8.35	69.58	8.59	0.24			NA
32X-2, 66-67	294.77	8.67	72.19	8.72	0.05			0.29
32X-3, 136-139	296.98	8.76	73.01	8.79	0.03			0.30
32X-5, 88-89	299.49	8.42	70.16	8.35	0.00			0.28
33X-1, 60-62	302.81	8.49	70.71	8.53	0.04			0.30
33X-3, 56-57	305.77	8.93	74.38	8.93	0.00			0.27
33X-3, 139-142	306.61	9.64	80.33	9.76	0.12			0.21
34X-3, 120-121	316.01	9.39	78.24	9.35	0.00			0.23
34X-6, 90-92	320.21	8.88	73.94	8.98	0.10			0.24
35X-1, 45-46	321.96	8.81	73.42	8.85	0.04			0.27
35X-3, 131-134	325.83	8.65	72.06	8.61	0.00			0.30
35X-5, 79-80	328.30	8.32	69.33	8.36	0.04			0.32
36X-1, 49-50	331.60	8.76	72.93	8.78	0.02			0.28
36X-3, 77-78	334.88	9.04	75.34	9.04	0.00			0.25
36X-3, 133-136	335.45	8.88	74.01	8.91	0.03			0.27
36X-6, 94-95	339.55	8.76	72.94	8.83	0.07			0.26
37X-1, 84-85	341.55	8.65	72.05	8.66	0.01			0.29
37X-3, 80-81	344.51	8.65	72.03	8.64	0.00			0.30
37X-3, 125-128	344.97	9.16	76.30	9.10	0.00			0.26
38X-2, 61-62	352.52	9.11	75.91	9.14	0.03			0.25
38X-4, 130-133	356.22	8.30	69.15	8.31	0.01			0.32
38X-5, 84-85	357.25	9.19	76.54	9.20	0.01			0.24
39X-1, 70-71	360.81	8.34	69.43	8.38	0.04			0.32
39X-3, 137-139	364.48	8.54	71.11	8.60	0.06			0.30
39X-6, 75-76	368.36	9.12	75.94	9.22	0.10			0.23
40X-1, 62-63	370.33	9.16	76.33	9.18	0.02			0.26
40X-3, 122-125	373.94	9.30	77.48	9.37	0.07	0.01		0.25
40X-5, 83-84	376.54	9.77	81.39	9.77	0.00			0.19
41X-1, 31-34	379.63	10.91	90.92	10.75	0.00			0.09
41X-1, 84-85	380.15	10.73	89.39	10.89	0.16			0.09
42X-1, 80-81	390.71	6.58	54.81	6.57	0.00			0.49
42X-3, 135-138	394.27	6.15	51.22	6.12	0.00			0.53
42X-6, 79-80	398.20	7.50	62.49	7.48	0.00			0.38
43X-1, 73-74	400.24	6.15	51.26	6.15	0.00			0.52
43X-3, 127-131	403.79	6.20	51.66	6.17	0.00			0.52
43X-4, 86-87	404.87	5.84	48.64	5.86	0.02			0.53
44X-1, 79-80	409.90	4.88	40.62	4.85	0.00			0.67
44X-6, 80-81	417.41	5.16	42.99	5.11	0.00			0.66
44X-6, 95-99	417.57	5.16	42.97	5.09	0.00	0.01		0.62
45X-1, 74-75	419.45	5.40	44.96	5.42	0.02			0.60
45X-3, 138-141	423.10	6.55	54.55	6.59	0.04			0.50
45X-6, 78-79	426.99	5.47	45.58	5.51	0.04			0.56
46X-1, 102-103	429.33	6.12	50.98	6.40	0.28			0.48
46X-3, 134-137	432.66	5.87	48.91	6.00	0.13			0.57
46X-6, 80-81	436.61	6.70	55.78	6.76	0.06			0.47
47X-1, 79-80	438.70	5.40	45.02	5.52	0.12			0.59
47X-3, 144-147	442.36	5.76	48.01	NA	NA	NA	NA	0.54
47X-5, 77-78	444.68	5.66	47.11	5.84	0.19			0.61
48X-1, 104-105	448.55	7.31	60.92	7.45	0.14			0.39
48X-3, 148-150	451.99	5.92	49.34	6.01	0.09			0.52
48X-6, 59-60	455.60	4.45	37.08	4.52	0.07			0.63
49X-1, 77-78	457.88	7.82	65.11	7.87	0.05			0.28
50X-1, 80-81	461.01	5.13	42.77	5.19	0.06			0.54
50X-3, 135-138	464.57	4.94	41.14	4.95	0.01	0.12		0.51
50X-4, 77-78	465.48	5.30	44.12	5.37	0.07			0.53
51X-1, 67-68	467.48	5.99	49.87	6.20	0.21			0.48
51X-3, 140-143	471.22	6.70	55.82	6.73	0.03	0.09		0.41
51X-6, 75-76	475.06	5.98	49.78	6.05	0.07	0.01		0.48
52X-1, 119-120	477.70	6.92	57.61	6.99	0.07			0.49
52X-3, 138-140	480.89	6.95	57.91	6.97	0.02			0.37
52X-4, 68-69	481.69	6.64	55.29	6.61	0.00			0.44
52X-6, 73-74	484.74	6.14	51.11	6.15	0.01			0.48
53X-1, 64-65	486.75	5.27	43.94	5.97	0.70			0.48
53X-3, 132-135	490.44	6.20	51.63	6.20	0.00	0.10		0.42
53X-5, 61-62	492.72	7.21	60.04	7.20	0.00			0.43
54X-1, 78-79	496.49	8.35	69.57	8.50	0.15			0.32
54X-1, 135-137	497.06	5.89	49.03	5.92	0.03	0.01		0.53
54X-2, 128-129	498.49	5.28	43.98	5.42	0.14	0.02		0.55
54X-3, 83-86	499.55	5.19	43.26	5.19	0.00			0.51
54X-3, 115-118	499.87	6.65	55.42	6.81	0.16	0.01	0.03	0.41
54X-3, 137-139	500.08	6.78	56.51	6.83	0.05			0.37
56X-5, 1-3	520.92	5.95	49.57	6.07	0.12			0.52
56X-6, 74-75	523.15	7.30	60.82	7.36	0.06			0.38
57X-1, 74-75	525.25	7.36	61.31	7.26	0.00			0.37
57X-5, 145-148	531.97	6.55	54.54	6.64	0.09	0.01		0.47
57X-6, 60-61	532.61	7.96	66.28	7.93	0.00			0.36
58X-1, 83-84	534.94	8.70	72.48	8.72	0.02			0.27
58X-3, 134-137	538.46	6.36	52.94	6.33	0.00			0.43
58X-5, 82-83	540.93	6.30	52.45	6.29	0.00	0.01		0.52
59X-1, 85-87	544.56	5.35	44.59	5.42	0.07	0.02		0.63
59X-5, 83-84	550.54	5.89	49.09	5.87	0.00			0.52
59X-6, 123-126	552.45	1.83	15.23	1.83	0.00			0.96
60X-1, 28-32	553.60	5.23	43.54	5.23	0.00			0.55
60X-1, 77-79	554.08	5.96	49.64	6.02	0.06			0.55

Table 16 (continued).

Core, section, interval (cm)	Midpoint (mbsf)	TIC (wt%)	CaCO₃ (wt%)	TC (wt%)	TOC (wt%)	N (wt%)	S (wt%)	H (wt%)
61X-1, 74-75	557.15	7.38	61.51	7.37	0.00			0.40
61X-3, 17-20	559.59	5.96	49.61	6.01	0.05			0.47
62X-1, 79-80	563.70	7.32	60.95	7.37	0.05			0.43
62X-5, 140-142	570.31	4.40	36.65	4.47	0.07	0.08		0.67
62X-6, 91-95	571.33	5.78	48.17	5.99	0.21			0.46
62X-, 41-43	572.45	5.65	47.06	5.76	0.11	0.06	1.71	0.49
63X-4, 28-30	577.29	2.68	22.35	2.84	0.16	0.11		0.81
64X-1, 77-78	582.88	3.18	26.50	3.25	0.07			0.75
64X-3, 147-150	586.59	3.96	33.03	4.06	0.10	0.12		0.73
64X-5, 60-61	588.71	3.69	30.73	3.86	0.17	0.12		0.74
65X-1, 75-76	592.56	4.03	33.54	4.10	0.07			0.65
65X-3, 129-132	596.11	3.38	28.15	3.50	0.12	0.07		0.79
65X-6, 77-78	600.08	4.07	33.92	4.24	0.17	0.10		0.65
66X-1, 109-110	602.60	5.48	45.65	5.55	0.07	0.12		0.52
66X-3, 143-146	605.95	3.89	32.37	4.03	0.14			0.65
66X-5, 76-77	608.27	5.27	43.94	5.55	0.28			0.47
67X-1, 83-84	611.94	5.42	45.17	5.74	0.32	0.13		0.47
67X-3, 137-141	615.49	4.38	36.49	4.49	0.11	0.01		0.60
67X-5, 70-71	617.81	4.62	38.48	4.57	0.00			0.58
68X-1, 72-73	621.43	4.48	37.32	4.69	0.21			0.51
68X-2, 130-132	623.51	5.43	45.22	5.59	0.16	0.02		0.51
69X-1, 49-50	624.80	4.66	38.85	4.75	0.09	0.02		0.54
69X-1, 50-52	624.81	4.60	38.34	4.71	0.11	0.08		0.63
70X-CC, 5-8	630.86	3.38	28.14	3.63	0.25	0.03		0.68
70X-CC, 19-20	630.99	3.53	29.40	3.72	0.19	0.08		0.64
72X-1, 53-56	640.55	5.14	42.81	5.21	0.07	0.01		0.52
72X-1, 99-100	641.00	6.12	50.97	6.24	0.12	0.01		0.40
73X-1, 118-119	642.79	5.21	43.39	5.23	0.02			0.49
73X-1, 146-149	643.08	4.69	39.08	4.79	0.10	0.01		0.58

Notes: TIC = total inorganic carbon; TC = total carbon; TOC = total organic carbon computed by difference (TC – TIC). Negative TOC values are reported as 0.00. wt% = weight percent. NA = not analyzed. Where no values are reported, concentrations are below detection limits.
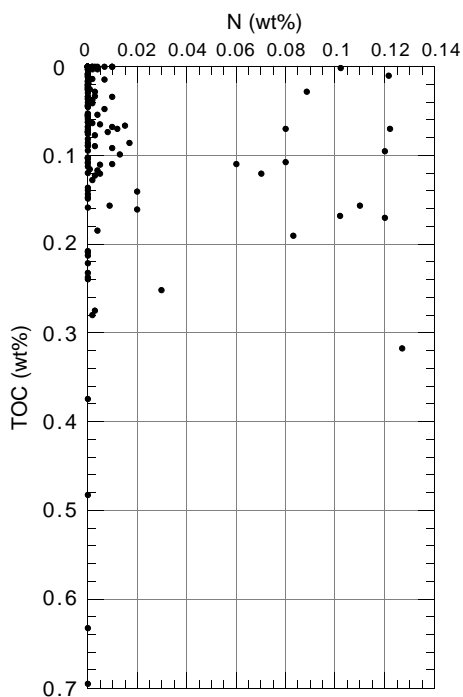
Figure 31. TOC vs. nitrogen content in Hole 1051A.

Figure 32. Nitrogen and TOC contents vs. depth in Hole 1051A. Lithologic units are described in the "Lithostratigraphy" section (this chapter).

defined as lithologic Subunit IVB, *P*-wave velocity increases steadily to a maximum value of 2.2 km/s. There is a positive correlation between bulk density and *P*-wave velocity (Fig. 41).

Undrained Shear Strength

Undrained shear strength was measured on sediments recovered from Hole 1051A by using the miniature vane-shear device and, when the sediment became too indurated to insert the vane-shear de-

vice, a pocket penetrometer (Table 27; Fig. 42). There is no systematic relationship between shear strength and depth in Hole 1051A, although the pocket penetrometer measurements are biased toward higher values compared with those obtained with the vane-shear device.

Normalized shear strength, the ratio of shear strength (S_u) to effective overburden pressure (P_0'), can be used to assess the stress history of a sediment column. Normalized shear strength ratios (S_u/P_0') de-

215

Table 17. Interstitial-water geochemical data for Hole 1051A.

Core, section, interval (cm)	Depth (mbsf)	pH	Alkalinity (mM)	Salinity (g/kg)	Cl (mM)	Na (mM)	Mg (mM)	Ca (mM)	SO$_4$ (mM)	NH$_4$ (μM)	H$_4$SiO$_4$ (μM)	K (mM)	Sr (μM)	Li (μM)	Rb (μM)	B (μM)
171B-1051A-																
2H-3, 145-150	10.25	7.67	3.05	35.5	558	479	53.76	10.63	29.3	17	676	12.3	91	30.2	1.92	280
3H-3, 145-150	19.75	7.49	2.89	36.0	560	481	53.50	11.06	29.7	62	661	11.8	106	31.2	1.84	482
4H-3, 145-150	29.25	7.54	3.14	36.0	561	481	53.64	11.33	29.9	8.7	740	12.6	114	33.2	1.97	598
5H-3, 145-150	38.75	7.54	3.23	35.5	565	485	53.10	11.78	29.2	22	694	11.6	122	31.6	1.86	504
6H-3, 145-150	48.25	7.50	3.36	36.0	564	483	52.83	12.30	29.1	52	705	11.9	130	38.7	1.87	519
7H-3, 145-150	57.75	7.54	3.49	35.5	564	485	51.94	12.38	28.8	12	757	11.5	138	38.3	1.98	446
10H-3, 145-150	87.75	7.56	4.06	35.5	562	480	52.02	13.43	28.5	65	792	11.7	169	49.0	2.00	468
13H-3, 145-150	114.75	7.51	4.48	35.5	565	484	50.91	14.13	28.2	42.0	803	11.5	192	58.2	2.02	547
16H-3, 145-150	143.20	7.51	4.88	35.5	566	479	50.40	14.97	24.6	62	810	10.2	223	70.8	2.05	519
19X-3, 140-150	172.20	7.44	4.81	36.0	567	486	48.85	15.95	27.8	81	871	11.6	246	88.0	2.23	461
22X-3, 140-150	201.00	7.43	4.87	36.0	570	485	48.84	16.69	26.5	120	858	11.4	277	97.4	2.15	461
25X-3, 140-150	229.80	7.42	5.11	36.0	568	485	47.34	17.54	26.6	122	936	11.9	324	120	2.19	454
28X-3, 140-140	258.60	7.47	4.86	36.0	570	487	47.04	18.33	27.4	149	982	11.8	355	133	2.20	468
31X-2, 140-150	285.90	7.30	6.35	36.0	574	489	46.97	20.00	26.7	172	1061	11.1	370	160	2.08	396
34X-3, 140-150	316.20	7.28	6.51	36.0	572	484	46.89	21.32	26.1	191	1065	10.4	386	172	1.94	555
37X-3, 140-150	345.10	7.29	6.55	36.0	578	492	46.26	21.69	26.7	186	1019	10.1	402	190	1.94	454
40X-3, 140-150	374.10	7.36	6.33	36.0	579	490	46.11	22.18	26.0	236	1052	10.4	409	202	1.88	381
43X-3, 140-150	403.90	7.81	8.05	36.0	590	492	41.12	29.65	22.1	336	1035	8.31	665	446	1.53	446
46X-3, 140-150	432.70	7.74	6.78	36.0	585	485	40.01	30.31	21.4	368	790	8.58	689	423	1.52	403
49X-1, 140-150	458.50	7.25	6.30	36.0	589	487	39.16	30.24	19.7	393	659	8.97	673	460	1.39	381
53X-3, 140-150	490.50	7.31	5.10	36.0	592	489	39.75	30.54	20.7	432	493	8.61	697	483	1.39	360
56X-5, 135-150	522.25	7.46	3.80	36.0	594	491	39.41	29.83	19.8	441	674	7.84	759	486	1.27	389
59X-3, 135-150	548.05	7.46	3.26	37.0	588	482	37.49	31.92	18.6	470	671	7.24	821	495	1.12	316
62X-3, 135-150	567.25			36.0	588		37.08	31.67	16.00			6.56	836		1.01	266
65X-3, 135-150	596.15	7.27	5.04	36.0	591	484	38.76	31.77	18.00	480		6.81	860	502	1.11	381
68X-3, 135-150	622.05				590				16.9		608	6.59	914	613	0.97	360

Note: Where no values are reported, data are absent.

termined for Hole 1051A are plotted against depth in Figure 43. A normally consolidated sediment has an S_u/P_0' between 0.2 and 0.22 (Ladd et al., 1977). Sediments above 30 mbsf in Hole 1051A have $S_u/P_0' > 0.22$ and are overconsolidated. Below 30 mbsf in Hole 1051A, S_u/P_0' are generally ≤0.22, suggesting that sediments below this depth are underconsolidated. Estimation of the overburden thickness (assuming that the sediment at 12 mbsf, where the maximum value of S_u was measured, was normally consolidated at maximum overburden thickness and that no changes in shear strength have occurred) suggests that 34 m of sediment may have accumulated and been removed in Hole 1051A between the late Eocene and the present.

Resistivity

The resistivity data from Hole 1051A were measured using the Scripps Institution of Oceanography probe (Table 28; Fig. 44). Resistivity values show a general increase in magnitude from 0.4 to 0.55 Ωm between 0 and 150 mbsf. At 100 mbsf, there is an abrupt increase in resistivity, which is just above the ooze to chalk transition at 120 mbsf (see "Lithostratigraphy" section, this chapter). The increase in resistivity across this interval is most likely because of a cementation process that has reduced sediment porosity, as resistivity and porosity in Hole 1051A are well correlated (Fig. 45).

Thermal Conductivity

Thermal conductivity data from the APC cores of Hole 1051A are listed in Table 29 and shown in Figure 46. Thermal conductivity measurements for Hole 1051A were obtained using the TK-04 instrument, and they display less scatter than measurements obtained in Holes 1049B and 1050B, which were determined using the Thermcon-85. Comparison of standard measurements from both instruments shows that the Thermcon-85 data are significantly more scattered and underestimate the values obtained with the TK-04. It is probable that the high degree of scatter observed in data from Holes 1049B and 1050B is caused by instrumental noise in the Thermcon-85 unit.

Thermal conductivity does not show any apparent change with depth in Hole 1051A. An average thermal conductivity of 1.14 ± 0.16 W/(m·K) is a representative estimate for the depth interval 0–130 mbsf in Hole 1051A.

Summary

Physical properties data at Site 1051 indicate that compaction and fluid expulsion, as well as physicochemical changes related to lithology, are the controlling factors on sediment properties. Physical properties data are influenced largely by sediment type; this is particularly apparent at the ooze to chalk transition at 120 mbsf and at the siliceous nannofossil chalk to clayey nannofossil chalk transition at 570 mbsf. Cementation and sediment lithification in the 0–120 mbsf interval influence *P*-wave velocity and resistivity by decreasing *P*-wave traveltime across grain contacts and by decreasing porosity, respectively. Porosity maxima in the upper 375 m of Hole 1051A correlate with ash layers and local percentage carbonate minima, suggesting that the ash layers were intervals of preferential fluid flow, which subsequently created secondary porosity in the enclosing carbonate sediments.

HEAT FLOW AND IN SITU TEMPERATURE MEASUREMENTS

The Adara tool was run three times in the upper section of Hole 1051B to measure in situ temperature (Table 30). The resulting time-temperature plot for the first run of the Adara tool is illustrated in Figure 47, and final temperature data are plotted in Figure 48. The sediment section above about 70 mbsf is essentially isothermal. This may be the result of seawater percolation into this portion of the sediment column either from above or laterally. Alternatively, significant amounts of heat may be conducted out the sides of the erosional remnant that constitutes the sediment block on which Site 1051 is located (see "Introduction" chapter, this volume).

Table 31 lists possible heat-flow values for this site, assuming various geothermal gradients, and using the measured downhole tem-
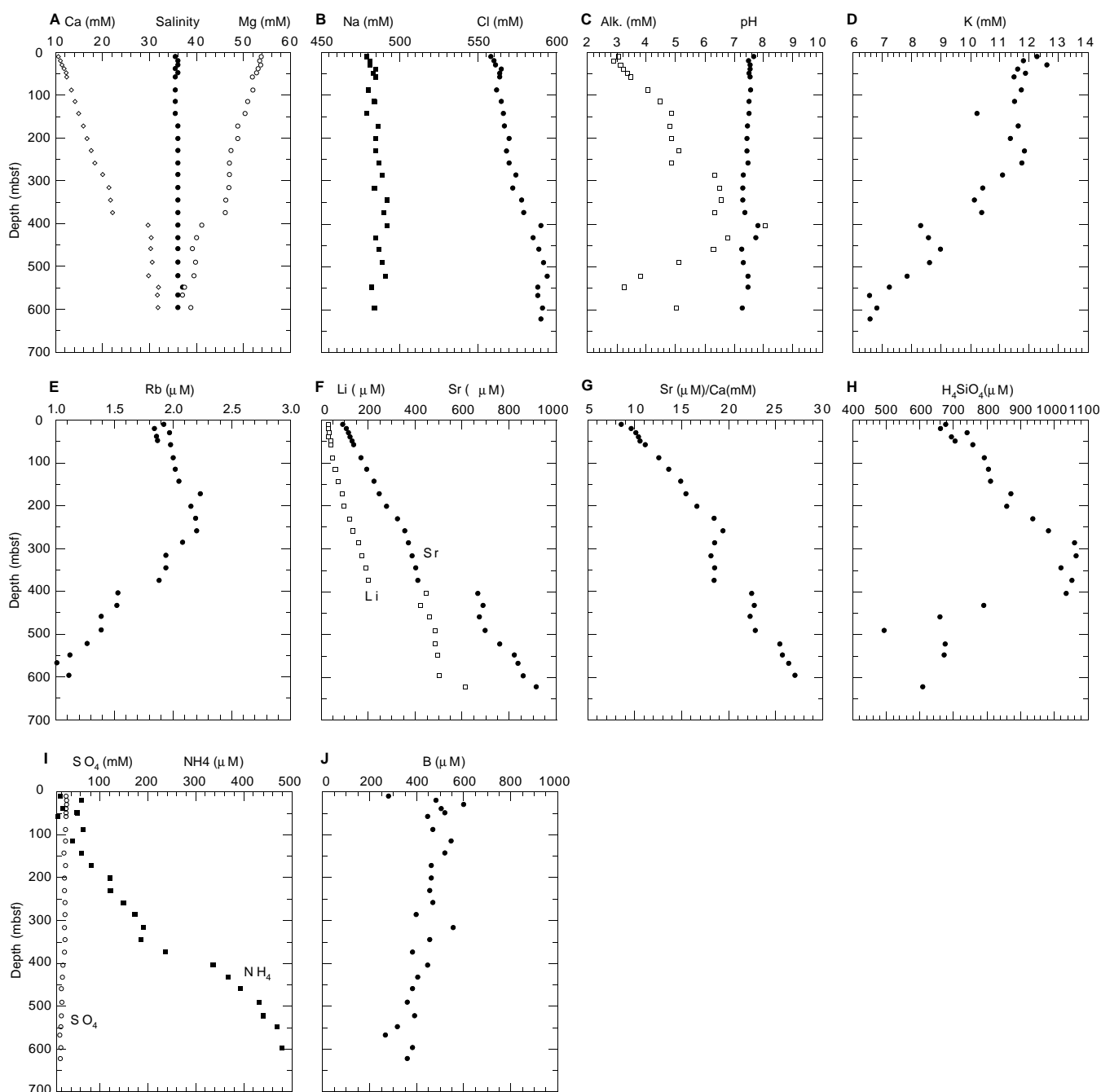
Figure 33. Interstitial-water geochemical data for Hole 1051A vs. depth. **A.** Calcium, salinity, and magnesium. **B.** Sodium and chloride. **C.** Alkalinity and pH. **D.** Potassium. **E.** Rubidium. **F.** Lithium and strontium. **G.** Strontium/calcium ratio. **H.** Silica. **I.** Sulfate and ammonium. **J.** Boron.

peratures and a thermal conductivity value of 1.14 W/(m·K) for the sediments (see "Physical Properties" section, this chapter). The range of heat-flow values obtained in Hole 1051B is low compared with values obtained at Deep Sea Drilling Project (DSDP) Site 534 in the Blake-Bahama Basin (42–57 mW/m²; Henderson and Davis, 1983) and sites to the north on the Blake Outer Ridge and the Carolina Rise area (46–48.4 mW/m²; Ruppell et al., 1995). These results indicate that the temperature distribution in the upper portion of the sediment column in Hole 1051B is not controlled by simple, one-dimensional heat flow from below.

DOWNHOLE LOGGING

Logging Operations

After Hole 1051A was drilled to a total depth of 645 mbsf, the lower limit of the BHA was placed at 110 mbsf. Three logging tool strings were deployed in Hole 1051A in the following order: triple-combo, FMS, and GHMT strings (see "Downhole Logging" section of the "Explanatory Notes" chapter, this volume). The Lamont-Doherty temperature-logging tool (TLT) was attached at the bottom

Hole 1051A

Hole 1051B
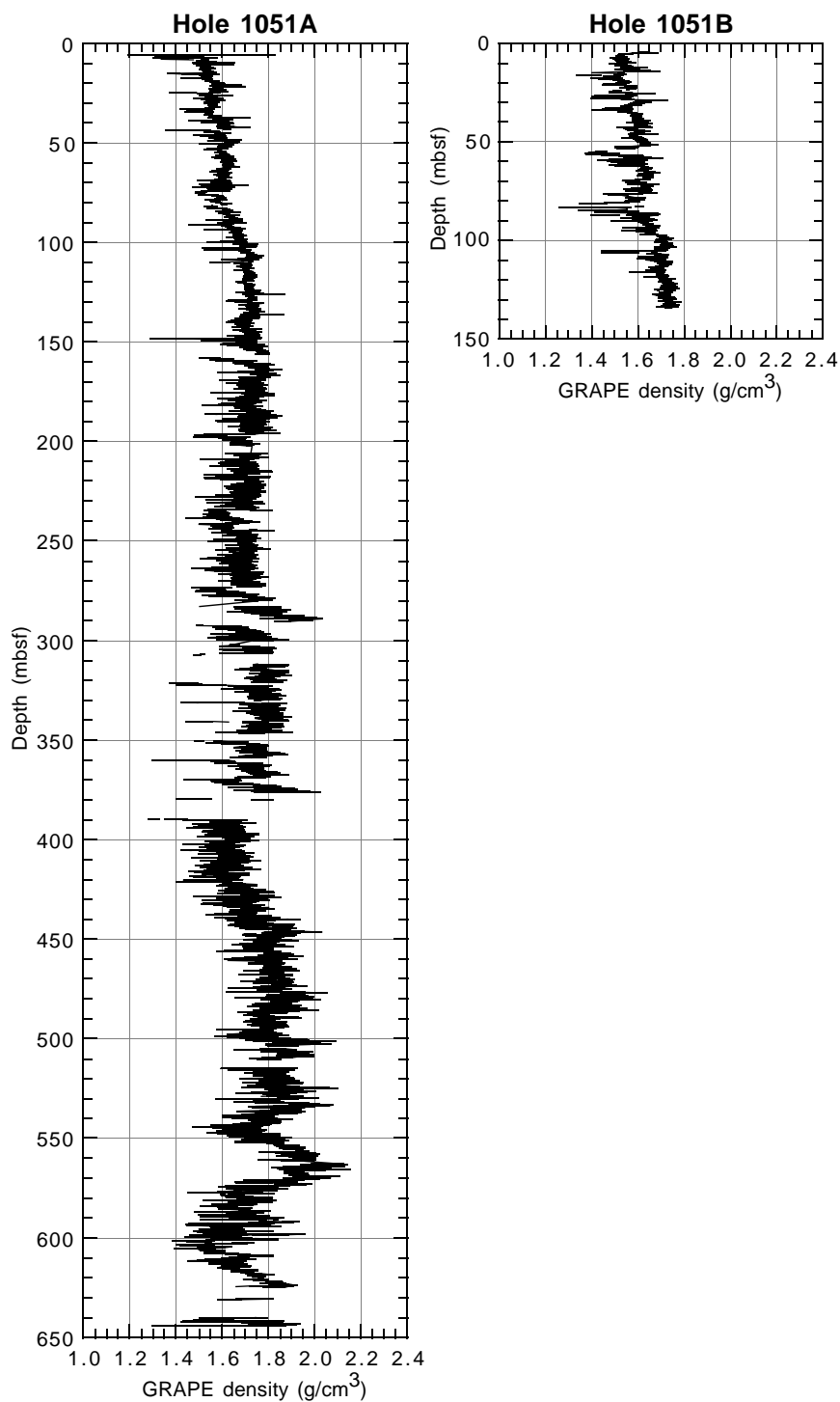
Figure 34. GRAPE bulk density for Holes 1051A and 1051B (see Tables 18, 19 [CD-ROM, back pocket, this volume] for data).

of the first logging run. The sonic digital tool was not operational, so it was not run with the FMS tool string. Each tool string was lowered to the bottom of the hole and pulled up at a rate between 300 and 600 m/hr to acquire high-resolution log data. All three tool strings reached the total depth drilled. A repeat interval was also run with each tool string to provide data quality control. A second pass of the FMS tool string was made in an attempt to increase borehole coverage.

The wireline heave compensator was not available for use during logging operations on Leg 171B. Fortunately, sea-state conditions were moderate (2.5-m swells) and had no obvious adverse effects on logging data. Table 32 shows the logging schedule and intervals logged with each tool string in Hole 1051A.

Data Quality

Overall, good hole conditions allowed high-quality logging data to be collected in Hole 1051A. Some post-cruise reprocessing of the log data is required to remove any effects of ship heave and "stick-and-slip" logging tool motion. The three-axis magnetometer-inclino-
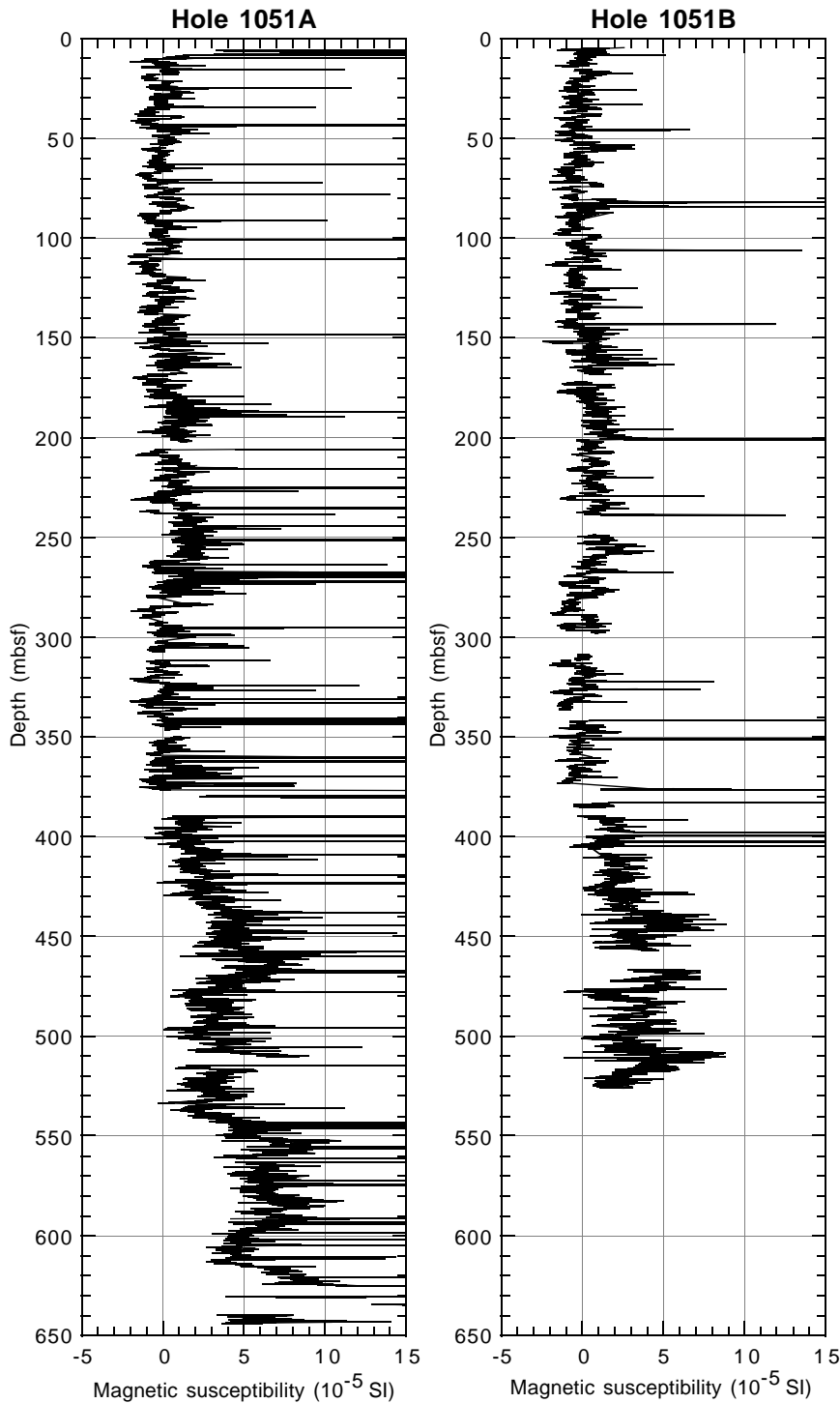
Figure 35. Magnetic susceptibility for Holes 1051A and 1051B (see Tables 20, 21 [CD-ROM, back pocket, this volume] for data).

meter tool (GPIT) indicates that the hole deviates by about 2°–3° between 110 and 400 mbsf. Below this depth, borehole inclination gradually increases to a maximum of ~17° near the base of the hole. The direction of borehole dip (borehole azimuth) varies between 155° and 160°N in the upper 400 m of the hole and gradually increases to about 185°N at the base of the hole. Hole diameter, measured by the Litho-Density sonde (HLDT) caliper, shows an overall uphole increase in diameter from about 9.9 in (25 cm) at the base to 15 in (38 cm) near the drill pipe. The outside diameter of the drill bit for this hole was 25 cm (9.875 in). Significant increases in borehole diameter, or "washouts," occur between 120 and 160 mbsf and between 280 and 310 mbsf. The FMS calipers (C1 perpendicular to C2) indicate a moderate degree of borehole elongation, or ovalization, on the order of 8–15 cm (i.e., the difference between C1 and C2).

Depth shifts for each of the logging runs were determined by correlating the natural gamma-ray logs and were made relative to the triple-combo tool string. The depth to the end of pipe, determined by wireline measurements, was 0.5 m shallower than that given by drill-pipe measurements. All logs were depth shifted from mbrf to mbsf by subtracting 1994 m (the distance between the rig floor and the bottom of the BHA). These preliminary adjustments will be replaced by more accurate depth shifts during post-cruise processing (post-cruise
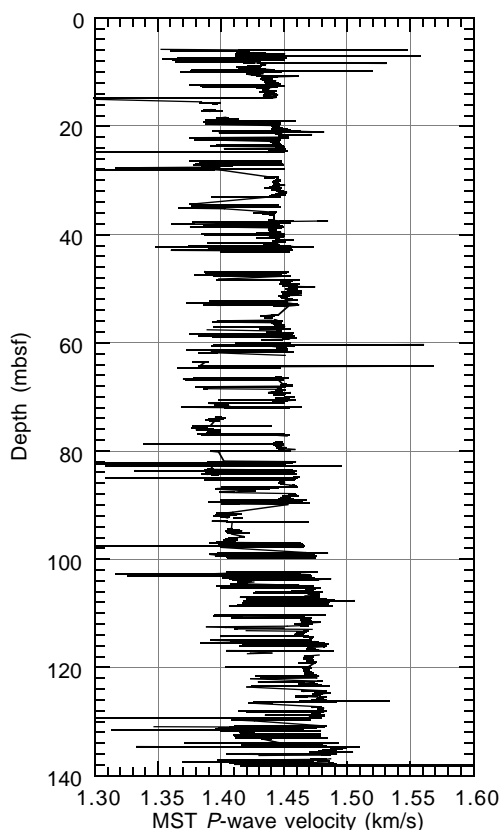
Figure 36. MST *P*-wave velocity for Hole 1051A (see Table 22 [CD-ROM, back pocket, this volume] for data). *P*-wave velocity was measured on APC cores only.

processed log data is available on CD-ROM, back pocket, this volume). The FMS microresistivity data have undergone shipboard image processing, improving the image for preliminary shipboard interpretation and integration with core observations.

Unfortunately, because of an electrical problem with the TLT and compatibility problems with the FMS tool, borehole temperature data were not collected in Hole 1051A. However, in situ temperature measurements were made using the Adara temperature probe (see "Heat Flow and In Situ Temperature Measurements" section, this chapter).

Logging Units

The three major logging units identified in Hole 1051A (Fig. 49) should not be confused with the lithologic units defined earlier (see "Lithostratigraphy" section, this chapter).

Logging Unit 1 (110–370 mbsf)

Between 110 mbsf (the base of the drill pipe) and 370 mbsf, the logs are distinguished by uniformly low resistivity (≤1 Ωm), less variable bulk density (RHOB <1.8 g/cm^3) and photoelectric effect (PEF = 3.2–3.6 barns/e$^-$), and slightly decreasing and more variable porosity than logging Unit 2 (Figs. 49, 50). Total gamma-ray counts (SGR) are relatively low throughout logging Unit 1 (<9 GAPI), indicating low clay content. Slightly higher gamma-ray values between 9 and 14 GAPI occur between 180 and 270 mbsf, coinciding with a slight increase in the mean potassium and thorium concentrations (Fig. 49). Thorium vs. potassium concentrations in the interval from
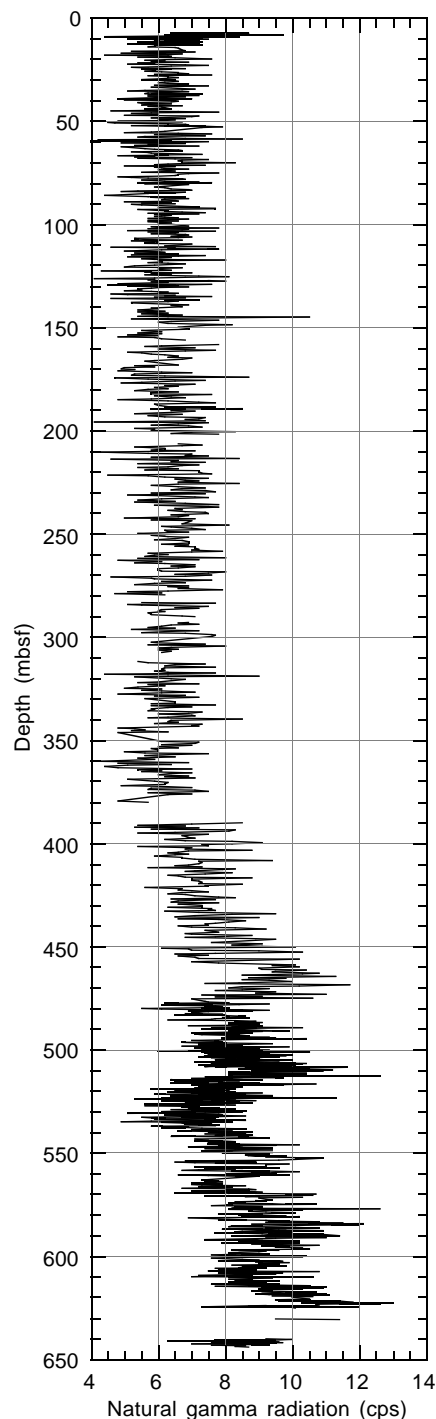
Figure 37. Composite plot of natural gamma radiation for Site 1051 (see Tables 23, 24 [CD-ROM, back pocket, this volume] for data).

110 to 370 mbsf fall largely within the montmorillonite (smectite) clay field (Fig. 51).

Magnetic susceptibility (MAGS) and Earth's conductivity (MAGC) show an overall decrease in mean values from 110 mbsf to the base of the unit at 370 mbsf (Fig. 52). In general, Unit 1 is characterized by low-amplitude variations in magnetic susceptibility, punctuated by sporadic

Table 25. Discrete index properties measurements for Hole 1051A.

Core, section, interval (cm)	Depth (mbsf)	Water content (total mass wt%)	Water content (solid mass wt%)	Bulk density (g/cm^3)	Grain density (g/cm^3)	Dry density (g/cm^3)	Porosity (%)	Void ratio
171B-1051A-								
2H-3, 75-77	9.56	41.6	71.1	1.60	2.65	0.93	64.8	1.84
2H-4, 75-77	11.06	43.0	75.3	1.57	2.61	0.89	65.8	1.92
2H-5, 75-77	12.56	41.6	71.1	1.58	2.58	0.93	64.2	1.79
2H-6, 75-77	14.06	43.3	76.4	1.56	2.60	0.88	65.9	1.94
3H-1, 75-77	16.06	42.8	74.9	1.57	2.59	0.90	65.5	1.90
3H-2, 75-77	17.56	42.2	73.1	2.01	6.72	1.16	82.7	4.80
3H-3, 75-77	19.06	41.0	69.4	1.59	2.60	0.94	63.8	1.76
3H-4, 75-77	20.56	41.4	70.6	1.59	2.61	0.93	64.3	1.80
3H-5, 75-77	22.06	41.1	69.8	1.59	2.59	0.94	63.9	1.77
3H-6, 75-77	23.56	39.4	65.0	1.62	2.62	0.98	62.4	1.66
4H-1, 75-77	25.56	40.9	69.3	1.60	2.61	0.94	63.8	1.76
4H-2, 75-77	27.06	42.7	74.4	1.58	2.63	0.90	65.7	1.91
4H-3, 75-77	28.56	41.7	71.5	1.58	2.59	0.92	64.4	1.81
4H-4, 75-77	30.06	41.7	71.6	1.59	2.61	0.92	64.6	1.83
4H-5, 75-77	31.56	41.3	70.5	1.59	2.61	0.93	64.2	1.80
4H-6, 75-77	33.06	42.4	73.6	1.58	2.61	0.91	65.3	1.88
5H-1, 75-77	35.06	42.2	72.9	1.57	2.56	0.91	64.6	1.82
5H-2, 75-77	36.56	41.1	69.8	1.59	2.59	0.94	63.8	1.76
5H-3, 75-77	38.06	39.0	63.8	1.63	2.64	1.00	62.2	1.64
5H-4, 75-77	39.56	39.5	65.2	1.63	2.64	0.98	62.7	1.68
5H-5, 75-77	41.06	39.0	63.8	1.62	2.60	0.99	61.8	1.62
5H-6, 75-77	42.56	38.3	61.9	1.64	2.63	1.02	61.4	1.59
6H-1, 75-77	44.56	40.1	66.8	1.61	2.62	0.97	63.1	1.71
6H-2, 75-77	46.06	39.5	65.4	1.62	2.63	0.98	62.7	1.68
6H-3, 75-77	47.56	40.1	67.0	1.61	2.61	0.96	63.1	1.71
6H-4, 75-77	49.06	38.5	62.6	1.64	2.63	1.01	61.7	1.61
6H-5, 74-76	50.55	38.4	62.3	1.64	2.64	1.01	61.6	1.61
6H-6, 75-77	52.06	38.8	63.4	1.64	2.63	1.00	62.0	1.63
7H-1, 75-77	54.06	39.0	63.8	1.63	2.62	1.00	62.0	1.63
7H-2, 75-77	55.56	39.6	65.6	1.62	2.62	0.98	62.7	1.68
7H-3, 71.5-73.5	57.03	37.4	59.8	1.66	2.64	1.04	60.6	1.54
7H-4, 75-77	58.56	37.3	59.5	1.66	2.63	1.04	60.5	1.53
7H-5, 75-77	60.06	38.9	63.7	1.62	2.59	0.99	61.7	1.61
7H-6, 75-77	61.56	38.3	62.0	1.64	2.61	1.01	61.3	1.58
8H-2, 75-77	63.85	38.9	63.6	1.64	2.64	1.00	62.1	1.64
8H-3, 75-77	65.35	39.0	63.9	1.63	2.64	1.00	62.2	1.65
8H-4, 75-77	66.85	39.1	64.2	1.62	2.58	0.99	61.8	1.62
8H-5, 75-77	68.35	39.9	66.5	1.61	2.59	0.97	62.7	1.68
8H-6, 75-77	69.85	38.7	63.2	1.63	2.61	1.00	61.7	1.61
8H-7, 75-77	71.35	40.9	69.2	1.60	2.60	0.94	63.8	1.76
8H-8, 75-77	72.35	37.1	59.0	1.66	2.60	1.04	60.0	1.50
9H-1, 75-77	73.06	41.2	70.2	1.59	2.59	0.93	64.0	1.78
9H-2, 75-77	74.56	41.3	70.5	1.59	2.61	0.93	64.3	1.80
9H-3, 75-77	76.06	44.6	80.5	1.54	2.58	0.85	67.0	2.03
9H-4, 75-77	77.56	38.8	63.3	1.63	2.60	1.00	61.6	1.61
9H-5, 74-76	79.05	40.5	68.2	1.60	2.60	0.95	63.4	1.73
9H-6, 75-77	80.56	39.1	64.3	1.62	2.61	0.99	62.1	1.64
10H-1, 75-77	82.56	41.1	69.7	1.60	2.61	0.94	64.0	1.78
10H-2, 75-77	84.06	37.5	59.9	1.65	2.59	1.03	60.3	1.52
10H-3, 75-77	85.56	38.9	63.7	1.63	2.63	1.00	62.0	1.63
10H-4, 75-77	87.06	37.6	60.3	1.65	2.63	1.03	60.8	1.55
10H-5, 74-76	88.55	37.1	59.0	1.67	2.64	1.05	60.3	1.52
10H-6, 65-67	89.96	35.6	55.3	1.69	2.63	1.09	58.7	1.42
11H-1, 75-77	92.06	37.5	59.9	1.66	2.64	1.04	60.7	1.55
11H-2, 75-77	93.56	37.0	58.7	1.67	2.66	1.05	60.4	1.53
11H-3, 75-77	95.06	35.8	55.8	1.75	2.90	1.12	61.2	1.58
11H-4, 75-77	96.56	36.4	57.3	1.67	2.60	1.06	59.2	1.45
11H-5, 75-77	98.06	36.3	57.1	1.67	2.60	1.06	59.2	1.45
11H-6, 75-77	99.56	34.3	52.2	1.71	2.64	1.13	57.4	1.35
12H-1, 75-77	101.56	33.1	49.6	1.74	2.66	1.16	56.3	1.29
12H-2, 75-77	103.06	34.9	53.6	1.69	2.61	1.10	57.8	1.37
12H-3, 75-77	104.56	34.0	51.6	1.72	2.64	1.13	57.1	1.33
12H-4, 75-77	106.06	33.8	51.1	1.73	2.66	1.14	57.0	1.33
12H-5, 75-77	107.56	31.8	46.6	1.76	2.66	1.20	54.7	1.21
12H-6, 75-77	109.06	34.4	52.3	1.72	2.65	1.13	57.5	1.36
13H-1, 75-77	111.06	34.2	51.9	1.72	2.66	1.13	57.4	1.35
13H-2, 75-77	112.56	35.9	55.9	1.69	2.65	1.08	59.1	1.45
13H-3, 75-77	114.06	34.7	53.2	1.71	2.67	1.12	58.1	1.39
13H-4, 75-77	115.56	33.3	50.0	1.72	2.61	1.15	56.0	1.27
13H-5, 75-77	117.06	33.5	50.4	1.73	2.64	1.15	56.5	1.30
13H-6, 75-77	118.56	33.4	50.2	1.73	2.66	1.15	56.6	1.31
14H-1, 75-77	120.56	34.6	52.9	1.71	2.65	1.12	57.8	1.37
14H-2, 75-77	122.06	34.1	51.7	1.71	2.63	1.13	57.0	1.33
14H-3, 75-77	123.56	32.9	49.0	1.74	2.64	1.17	55.8	1.26
14H-4, 75-77	125.06	33.1	49.6	1.73	2.64	1.16	56.1	1.28
14H-5, 75-77	126.56	32.9	49.0	1.74	2.65	1.17	55.9	1.27
14H-6, 75-77	128.06	32.7	48.7	1.73	2.62	1.17	55.5	1.25
15H-1, 75-77	130.06	34.9	53.5	1.70	2.61	1.10	57.7	1.36
15H-2, 75-77	131.56	33.3	50.0	1.73	2.65	1.15	56.4	1.29
15H-3, 75-77	133.06	33.0	49.3	1.74	2.65	1.17	56.1	1.28
15H-4, 75-77	134.56	33.6	50.5	1.72	2.63	1.15	56.5	1.30
15H-5, 75-77	136.06	33.8	50.9	1.72	2.64	1.14	56.8	1.32
15H-6, 72-74	137.53	35.4	54.9	1.70	2.66	1.10	58.8	1.43
16H-1, 75-77	139.56	34.4	52.4	1.71	2.64	1.12	57.5	1.35
16H-2, 75-77	141.06	34.8	53.4	1.70	2.63	1.11	57.9	1.37
16H-3, 75-77	142.56	35.6	55.2	1.69	2.63	1.09	58.7	1.42
16H-4, 75-77	144.06	36.1	56.5	1.69	2.66	1.08	59.4	1.47
16H-5, 75-77	145.56	33.2	49.8	1.73	2.64	1.16	56.2	1.28

Table 25 (continued).

Core, section, interval (cm)	Depth (mbsf)	Water content (total mass wt%)	Water content (solid mass wt%)	Bulk density (g/cm³)	Grain density (g/cm³)	Dry density (g/cm³)	Porosity (%)	Void ratio
16H-6, 75-77	147.06	37.1	58.9	1.69	2.75	1.07	61.2	1.58
17X-1, 78-80	149.09	33.8	51.0	1.72	2.63	1.14	56.7	1.31
17X-2, 66-68	150.47	32.5	48.1	1.75	2.65	1.18	55.5	1.25
17X-3, 68-70	151.99	35.6	55.4	1.70	2.66	1.09	59.0	1.44
17X-4, 65-67	153.46	31.8	46.5	1.75	2.62	1.20	54.4	1.19
17X-5, 66-68	154.97	31.9	46.7	1.76	2.63	1.20	54.6	1.20
17X-6, 71-73	156.52	30.8	44.4	1.77	2.63	1.23	53.3	1.14
18X-1, 79-81	159.00	31.5	46.1	1.77	2.65	1.21	54.4	1.19
18X-2, 75-77	160.46	31.2	45.3	1.76	2.61	1.21	53.6	1.15
18X-3, 81-83	162.02	30.0	42.8	1.79	2.62	1.25	52.3	1.10
18X-4, 65-67	163.36	30.7	44.2	1.78	2.64	1.23	53.2	1.14
18X-5, 70-72	164.91	30.4	43.6	1.79	2.66	1.25	53.1	1.13
18X-6, 78-80	166.49	30.4	43.7	1.78	2.63	1.24	52.9	1.12
19X-1, 77-79	168.58	30.9	44.7	1.78	2.66	1.23	53.7	1.16
19X-2, 95-97	170.26	31.3	45.6	1.77	2.66	1.22	54.2	1.19
19X-3, 66-68	171.47	30.6	44.0	1.79	2.66	1.24	53.4	1.14
19X-4, 63-65	172.94	29.8	42.4	1.79	2.63	1.26	52.1	1.09
19X-5, 61-63	174.42	30.0	42.8	1.79	2.64	1.26	52.5	1.11
19X-6, 88-90	176.19	28.9	40.6	1.82	2.67	1.30	51.4	1.06
20X-1, 71-73	178.12	29.5	41.9	1.81	2.66	1.27	52.1	1.09
20X-2, 56-58	179.47	29.8	42.4	1.79	2.61	1.25	51.9	1.08
20X-3, 70-72	181.11	29.1	41.1	1.80	2.63	1.28	51.3	1.05
20X-4, 59-61	182.50	30.3	43.6	1.78	2.64	1.24	52.9	1.12
20X-5, 81-83	184.22	29.2	41.2	1.81	2.64	1.28	51.6	1.07
20X-6, 42-44	185.33	30.7	44.4	1.77	2.60	1.22	53.0	1.13
21X-1, 80-82	187.81	30.3	43.4	1.79	2.64	1.25	52.8	1.12
21X-2, 78-80	189.29	33.8	51.1	1.72	2.63	1.14	56.7	1.31
21X-3, 75-77	190.76	31.3	45.6	1.77	2.66	1.22	54.2	1.19
21X-4, 73-75	192.24	31.2	45.3	1.76	2.62	1.21	53.6	1.16
21X-5, 73-75	193.74	30.0	42.8	1.79	2.64	1.25	52.5	1.10
21X-6, 78-80	195.29	31.6	46.2	1.75	2.61	1.20	54.1	1.18
22X-1, 77-79	197.38	32.8	48.8	1.74	2.65	1.17	55.8	1.26
22X-2, 76-78	198.87	32.8	48.8	1.73	2.60	1.16	55.3	1.24
22X-3, 77-79	200.38	34.2	51.9	1.71	2.60	1.12	56.9	1.32
22X-4, 75-77	201.86	34.2	51.9	1.72	2.64	1.13	57.2	1.34
23X-1, 74-76	206.95	31.4	45.9	1.76	2.62	1.21	54.0	1.17
23X-2, 83-85	208.54	32.6	48.5	1.73	2.59	1.16	55.1	1.23
23X-3, 70-72	209.91	33.8	51.0	1.72	2.61	1.14	56.6	1.30
23X-4, 75-77	211.46	31.5	46.0	1.77	2.67	1.21	54.5	1.20
23X-5, 67-69	212.88	30.1	43.2	1.80	2.66	1.25	52.8	1.12
23X-6, 69-71	214.40	30.8	44.5	1.76	2.58	1.22	52.8	1.12
24X-1, 86-88	216.67	33.1	49.5	1.72	2.59	1.15	55.6	1.25
24X-2, 73-75	218.04	32.0	47.1	1.75	2.64	1.19	54.8	1.21
24X-3, 73-75	219.54	29.7	42.3	1.80	2.66	1.27	52.4	1.10
24X-4, 86-88	221.17	31.1	45.2	1.75	2.57	1.20	53.1	1.13
24X-5, 77-79	222.58	30.2	43.3	1.78	2.61	1.24	52.4	1.10
24X-6, 88-90	224.19	29.7	42.3	1.80	2.63	1.26	52.1	1.09
25X-1, 81-83	226.22	30.2	43.3	1.78	2.62	1.24	52.6	1.11
25X-2, 72-74	227.63	31.7	46.5	1.74	2.59	1.19	54.0	1.18
25X-3, 83-85	229.24	30.7	44.3	1.77	2.61	1.23	53.0	1.13
25X-4, 72-74	230.63	30.5	44.0	1.77	2.62	1.23	52.9	1.12
25X-5, 77-79	232.18	29.4	41.7	1.81	2.65	1.27	51.9	1.08
25X-6, 71-73	233.62	30.3	43.5	1.76	2.56	1.23	52.1	1.09
26X-1, 80-82	235.81	30.1	43.0	1.78	2.62	1.25	52.3	1.10
26X-2, 78-80	237.29	30.7	44.4	1.77	2.61	1.23	53.1	1.13
26X-3, 75-77	238.76	32.2	47.4	1.74	2.60	1.18	54.7	1.21
26X-4, 75-77	240.26	28.7	40.3	1.81	2.62	1.29	50.8	1.03
26X-5, 79-81	241.80	29.9	42.7	1.78	2.59	1.24	51.9	1.08
26X-6, 75-77	243.26	30.7	44.4	1.78	2.66	1.24	53.5	1.15
27X-1, 78-80	245.39	37.7	60.5	1.62	2.50	1.01	59.7	1.48
27X-2, 81-83	246.92	30.3	43.5	1.76	2.56	1.23	52.0	1.09
27X-3, 88-90	248.49	32.6	48.3	1.73	2.59	1.17	55.0	1.22
27X-4, 87-89	249.98	29.6	42.1	1.79	2.61	1.26	51.8	1.07
27X-5, 73-75	251.34	31.8	46.6	1.75	2.61	1.19	54.3	1.19
27X-6, 73-75	252.84	30.8	44.4	1.76	2.58	1.22	52.8	1.12
28X-1, 76-78	254.97	30.2	43.3	1.77	2.60	1.24	52.3	1.10
28X-2, 81-83	256.52	31.3	45.5	1.76	2.61	1.21	53.7	1.16
28X-3, 73-75	257.94	30.4	43.7	1.78	2.63	1.24	52.9	1.13
28X-4, 76-78	259.47	32.4	48.0	1.74	2.60	1.17	54.9	1.22
28X-5, 74-76	260.95	34.4	52.4	1.70	2.60	1.12	57.1	1.33
28X-6, 77-79	262.48	31.8	46.5	1.76	2.64	1.20	54.5	1.20
29X-1, 67-69	264.48	32.5	48.1	1.73	2.59	1.17	54.9	1.22
29X-2, 72-74	266.03	32.3	47.7	1.72	2.55	1.17	54.2	1.19
29X-3, 74-76	267.55	32.9	49.1	1.72	2.59	1.16	55.4	1.24
29X-4, 79-81	269.10	32.5	48.1	1.73	2.58	1.17	54.8	1.21
29X-5, 69-71	270.50	33.1	49.5	1.72	2.60	1.15	55.7	1.26
29X-6, 75-77	272.06	31.5	46.0	1.74	2.58	1.19	53.7	1.16
30X-1, 75-77	274.16	31.2	45.4	1.75	2.56	1.20	53.2	1.14
30X-2, 75-77	275.66	31.0	44.9	1.76	2.61	1.22	53.3	1.14
30X-3, 59-61	277.00	35.7	55.6	1.67	2.59	1.08	58.4	1.41
30X-4, 19-21	278.10	32.5	48.1	1.73	2.60	1.17	54.9	1.22
30X-5, 48-50	279.89	32.0	47.0	1.74	2.58	1.18	54.2	1.19
32X-1, 71-73	293.32	31.4	45.8	1.75	2.60	1.20	53.8	1.16
32X-2, 72-74	294.83	30.2	43.4	1.78	2.61	1.24	52.5	1.10
32X-3, 72-74	296.33	30.1	43.0	1.77	2.58	1.24	52.0	1.08
32X-4, 72-74	297.83	30.6	44.0	1.77	2.59	1.23	52.7	1.12
32X-5, 88-90	299.49	29.5	41.9	1.79	2.59	1.26	51.4	1.06

Table 25 (continued).

Core, section, interval (cm)	Depth (mbsf)	Water content (total mass wt%)	Water content (solid mass wt%)	Bulk density (g/cm³)	Grain density (g/cm³)	Dry density (g/cm³)	Porosity (%)	Void ratio
33X-1, 62-64	302.83	29.4	41.7	1.79	2.60	1.26	51.4	1.06
33X-2, 83-85	304.54	30.2	43.3	1.77	2.59	1.24	52.3	1.10
33X-3, 56-58	305.77	29.6	42.1	1.79	2.61	1.26	51.8	1.07
33X-4, 42-44	307.13	27.1	37.1	1.85	2.65	1.35	49.0	0.96
34X-1, 52-54	312.33	29.0	40.8	1.81	2.64	1.29	51.2	1.05
34X-2, 74-76	314.05	30.2	43.3	1.77	2.59	1.24	52.3	1.10
34X-3, 75-77	315.56	30.0	42.9	1.79	2.63	1.25	52.4	1.10
34X-4, 74-76	317.05	29.2	41.3	1.81	2.65	1.28	51.6	1.07
34X-5, 87-89	318.68	29.9	42.6	1.79	2.64	1.26	52.3	1.10
34X-6, 90-92	320.21	29.7	42.3	1.79	2.63	1.26	52.0	1.09
35X-1, 69-71	322.20	28.8	40.5	1.81	2.63	1.29	51.0	1.04
35X-2, 60-62	323.61	30.3	43.6	1.78	2.63	1.24	52.8	1.12
35X-3, 74-76	325.25	30.2	43.2	1.79	2.65	1.25	52.7	1.12
35X-4, 70-72	326.71	29.8	42.4	1.78	2.60	1.25	51.9	1.08
35X-5, 72-74	328.23	29.8	42.5	1.78	2.61	1.25	52.0	1.08
35X-6, 61-63	329.62	29.8	42.5	1.79	2.64	1.26	52.2	1.09
36X-1, 50-52	331.61	28.9	40.6	1.80	2.59	1.28	50.7	1.03
36X-2, 73-75	333.34	29.2	41.2	1.81	2.65	1.28	51.6	1.07
36X-3, 76-78	334.87	28.4	39.7	1.82	2.62	1.30	50.4	1.02
36X-4, 81-83	336.42	30.8	44.6	1.76	2.58	1.22	52.9	1.12
36X-5, 46-48	337.57	29.7	42.2	1.79	2.60	1.26	51.8	1.07
36X-6, 94-96	339.55	29.3	41.5	1.80	2.62	1.27	51.5	1.06
37X-1, 77-79	341.48	28.2	39.2	1.82	2.61	1.30	50.0	1.00
37X-2, 78-80	342.99	26.8	36.6	1.88	2.70	1.37	49.1	0.97
37X-3, 86-88	344.57	29.1	41.1	1.80	2.62	1.28	51.2	1.05
37X-4, 143-145	346.64	28.4	39.8	1.81	2.61	1.30	50.4	1.01
38X-1, 87-89	351.28	29.9	42.6	1.77	2.56	1.24	51.6	1.07
38X-2, 64-66	352.55	28.8	40.4	1.81	2.63	1.29	51.0	1.04
38X-3, 87-89	354.28	29.8	42.5	1.78	2.59	1.25	51.8	1.08
38X-4, 88-90	355.79	30.6	44.1	1.75	2.55	1.22	52.3	1.10
38X-5, 91-93	357.32	28.4	39.7	1.82	2.62	1.30	50.4	1.02
38X-6, 118-120	359.09	29.3	41.3	1.79	2.59	1.27	51.1	1.04
39X-1, 75-77	360.86	31.3	45.5	1.75	2.59	1.20	53.5	1.15
39X-2, 69-71	362.30	31.5	46.0	1.75	2.59	1.20	53.8	1.17
39X-3, 75-77	363.86	29.7	42.3	1.79	2.63	1.26	52.1	1.09
39X-4, 73-75	365.34	32.5	48.1	1.73	2.60	1.17	55.0	1.22
39X-5, 74-76	366.85	31.1	45.1	1.78	2.67	1.23	54.0	1.17
39X-6, 78-80	368.39	31.7	46.5	1.74	2.57	1.19	53.8	1.17
40X-1, 78-80	370.49	27.7	38.4	1.82	2.59	1.31	49.2	0.97
40X-2, 73-75	371.94	30.1	43.1	1.77	2.58	1.24	52.1	1.09
40X-3, 73.5-75.5	373.45	27.4	37.7	1.83	2.60	1.33	48.9	0.96
40X-4, 73-75	374.94	25.6	34.4	1.88	2.65	1.40	47.1	0.89
40X-5, 69-71	376.40	27.9	38.7	1.85	2.70	1.34	50.5	1.02
41X-1, 85-87	380.16	38.7	63.2	1.66	2.73	1.02	62.8	1.69
42X-1, 85-87	390.76	36.8	58.3	1.64	2.52	1.04	58.9	1.43
42X-2, 78-80	392.19	33.9	51.2	1.67	2.48	1.11	55.4	1.24
42X-3, 80-82	393.71	31.3	45.6	1.73	2.52	1.19	52.9	1.12
42X-4, 71-73	395.12	34.3	52.1	1.67	2.49	1.10	55.9	1.27
42X-5, 85-87	396.76	32.3	47.7	1.72	2.53	1.16	54.1	1.18
42X-6, 69.5-71.5	398.11	32.6	48.3	1.71	2.53	1.15	54.4	1.19
43X-1, 75-77	400.26	34.4	52.4	1.67	2.51	1.10	56.2	1.28
43X-2, 69-71	401.70	37.0	58.8	1.62	2.47	1.02	58.6	1.42
43X-3, 75-77	403.26	34.8	53.3	1.66	2.49	1.08	56.4	1.29
43X-4, 84-86	404.85	37.0	58.8	1.62	2.46	1.02	58.6	1.41
43X-5, 75-77	406.26	37.1	59.1	1.63	2.51	1.03	59.1	1.45
43X-6, 78-80	407.79	33.8	51.1	1.69	2.51	1.12	55.6	1.25
44X-1, 77-79	409.88	32.5	48.2	1.71	2.53	1.15	54.3	1.19
44X-2, 70-72	411.31	30.0	42.8	1.74	2.49	1.22	51.0	1.04
44X-3, 77-79	412.88	33.2	49.7	1.68	2.47	1.12	54.5	1.20
44X-4, 83-85	414.44	34.2	52.1	1.66	2.44	1.09	55.3	1.24
44X-5, 83-85	415.94	31.6	46.1	1.73	2.54	1.19	53.4	1.14
44X-6, 78-80	417.39	38.1	61.4	1.61	2.49	1.00	59.9	1.50
45X-1, 75-77	419.46	32.0	47.0	1.71	2.51	1.17	53.6	1.15
45X-2, 81-83	421.02	35.6	55.2	1.63	2.43	1.05	56.7	1.31
45X-3, 70-72	422.41	31.5	46.1	1.72	2.49	1.17	52.8	1.12
45X-4, 87-89	424.08	29.4	41.6	1.77	2.53	1.25	50.7	1.03
45X-5, 73-75	425.44	29.8	42.4	1.76	2.54	1.24	51.2	1.05
45X-6, 77-79	426.98	29.8	42.4	1.76	2.53	1.24	51.2	1.05
46X-1, 72-74	429.03	26.5	36.0	1.84	2.58	1.35	47.5	0.91
46X-2, 82-84	430.63	27.0	37.0	1.82	2.57	1.33	48.1	0.93
46X-3, 78-80	432.09	26.8	36.6	1.82	2.55	1.33	47.7	0.91
46X-4, 81-83	433.62	27.5	37.8	1.80	2.53	1.31	48.3	0.93
46X-5, 72-74	435.03	25.2	33.7	1.86	2.56	1.39	45.7	0.84
46X-6, 80.5-82.5	436.62	26.6	36.1	1.84	2.58	1.35	47.6	0.91
47X-1, 78-80	438.69	27.9	38.7	1.80	2.53	1.29	48.9	0.96
47X-2, 71-73	440.12	23.5	30.8	1.91	2.59	1.46	43.8	0.78
47X-3, 65-67	441.56	26.0	35.2	1.83	2.53	1.35	46.5	0.87
47X-4, 77-79	443.18	27.0	37.0	1.83	2.58	1.34	48.3	0.93
47X-5, 75-77	444.66	26.1	35.4	1.85	2.58	1.36	47.2	0.89
47X-6, 75-77	446.16	23.1	30.1	1.91	2.57	1.47	43.0	0.76
48X-1, 102-104	448.53	20.6	26.0	1.97	2.60	1.56	39.7	0.66
48X-2, 96-98	449.97	21.2	27.0	1.94	2.56	1.53	40.3	0.67
48X-3, 67-69	451.18	19.0	23.4	2.01	2.60	1.63	37.3	0.60
48X-4, 76-78	452.77	23.3	30.4	1.89	2.54	1.45	43.0	0.75
48X-5, 86-88	454.37	21.1	26.7	1.95	2.57	1.54	40.1	0.67
48X-6, 38-40	455.39	20.2	25.4	1.99	2.61	1.59	39.3	0.65
49X-1, 78-80	457.89	16.1	19.2	2.09	2.61	1.75	32.8	0.49
49X-2, 45-47	459.06	18.7	23.0	1.99	2.53	1.62	36.2	0.57
50X-1, 85-87	461.06	22.5	29.0	1.91	2.54	1.48	41.8	0.72
50X-2, 80-82	462.51	17.8	21.7	2.04	2.60	1.68	35.5	0.55

Table 25 (continued).

Core, section, interval (cm)	Depth (mbsf)	Water content (total mass wt%)	Water content (solid mass wt%)	Bulk density (g/cm^3)	Grain density (g/cm^3)	Dry density (g/cm^3)	Porosity (%)	Void ratio
50X-3, 79-81	464.00	18.9	23.4	2.01	2.60	1.63	37.2	0.59
50X-4, 75-77	465.46	18.9	23.3	1.99	2.55	1.61	36.7	0.58
51X-1, 66-68	467.47	18.7	23.0	1.99	2.54	1.62	36.3	0.57
51X-3, 75-77	470.56	20.2	25.3	1.98	2.59	1.58	39.0	0.64
51X-5, 83-85	473.64	18.4	22.6	2.01	2.56	1.64	36.1	0.57
52X-1, 119-121	477.70	20.2	25.4	1.97	2.57	1.57	38.9	0.64
52X-4, 74-76	481.75	22.1	28.3	1.92	2.55	1.50	41.4	0.71
52X-6, 76-78	484.77	23.2	30.2	1.87	2.49	1.44	42.3	0.73
53X-1, 63-65	486.74	24.3	32.2	1.85	2.50	1.40	44.0	0.78
53X-3, 88-90	489.99	20.3	25.4	1.96	2.55	1.56	38.7	0.63
53X-5, 60-62	492.71	20.5	25.8	1.93	2.51	1.54	38.7	0.63
54X-2, 72-74	497.93	23.3	30.4	1.88	2.51	1.44	42.8	0.75
54X-3, 74-76	499.45	20.1	25.1	1.95	2.52	1.56	38.3	0.62
54X-5, 69.5-71.5	502.41	15.3	18.1	2.13	2.65	1.80	31.9	0.47
56X-5, 76-78	521.67	18.6	22.9	2.00	2.56	1.63	36.5	0.57
56X-CC, 28-30	524.49	19.2	23.8	2.01	2.61	1.62	37.7	0.61
57X-1, 68.5-70.5	525.20	19.3	23.9	2.00	2.58	1.61	37.6	0.60
57X-3, 71.5-73.5	528.23	21.5	27.4	1.94	2.57	1.52	40.7	0.69
57X-5, 70-72	531.21	22.5	29.0	1.93	2.58	1.49	42.2	0.73
58X-1, 83-85	534.94	18.0	22.0	2.05	2.62	1.68	36.0	0.56
58X-3, 75-77	537.86	20.0	25.1	1.96	2.54	1.57	38.4	0.62
58X-5, 81-83	540.92	22.3	28.6	1.91	2.55	1.49	41.6	0.71
59X-1, 81-83	544.52	24.5	32.4	1.86	2.52	1.40	44.4	0.80
59X-3, 77-79	547.48	22.8	29.5	1.91	2.56	1.48	42.4	0.74
59X-5, 81-83	550.52	22.3	28.7	1.94	2.60	1.51	42.2	0.73
60X-1, 73-75	554.04	19.7	24.5	2.00	2.61	1.61	38.4	0.62
61X-1, 68-70	557.09	15.6	18.5	2.11	2.62	1.78	32.2	0.47
61X-3, 86-88	560.27	17.3	21.0	2.06	2.62	1.70	34.9	0.54
62X-1, 73-75	563.64	21.1	26.8	1.97	2.61	1.55	40.5	0.68
62X-3, 79-81	566.70	17.6	21.3	2.06	2.63	1.70	35.4	0.55
62X-5, 71.5-73.5	569.63	18.8	23.1	2.01	2.58	1.63	36.8	0.58
63X-1, 72-74	573.23	18.7	23.0	2.02	2.61	1.65	36.9	0.59
63X-3, 89-91	576.40	27.4	37.7	1.82	2.56	1.32	48.5	0.94
63X-5, 81-83	579.32	29.3	41.5	1.75	2.49	1.24	50.2	1.01
64X-1, 76-78	582.87	30.2	43.3	1.75	2.53	1.22	51.7	1.07
64X-3, 72-74	585.83	30.5	43.9	1.75	2.53	1.21	52.0	1.08
64X-5, 77-79	588.88	23.9	31.4	1.88	2.56	1.43	44.0	0.79
65X-1, 46-48	592.27	23.7	31.0	1.88	2.54	1.44	43.4	0.77
65X-4, 5-7	596.36	30.6	44.0	1.74	2.50	1.21	51.8	1.07
65X-6, 88-90	600.19	28.6	40.0	1.77	2.50	1.26	49.4	0.98
66X-1, 110-112	602.61	24.2	32.0	1.86	2.53	1.41	44.1	0.79
66X-3, 78-80	605.29	29.1	41.0	1.76	2.49	1.25	49.9	1.00
66X-5, 74-76	608.25	24.7	32.9	1.84	2.50	1.39	44.5	0.80
67X-1, 86-88	611.97	24.0	31.6	1.86	2.50	1.41	43.6	0.77
67X-3, 55-57	614.66	23.6	30.9	1.88	2.52	1.43	43.2	0.76
67X-5, 71-73	617.82	24.4	32.3	1.86	2.52	1.41	44.3	0.80
68X-1, 70-72	621.41	19.5	24.3	1.98	2.55	1.59	37.7	0.61

abrupt spikes (related to the presence of Mn oxide flecks; see "Lithostratigraphy" section, this chapter). The more variable susceptibility values between 110 and 120 mbsf are caused by the proximity to the highly magnetic BHA.

Logging Unit 1 corresponds to the bottom part of lithologic Subunit IC (63.64–119.8 mbsf) and all of Subunit ID (119.8–377.11 mbsf). The relatively low natural gamma-ray counts, bulk density, and PEF values and variable high porosity are consistent with the high carbonate content (~70%−80%) and low clay content of the nannofossil ooze and chalks of lithologic Units I and II (see "Lithostratigraphy" section, this chapter).

The shipboard-processed FMS images (using static normalization; Serra, 1989) of Unit 1 are difficult to interpret because of the low resistivity of the interval. The lower part of Unit 1, however, displays ~1-m-thick, cyclic, light–dark alternations, corresponding to high-to-low fluctuations in microresistivity.

Logging Unit 2 (370–420 mbsf)

Logging Unit 2 is distinguished by an abrupt decrease in average bulk density and PEF values and a slight increase in mean porosity and natural gamma-ray counts (Figs. 49, 50). Log magnetic susceptibility and Earth's conductivity values throughout logging Unit 2 are characterized by a distinct increase in amplitude and frequency of variation (Fig. 52).

Logging Unit 2 corresponds to lithologic Unit II (379.3−381.6 mbsf) and the upper part of Unit III (389.9−534.1 mbsf), an interval of strongly altered porcellanitic smectite clay, porcellanized foraminifer packstone, and siliceous nannofossil chalk to siliceous nannofossil chalk with clay (see "Lithostratigraphy" section, this chapter). This is the only interval in Hole 1051A with chert. The FMS data show an interval of strongly contrasting high- and low-resistivity beds, consistent with the occurrence of clay- and chert-rich intervals. The transition between logging Units 2 and 3 on the standard logs is a bit arbitrary and is based on a slight decrease in the porosity logs at a depth of about 420 mbsf.

Logging Unit 3 (420–565 mbsf)

Logging Unit 3 is characterized by a distinct increase in the amplitude and frequency of variation in resistivity, bulk density, PEF, porosity, and natural gamma-ray values. This unit is also distinguished by the maximum values of magnetic susceptibility, resistivity, and bulk density and by gradually decreasing mean porosity. The natural gamma-ray counts are elevated (>18 GAPI) and are dominated by significant fluctuations in thorium and potassium contents.

Logging Unit 3 corresponds to the middle and lower portions of lithologic Unit III (389.9−534.1 mbsf) (see "Lithostratigraphy" section, this chapter). The maximum gamma-ray counts and relatively low porosity are consistent with the generally low carbonate content
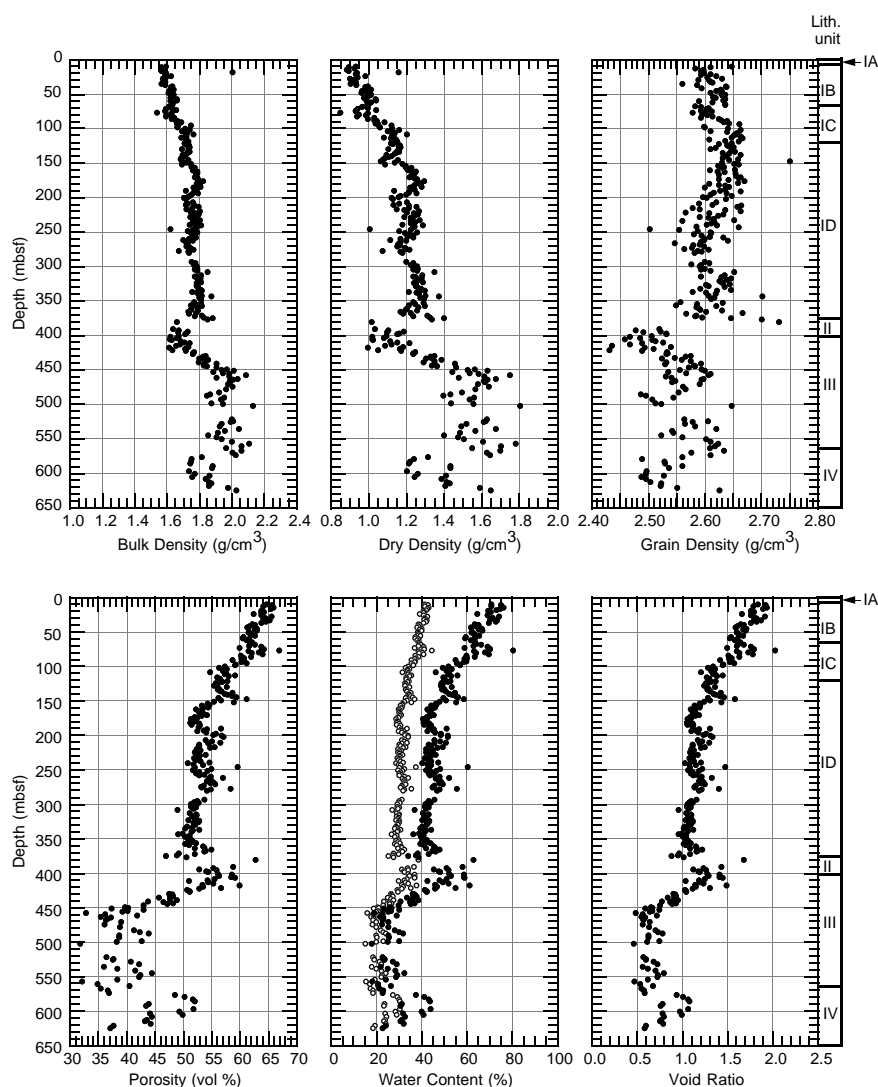
Figure 38. Discrete measurements of bulk density, dry density, grain density, porosity, water content, and void ratio for Hole 1051A. In the water content plot, open circles = values expressed in terms of total mass; solid circles = values expressed in terms of the total mass of solids.

(~50%−60%) (see "Physical Properties" section, this chapter) of the siliceous nannofossil chalks with clay-rich intervals of lithologic Unit III (see "Lithostratigraphy" section, this chapter).

FMS imaging of logging Unit 3 clearly shows three zones of higher resistivity recognized in the geophysical logs, which correspond to the log intervals 460−466, 510−545, and 560−585 mbsf (Fig. 50). These zones are characterized by more abundant, thin, resistive beds (<40 cm in thickness). The FMS images also show that the beds display similar dip and azimuth to those observed in logging Unit 1.

Logging Unit 4 (565−644 mbsf)

The top of logging Unit 4 is marked by a sharp decrease in resistivity and bulk density, increasing porosity and natural gamma-ray values, and a change to more variable and significantly lower magnetic susceptibility values (<200 × 10^{-6} SI; Figs. 50, 52). The Earth's conductivity also shows an abrupt increase in value at the boundary between logging Units 3 and 4. Bulk density remains consistently low (<1.8 g/cm³) throughout logging Unit 4. Mean values of bulk density, resistivity, and PEF gradually increase toward the bottom of the unit, whereas the average porosity value decreases slightly over this interval.

Logging Unit 4 corresponds to lithologic Unit IV, a sequence of predominantly siliceous nannofossil chalks to siliceous claystones or clayey spiculite (see "Lithostratigraphy" section, this chapter). The generally high gamma-ray counts are consistent with the low-carbonate (<60%), clay-rich interval, and the FMS images clearly show the presence of highly resistive siliceous material.

Comparison of Core-Log Physical Properties Data

Comparison of logging data with index and physical properties measured on cores (see "Physical Properties" section, this chapter) shows good agreement. The magnetic susceptibility data are generally of good quality, indicating that there were few measurement errors, and they correlate well with the MST core measurements—particularly in the lower part of the hole (Figs. 53, 54). The core measurements have a higher frequency because the MST has a higher vertical resolution than the GHMT-SUMS tool (see "Explanatory Notes" chapter, this volume). The only significant difference between these two data sets occurs between 560 and 640 mbsf and may be related to elevated bottom-hole temperatures and thermal drift of the measurement coils (Fig. 53). Similarly, the core (GRAPE) and log (RHOB) measurements of sediment bulk density and porosity are

similar over the common depth interval (Fig. 55). The good agreement between log and core porosity indicates that free water (pore space) and molecular-bound water (clays and other minerals) did not significantly affect the log porosity data.

REFERENCES

Berggren, W.A., Kent, D.V., Swisher, C.C., III, and Aubry, M.-P., 1995. A revised Cenozoic geochronology and chronostratigraphy. *In* Berggren, W.A., Kent, D.V., Aubry, M.-P., and Hardenbol, J. (Eds.), *Geochronology, Time Scales and Global Stratigraphic Correlation.* Spec. Publ.—Soc. Econ. Paleontol. Mineral., 54:129−212.

Blome, C.D., 1992. Radiolarians from Leg 122, Exmouth and Wombat Plateaus, Indian Ocean. *In* von Rad, U., Haq, B.U., et al., *Proc. ODP, Sci. Results,* 122: College Station, TX (Ocean Drilling Program), 633−652.

Henderson, J., and Davis, E.E., 1983. An estimate of the heat flow in the western North Atlantic at Deep Sea Drilling Project Site 534. *In* Sheridan, R.E., Gradstein, F.M., et al., *Init. Repts. DSDP,* 76: Washington (U.S. Govt. Printing Office), 719−724.

Ladd, D.D., Foott, R., Ishihara, K., Schlosser, F., and Poulos, H.G., 1977. Stress-deformation and strength characteristics: state-of-the-art report. *Proc. 9th Int. Conf. Soil Mechanics Foundation Engineering,* Tokyo, 2:421−482.

Nishimura, A., 1992. Paleocene radiolarian biostratigraphy in the northwest Atlantic at Site 384, Leg 43, of the Deep Sea Drilling Project. *Micropaleontology,* 38:317−362.

Quirein, J.A., Gardner, J.S., and Watson, J.T., 1982. Combined natural gamma-ray spectral/litho-density measurements applied to complex lithology. *SPE of AIME, 57th Annual Fall Technical Conf. and Exhibit.,* New Orleans, paper SPE 11143.

Rashid, M.A. (Ed.), 1985. *Geochemistry of Marine Humic Compounds:* Berlin (Springer-Verlag).

Riedel, W.R., and Sanfilippo, A., 1978. Stratigraphy and evolution of tropical Cenozoic radiolarians. *Micropaleontology,* 24:61−96.

Ruppell, C., Von Herzen, R.P., and Bonneville, A, 1995. Heat flux through an old (~175 Ma) passive margin: offshore southeastern United States. *J. Geophys. Res.,* 100:20037−20057.

Serra, O., 1989. *Formation MicroScanner Image Interpretation:* Houston (Schlumberger Educ. Services), SMP-7028.

Tjalsma, R.C., and Lohmann, G.P., 1983. Paleocene-Eocene bathyal and abyssal benthic foraminifera from the Atlantic Ocean. *Micropaleontol. Spec. Publ.,* 4.

van Morkhoven, F.P.C.M., Berggren, W.A., and Edwards, A.S., 1986. Cenozoic cosmopolitan deep-water benthic foraminifera. *Bull. Cent. Rech. Explor.—Prod. Elf-Aquitaine,* Mem. 11.

Ms 171BIR-105
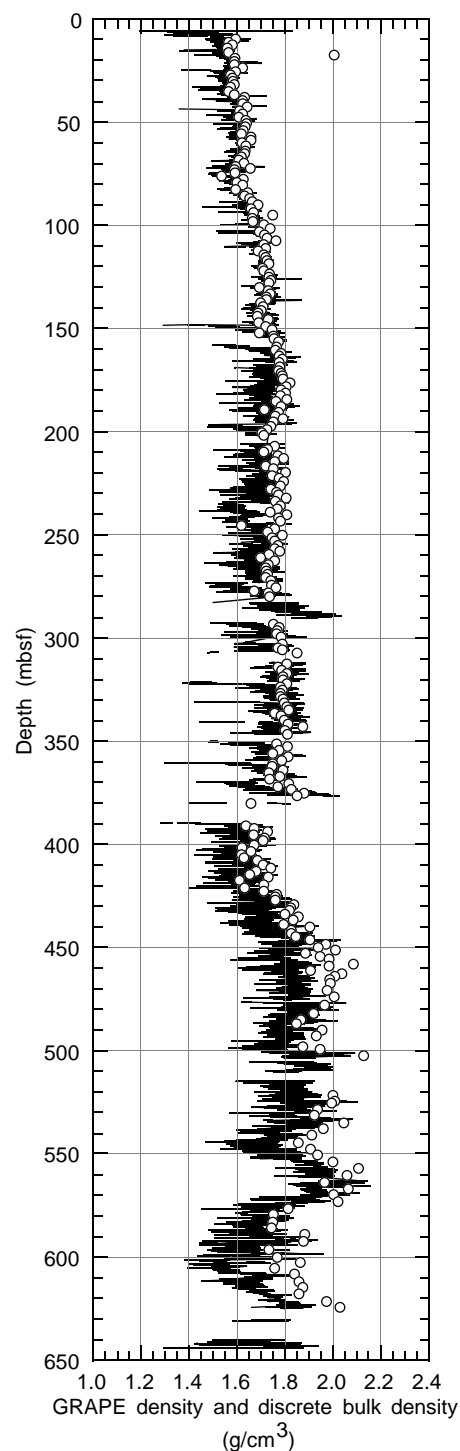
Figure 39. Comparison of GRAPE bulk density (line) with discrete measurements of bulk density (open circles) for Hole 1051A.

NOTE: Core description forms ("barrel sheets") and core photographs can be found in Section 4, beginning on page 363. Forms containing smear-slide data and shore-based log processing data can be found on CD-ROM. See Table of Contents for material contained on CD-ROM.

Table 26. Discrete measurements of uncorrected *P*-wave velocity for Hole 1051A.

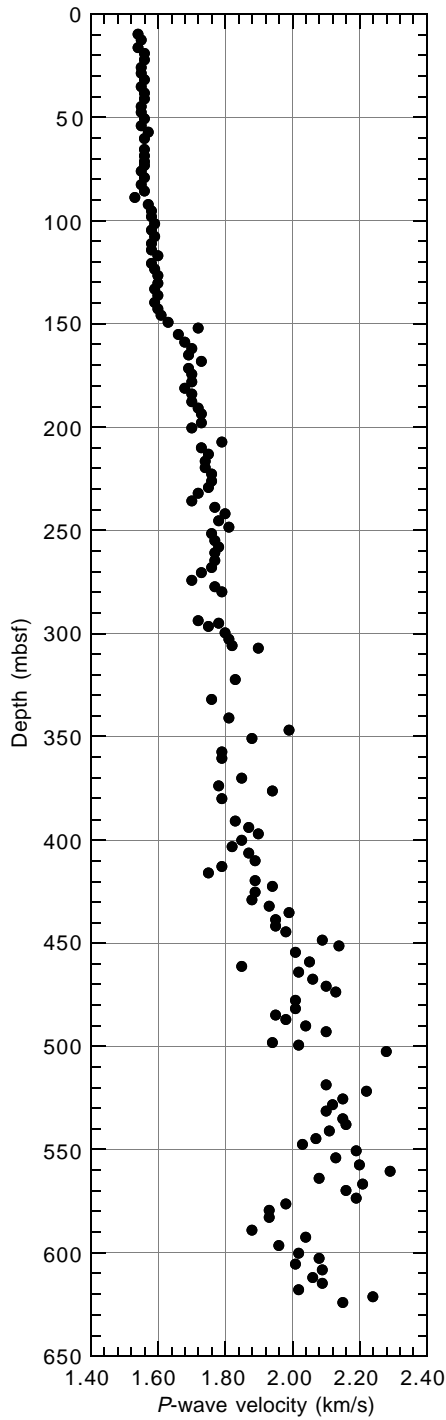| Core, section, interval (cm)	Depth (mbsf)	*P*-wave velocity (m/s)	Core, section, interval (cm)	Depth (mbsf)	*P*-wave velocity (m/s)
171B-1051A-			32X-2, 69.7-71.7	294.80	1784.6
2H-3, 82.4-84.4	9.62	1541.4	32X-5, 88.7-90.7	299.49	1797.8
2H-5, 74.1-76.1	12.54	1548.6	32X-3, 72-74	296.32	1746.3
3H-1, 74.1-76.1	16.04	1543.4	33X-1, 62-64	302.82	1812.8
3H-3, 74.2-76.2	19.04	1560.9	33X-3, 56-58	305.76	1820.5
3H-5, 74-76	22.04	1561.2	33X-4, 42-44	307.12	1898.2
4H-1, 74-76	25.54	1552.4	35X-1, 69-71	322.19	1833.2
4H-3, 74.2-76.2	28.54	1554.9	36X-1, 54.3-56.3	331.64	1764.3
4H-5, 74-76	31.54	1555.0	37X-1, 25.2-27.2	340.95	1809.7
5H-1, 74-76	35.04	1551.9	37X-4, 131.4-133.4	346.51	1986.9
5H-3, 74-76	38.04	1559.4	38X-1, 21.5-23.5	350.62	1884.1
5H-5, 72-74	41.02	1558.9	38X-5, 106.1-108.1	357.46	1788.0
6H-1, 74-76	44.54	1550.4	39X-1, 23.9-25.9	360.34	1794.6
6H-3, 75.2-77.2	47.55	1554.2	40X-1, 20.1-22.1	369.90	1851.0
6H-5, 74-76	50.54	1563.4	40X-3, 84.9-86.9	373.55	1778.2
7H-1, 74-76	54.04	1553.3	40X-5, 61.3-63.3	376.31	1939.9
7H-3, 71-73	57.01	1566.0	41X-1, 65.3-67.3	379.95	1792.2
7H-5, 74-76	60.04	1555.5	42X-1, 82.6-84.6	390.73	1825.9
8H-3, 74-76	65.33	1557.2	42X-3, 77.5-79.5	393.68	1872.5
8H-5, 74-76	68.33	1555.7	42X-5, 81.8-83.8	396.72	1901.7
8H-7, 75-77	71.34	1559.7	43X-1, 69.3-71.3	400.19	1853.2
9H-1, 74-76	73.04	1561.2	43X-3, 61.9-63.9	403.12	1815.0
9H-3, 74.1-76.1	76.04	1549.6	43X-5, 83.5-85.5	406.34	1874.4
9H-5, 67-69	78.97	1558.3	44X-1, 74.1-76.1	409.84	1888.8
10H-1, 74.1-76.1	82.54	1553.9	44X-3, 61.7-63.7	412.72	1787.4
10H-3, 74-76	85.54	1564.0	44X-5, 88-90	415.98	1746.3
10H-5, 74-76	88.54	1525.7	45X-1, 83-85	419.53	1891.7
11H-1, 74.1-76.1	92.04	1570.3	45X-3, 74.1-76.1	422.44	1942.0
11H-3, 74-76	95.04	1580.7	45X-5, 54.1-56.1	425.24	1885.2
11H-5, 74-76	98.04	1584.1	46X-1, 69.9-71.9	429.00	1875.2
12H-1, 74.1-76.1	101.54	1594.0	46X-3, 69.8-71.8	432.00	1933.9
12H-3, 74-76	104.54	1580.8	46X-5, 74.2-76.2	435.04	1988.3
12H-5, 69.5-71.5	107.50	1591.2	47X-1, 73.8-75.8	438.64	1948.4
13H-1, 74-76	111.04	1581.7	47X-3, 74.9-76.9	441.65	1953.8
13H-3, 74-76	114.04	1579.7	47X-5, 58.3-60.3	444.48	1976.5
13H-5, 74-76	117.04	1601.1	48X-1, 102-104	448.52	2089.3
14H-1, 74-76	120.54	1579.8	48X-3, 67-69	451.17	2137.0
14H-3, 74-76	123.54	1592.0	48X-5, 86-88	454.36	2013.5
14H-5, 74-76	126.54	1599.8	49X-1, 78-80	457.88	2495.0
15H-1, 74-76	130.04	1604.4	49X-2, 45-47	459.05	2045.1
15H-3, 74-76	133.04	1590.4	50X-1, 85-87	461.05	1848.1
15H-5, 74-76	136.04	1596.2	50X-3, 79-81	463.99	2016.8
16H-1, 74-76	139.54	1587.1	51X-1, 66-68	467.46	2062.5
16H-3, 74-76	142.54	1603.9	51X-3, 75-77	470.55	2103.2
16H-5, 74-76	145.54	1609.4	51X-5, 83-85	473.63	2128.7
17X-1, 77.3-79.3	149.07	1631.3	52X-1, 119-121	477.69	2008.3
17X-3, 74-76	152.04	1716.9	52X-4, 74-76	481.74	2011.0
17X-5, 72.9-74.9	155.03	1661.7	52X-6, 76-78	484.76	1952.3
18X-1, 43-45	158.63	1676.7	53X-1, 74-76	486.73	1981.4
18X-3, 79.9-81.9	162.00	1698.9	53X-3, 88-90	489.98	2035.1
18X-5, 70.1-72.1	164.90	1688.0	53X-5, 60-62	492.7	2099.4
19X-1, 22.9-24.9	168.03	1726.8	54X-2, 83.4-85.4	498.03	1938.2
19X-3, 66.5-68.5	171.47	1693.1	54X-3, 73.4-75.4	499.43	2022.6
19X-5, 60.6-62.6	174.41	1702.8	54X-5, 79.4-81.4	502.49	2275.8
20X-1, 73.1-75.1	178.13	1701.5	56X-3, 73.9-75.9	518.64	2099.8
20X-3, 75.1-77.1	181.15	1680.8	56X-5, 74.3-76.3	521.64	2221.8
20X-5, 56-58	183.96	1699.9	57X-1, 74.1-76.1	525.24	2146.7
21X-1, 56.1-58.1	187.56	1696.4	57X-3, 77-79	528.27	2116.9
21X-3, 67-69	190.67	1721.6	57X-5, 75-77	531.25	2098.2
21X-5, 56.4-58.4	193.56	1731.7	58X-1, 74-76	534.84	2146.7
22X-1, 119.3-121.3	197.79	1733.1	58X-3, 70-72	537.80	2164.0
22X-3, 63.8-65.8	200.24	1703.0	58X-5, 74.1-76.1	540.84	2114.0
23X-1, 77.6-79.6	206.98	1790.0	59X-1, 74-76	544.44	2070.8
23X-3, 74-76	209.94	1729.8	59X-3, 74.1-76.1	547.44	2026.7
23X-5, 71.9-73.9	212.92	1745.5	59X-5, 74-76	550.44	2193.2
24X-1, 50.2-52.2	216.30	1737.1	60X-1, 72.3-74.3	554.02	2132.5
24X-3, 69.4-71.4	219.49	1735.1	61X-1, 73.7-75.7	557.14	2200.5
24X-5, 80.4-82.4	222.60	1756.6	61X-3, 91.4-93.4	560.31	2285.2
25X-1, 67.8-69.8	226.08	1760.6	62X-1, 80.7-82.7	563.71	2083.0
25X-3, 90.5-92.5	229.31	1745.0	62X-3, 73.2-75.2	566.63	2213.2
25X-5, 71.2-73.2	232.11	1719.3	62X-5, 74-76	569.64	2162.2
26X-1, 74-76	235.74	1703.0	63X-1, 78.5-80.5	573.29	2191.8
26X-3, 88.1-90.1	238.88	1774.9	63X-3, 74.3-76.3	576.24	1977.3
26X-5, 79.6-81.6	241.80	1798.4	63X-5, 68.9-70.9	579.19	1930.0
27X-1, 70.3-72.3	245.30	1777.9	64X-1, 64.9-66.9	582.75	1934.5
27X-3, 78-80	248.38	1809.8	64X-5, 80.1-82.1	588.90	1878.6
27X-5, 77.1-79.1	251.37	1761.5	65X-1, 46-48	592.26	2038.3
28X-1, 80.9-82.9	255.01	1765.5	65X-4, 5-7	596.35	1955.9
28X-3, 79.3-81.3	257.99	1783.4	65X-6, 89-91	600.19	2015.7
28X-5, 83.3-85.3	261.03	1771.3	66X-1, 110-112	602.60	2083.1
29X-1, 77.3-79.3	264.57	1768.9	66X-3, 78-80	605.28	2009.3
29X-3, 106.2-108.2	267.86	1758.0	66X-5, 75-77	608.25	2089.5
29X-5, 72.3-74.3	270.52	1731.9	67X-1, 86-88	611.96	2055.9
30X-1, 84.5-86.5	274.25	1701.6	67X-3, 55-57	614.65	2085.7
30X-3, 62.7-64.7	277.03	1773.9	67X-5, 71-73	617.81	2024.8
30X-5, 27.3-29.3	279.67	1793.2	68X-1, 70-72	621.40	2241.3
32X-1, 120.1-122.1	293.80	1718.3	68X-3, 45-47	624.15	2149.2

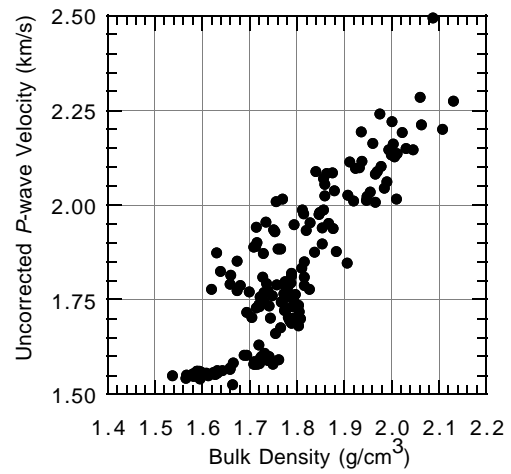Figure 40. Discrete *P*-wave velocity for Hole 1051A.

Figure 41. Comparison of discrete *P*-wave velocity and discrete bulk density for Hole 1051A. The *P*-wave velocity values are uncorrected for in situ pressure and temperature conditions.

Table 27. Discrete measurements of shear strength for Hole 1051A.

Core, section, interval (cm)	Depth (mbsf)	Peak (kPa)	Residual (kPa)	Penetrometer (kPa)
171B-1051A-				
2H-3, 63.5-64.5	9.44	19.44		
2H-5, 68.6-69.6	12.49	49.22	18.64	
3H-1, 79.3-80.3	16.10	29.16	13.33	
3H-3, 67.7-68.7	18.98	34.59	12.92	
3H-5, 78.1-79.1	22.09	55.18	16.83	
4H-1, 78.2-79.2	25.59	34.12	16.72	
4H-3, 78.2-79.2	28.59	34.64	16.05	
4H-5, 70.3-71.3	31.51	51.25	18.62	
5H-1, 78.4-79.4	35.09	31.45	14.75	
5H-3, 78.7-79.7	38.09	14.48	6.27	
5H-5, 67.5-68.5	40.98	35.08	15.67	
6H-1, 80.2-81.2	44.61	25.43	19.95	
6H-3, 74-75	47.55	47.23	20.68	
6H-5, 77.4-78.4	50.58	81.50	36.13	
7H-1, 77.1-78.1	54.08	39.29	18.86	
7H-3, 74.5-75.5	57.05	48.38	23.71	
7H-5, 77.4-78.4	60.08	58.34	28.59	
8H-3, 77.6-78.6	65.37	42.21	18.61	
8H-5, 77.5-78.5	68.37	62.12	22.16	
8H-7, 78.6-79.6	71.38	47.40	19.12	
9H-1, 77.3-78.3	73.08	25.22	12.44	
9H-3, 77.2-78.2	76.08	40.04	13.22	
9H-5, 77.5-78.5	79.08	34.96	14.57	
10H-1, 80.2-81.2	82.61	33.77	15.53	
10H-3, 77.8-78.8	85.58	26.65	12.83	
10H-5, 77.7-78.7	88.58	46.97	19.10	
11H-1, 77.8-78.8	92.08	24.03	9.53	
11H-3, 77.5-78.5	95.08	26.73	12.74	
11H-5, 78.1-79.1	98.09	47.19	18.25	
12H-1, 78.3-79.3	101.59	64.83	25.93	
12H-3, 79.1-80.1	104.60	65.80	30.93	88.3
12H-5, 73.4-74.4	107.54	43.51	14.94	
13H-1, 77.6-78.6	111.08	40.26	15.30	83.4
13H-3, 77.7-78.7	114.08	37.34	15.43	73.6
13H-5, 78.1-79.1	117.09	60.61	27.88	115.2
14H-1, 77.9-78.9	120.58	41.24	18.56	78.5
14H-3, 77.8-78.8	123.58	43.83	23.38	61.3
14H-5, 77.4-78.4	126.58	65.70	28.07	110.3
15H-1, 78.1-79.1	130.09	21.10	11.54	36.8
15H-3, 80-81	133.11	31.93	18.94	68.6
15H-5, 77.6-78.6	136.08	50.87	22.04	79.4
16H-1, 77.7-78.7	139.58	66.13	35.27	122.6
16H-3, 78.4-79.4	142.59	25.76	13.14	36.8
16H-5, 77.7-78.7	145.58	110.39	75.80	107.9
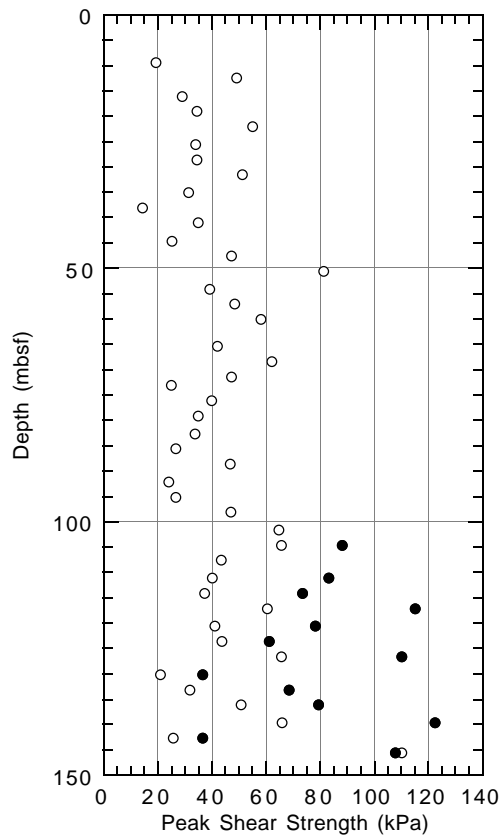
Figure 42. Shear strength for Hole 1051A. The open circles = vane-shear device measurements; the solid circles = pocket penetrometer measurements.
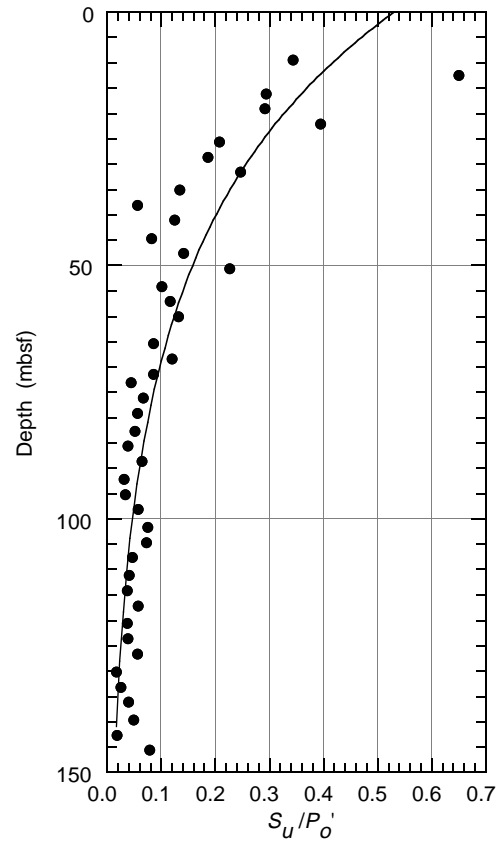
Figure 43. S_u/P_0' for Hole 1051A. The S_u/P_0' values are calculated from bulk density and undrained shear strength data (see "Physical Properties" section [this chapter] for further details). The line is a logarithmic fit to the data.

Table 28. Discrete measurements of resistivity for Hole 1051A.

Core, section, interval (cm)	Depth (mbsf)	Longitudinal resistivity (Ωm)	Transverse resistivity (Ωm)
171B-1051A-			
2H-3, 79.5-82.5	9.61	0.4040	0.4994
2H-5, 76.5-79.5	12.58	0.4127	0.4001
3H-1, 81.5-84.5	16.13	0.4358	0.4117
3H-3, 60.5-63.5	18.92	0.4923	0.4549
3H-5, 81.5-84.5	22.13	0.4485	0.4360
4H-1, 81.5-84.5	25.63	0.4413	0.4260
4H-3, 80.5-83.5	28.62	0.4735	0.4469
4H-5, 76.5-79.5	31.58	0.4731	0.4497
5H-1, 81.5-84.5	35.13	0.4212	0.4106
5H-3, 81.5-84.5	38.13	0.4380	0.4190
5H-5, 78.5-81.5	41.10	0.4332	0.4510
6H-1, 82.5-85.5	44.64	0.4695	0.4592
6H-3, 82-85	47.64	0.4406	0.4417
6H-5, 81.5-84.5	50.63	0.4758	0.4719
7H-1, 81.5-84.5	54.13	0.4456	0.4504
7H-3, 64.5-67.5	56.96	0.4623	0.4572
7H-5, 81.5-84.5	60.13	0.4565	0.4612
8H-3, 82-85	65.43	0.4563	0.4588
8H-5, 80.5-83.5	68.41	0.4482	0.4537
8H-7, 71-74	71.32	0.4854	0.4732
9H-1, 81-84	73.13	0.4151	0.4125
9H-3, 81-84	76.13	0.4420	0.4439
9H-5, 76-79	79.08	0.4573	0.4490
10H-1, 84.5-87.5	82.66	0.4299	0.4274
10H-3, 81-84	85.63	0.4268	0.4441
10H-5, 81.5-84.5	88.63	0.4702	0.4836
11H-1, 82-85	92.14	0.4942	0.4815
11H-3, 81.5-84.5	95.13	0.4733	0.4646
11H-5, 82-85	98.14	0.4977	0.4868
12H-1, 83-86	101.65	0.5448	0.5323
12H-3, 81-84	104.63	0.6343	0.6761
12H-5, 76.5-79.5	107.58	0.6447	0.5567
13H-1, 80.5-83.5	111.12	0.5126	0.5076
13H-3, 82-85	114.14	0.4991	0.5171
13H-5, 81.5-84.5	117.13	0.5136	0.5292
14H-1, 81.5-84.5	120.63	0.5038	0.5132
14H-3, 80.5-83.5	123.62	0.5268	0.5377
14H-5, 81.5-84.5	126.63	0.5481	0.5348
15H-1, 81.5-84.5	130.13	0.5268	0.4877
15H-3, 81.5-84.5	133.13	0.5268	0.5217
15H-5, 81.5-84.5	136.13	0.5598	0.5186
16H-1, 81.5-84.5	139.63	0.5523	0.5143
16H-3, 81.5-84.5	142.63	0.5110	0.4957
16H-5, 81.5-84.5	145.63	0.5784	0.5504
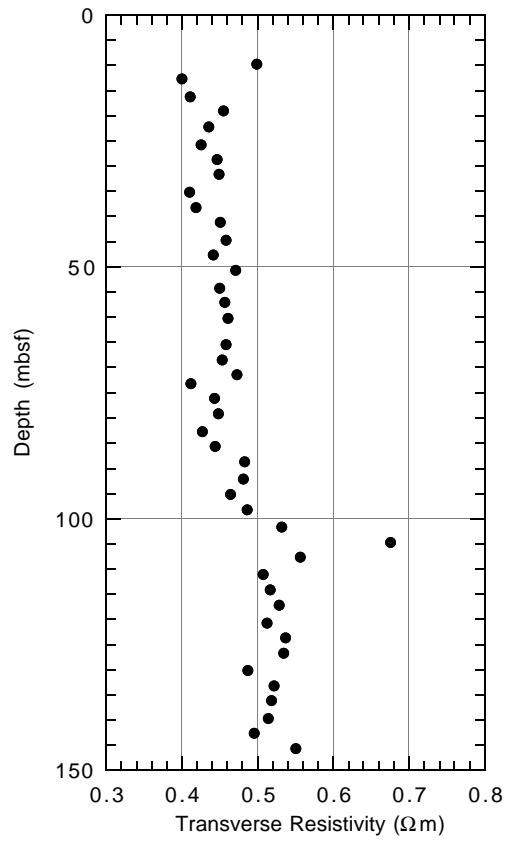
Figure 44. Sediment resistivity for Hole 1051A. Transverse resistivity measurements are considered more reliable than longitudinal measurements because planar unloading cracks that are perpendicular to the core axis bias longitudinal resistivity measurements to higher values.
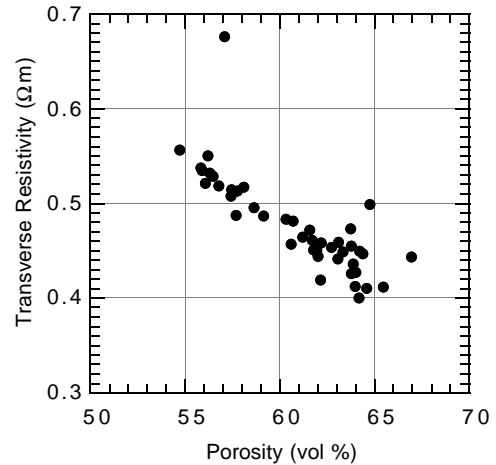
Figure 45. Comparison of transverse resistivity and sediment porosity for Hole 1051A.
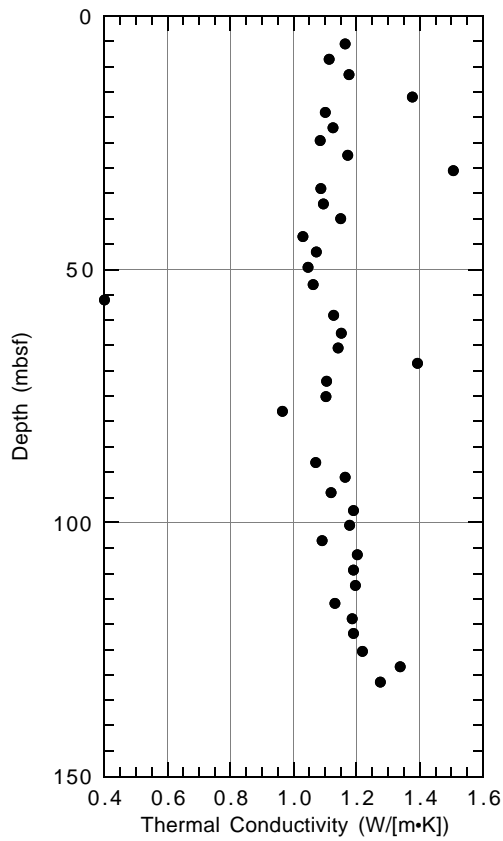
Figure 46. Thermal conductivity for Hole 1051A.

Table 29. Discrete measurements of thermal conductivity for Hole 1051A.

Core, section, interval (cm)	Depth (mbsf)	Thermal conductivity (W/[m·K])
171B-1051A-		
2H-1, 72-74	5.52	1.17
2H-3, 70-72	8.50	1.11
2H-5, 70-72	11.50	1.18
3H-2, 69-71	15.99	1.38
3H-4, 69-71	18.99	1.10
3H-6, 69-71	21.99	1.13
4H-1, 69-71	24.49	1.09
4H-3, 69-71	27.49	1.17
4H-5, 69-71	30.49	1.51
5H-1, 69-71	33.99	1.09
5H-3, 69-71	36.99	1.10
5H-5, 69-71	39.99	1.15
6H-1, 69-71	43.49	1.03
6H-3, 69-71	46.49	1.07
6H-5, 69-71	49.49	1.05
7H-1, 69-71	52.99	1.06
7H-3, 69-71	55.99	0.40
7H-5, 69-71	58.99	1.13
8H-1, 69-71	62.49	1.15
8H-3, 69-71	65.49	1.14
8H-5, 69-71	68.49	1.40
9H-1, 69-71	71.99	1.11
9H-3, 69-71	74.99	1.10
9H-5, 69-71	77.99	0.97
11H-1, 69-71	87.99	1.07
11H-3, 69-71	90.99	1.16
11H-5, 69-71	93.99	1.12
12H-1, 69-71	97.49	1.19
12H-3, 69-71	100.49	1.18
12H-5, 69-71	103.49	1.09
13H-1, 69-71	106.31	1.20
13H-3, 69-71	109.31	1.19
13H-5, 69-71	112.31	1.20
14H-1, 69-71	115.81	1.13
14H-3, 69-71	118.81	1.19
14H-5, 69-71	121.81	1.19
15H-1, 69-71	125.31	1.22
15H-3, 69-71	128.31	1.34
15H-5, 69-71	131.31	1.28

171-1051B-4H, 33.3 mbsf: 3.42 °C

Table 30. In situ Adara temperature tool measurements in Hole 1051B.

Depth (mbsf)	Bottom water temperature (°C)	Sediment temperature (°C)
0	3.717	
33.3		3.419
61.8		3.471
87.3		4.144
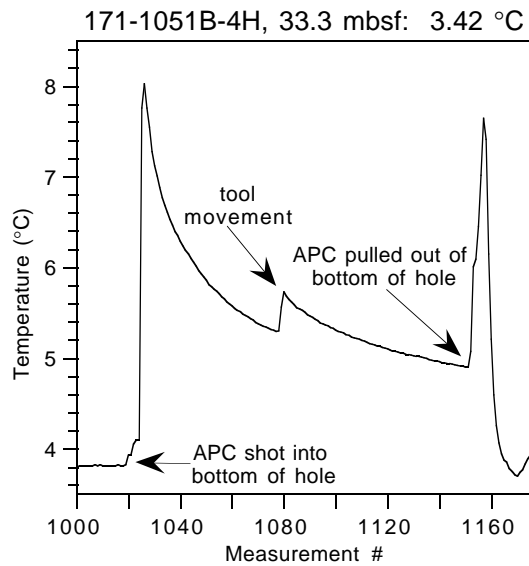
Figure 47. A time-temperature plot of one of the three Adara measurements taken in Hole 1051B. Slight tool movement during this measurement caused only a small difference in computed equilibrium temperatures between the first and second decay curves. The equilibrium temperature for the second curve is reported in Table 30.
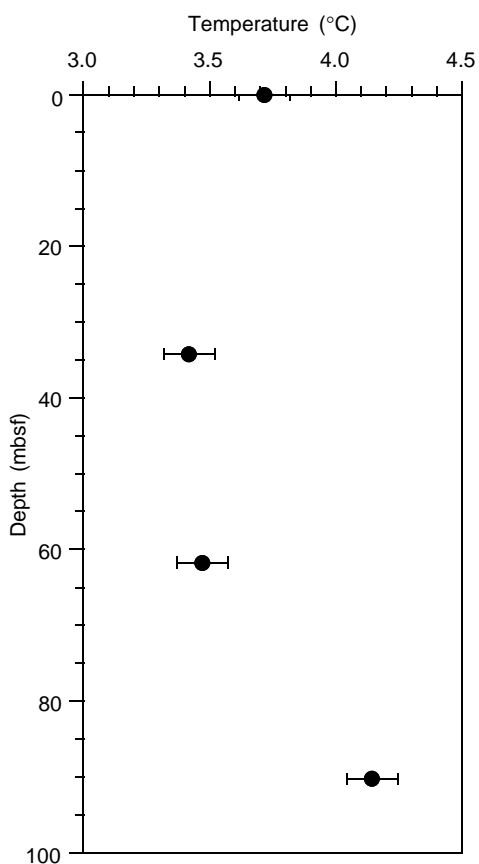
Temperature (°C)

Figure 48. In situ temperature for Hole 1051B. Error bars show the nominal accuracy associated with the Adara temperature measurements (±0.1°C).

Table 31. Estimated heat flow for Hole 1051B.

Temperature measurements used in regression (depths in mbsf)	Geothermal gradient (°C/km)	Heat flow (mW/m²)
0, 33.3, 61.8, 87.3	4.2	4.8
33.3, 61.8, 87.3	13.0	14.8
61.8, 87.3	26.4	30.0

Table 32. Logging operations in Hole 1051.

Time	Operations
26 January 1997	
21:00	Triple combo assembled and prepared for logging.
22:30	Run in hole with triple combo.
0:00	Begin logging first upward pass (644-0 mbsf). Pull pipe up to 146 mbsf. Log 100 m repeat section (456-356 mbsf).
3:00	Triple combo pulled out of drill string.
4:00	Triple combo disassembled and removed from rig floor.
4:30	FMS assembled and prepared for logging. SDT not run.
12:00	Run in hole with FMS.
13:40	Begin logging first upward pass (645.7-126.8 mbsf). Complete second logging run (644.5-130.7 mbsf).
27 January 1997	
19:00	FMS disassembled and removed from rig floor.
19:15	GHMT assembled and prepared for logging.
19:30	Run in hole with GHMT.
20:00	Begin logging first upward pass (638-124.8 mbsf). Log 2 repeat sections (389-360.9 mbsf and 206-175.3 mbsf).
00:00	GHMT disassembled and removed from rig floor.

Notes: Drillers total depth = 2363.6 mbrf (644.6 mbsf). Water depth = 1994 mbrf.
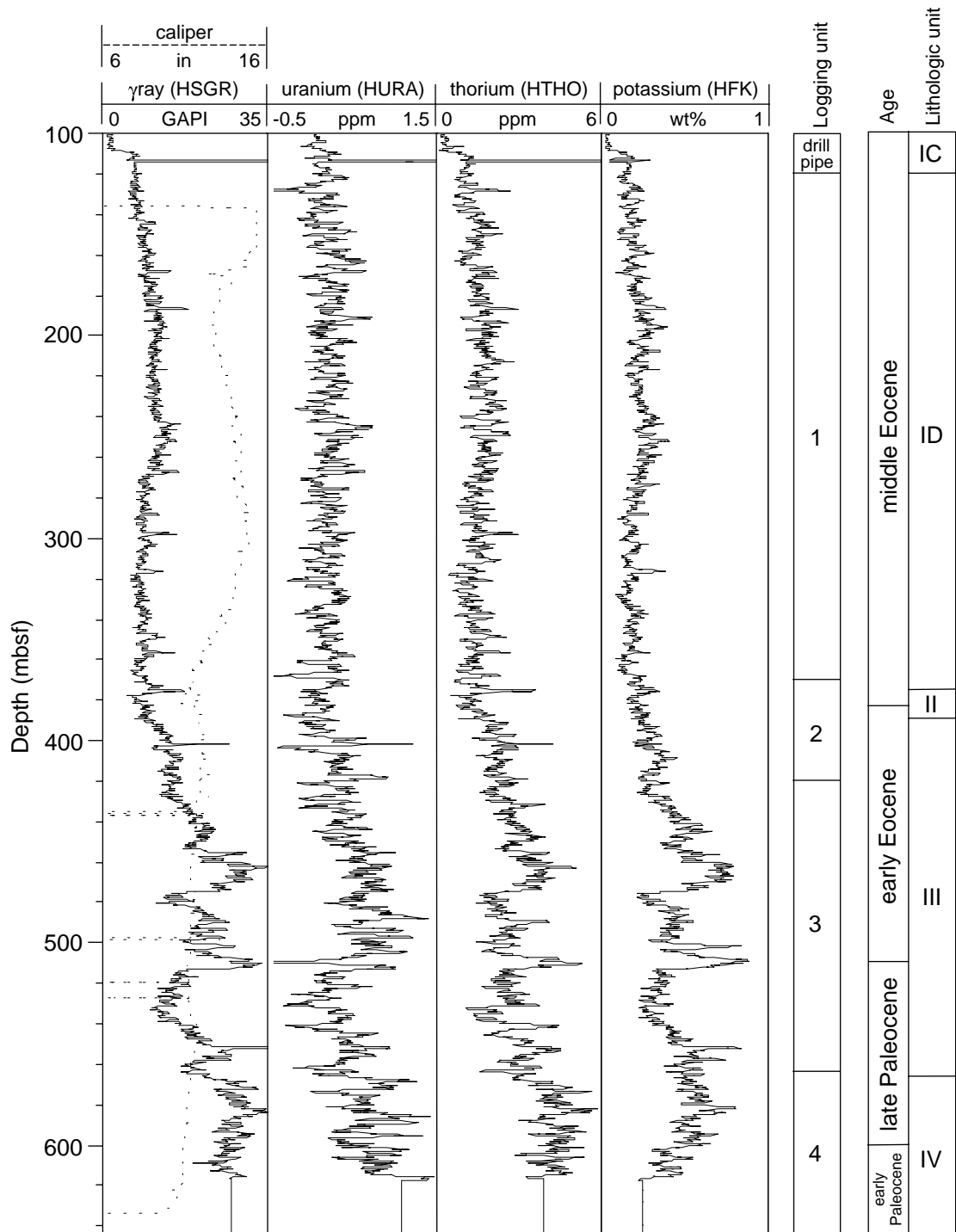
Figure 49. Spectral natural gamma-ray results from the triple-combo tool string for the interval 100–644 mbsf and a lithologic summary column for Hole 1051A (see "Lithostratigraphy" section, this chapter).
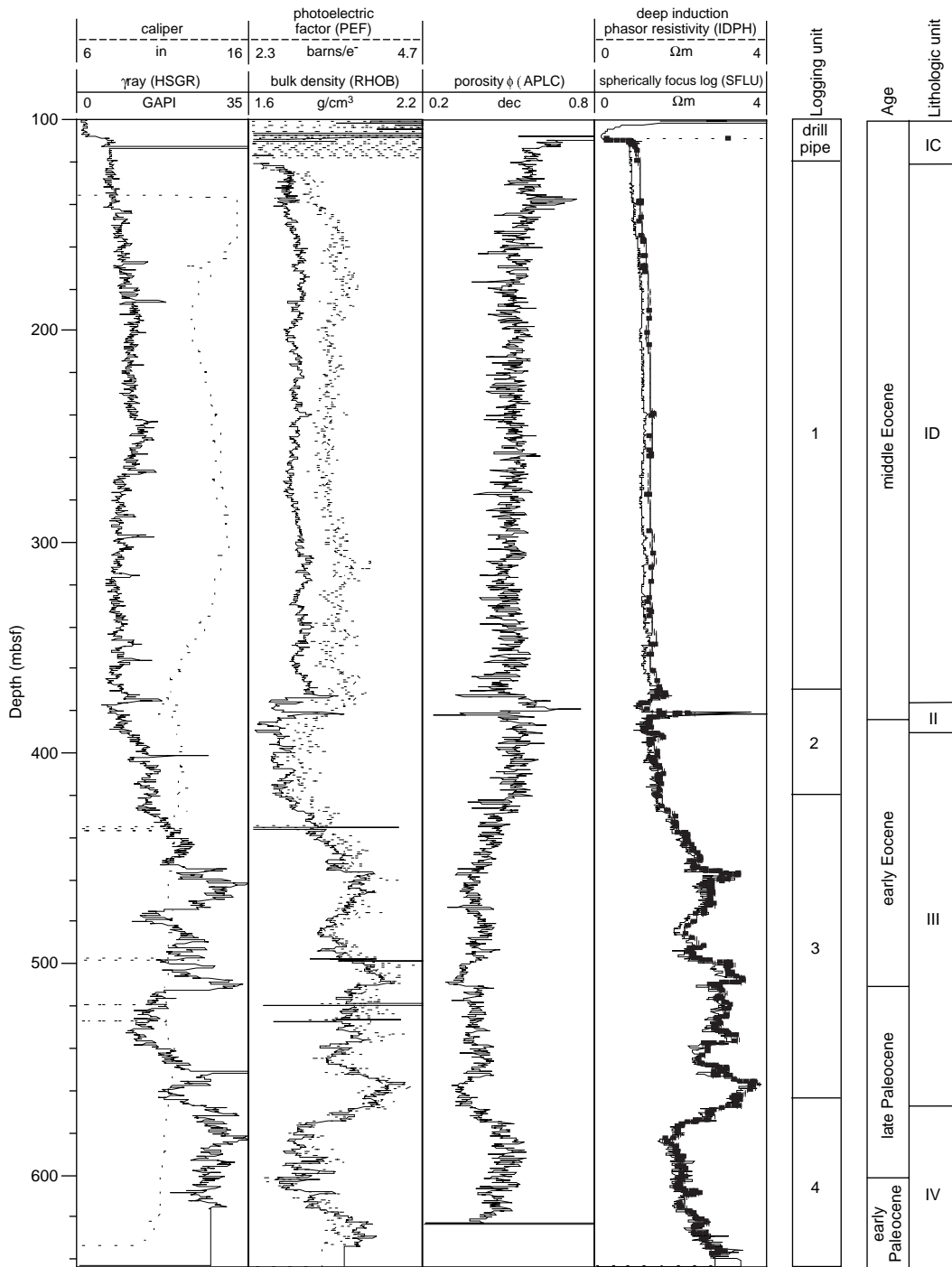
Figure 50. Summary of key geophysical logs acquired with the triple-combo tool string. From left to right, the tracks are the natural gamma ray and caliper, bulk density (RHOB), photoelectric effect (PEF), porosity (APLC), and shallow (SFLU) and deep resistivity (IDPH). The logging units are discussed in the "Downhole Logging" section (this chapter); the lithologic units are discussed in the "Lithostratigraphy" section (this chapter).

A

110-370 mbsf

B
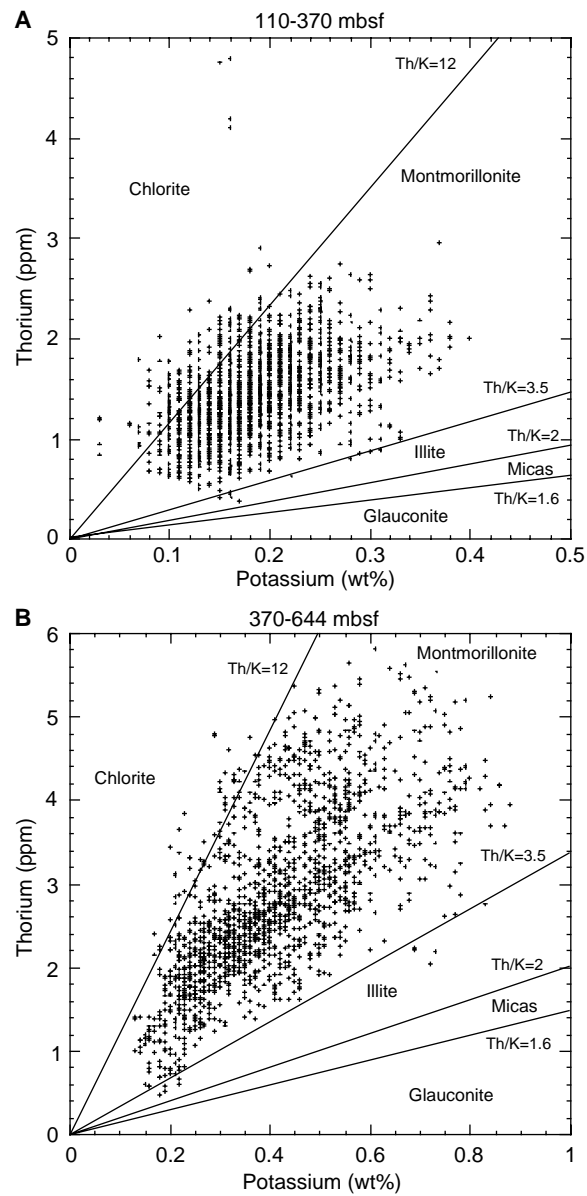
370-644 mbsf

Figure 51. Identification of clay minerals as a function of thorium and potassium concentrations within two different depth intervals in Hole 1051A, as recorded by the natural gamma-ray spectrometry tool (HNGS). **A.** 110–370 mbsf. **B.** 370–644 mbsf. Graph modified after Quirein et al. (1982).
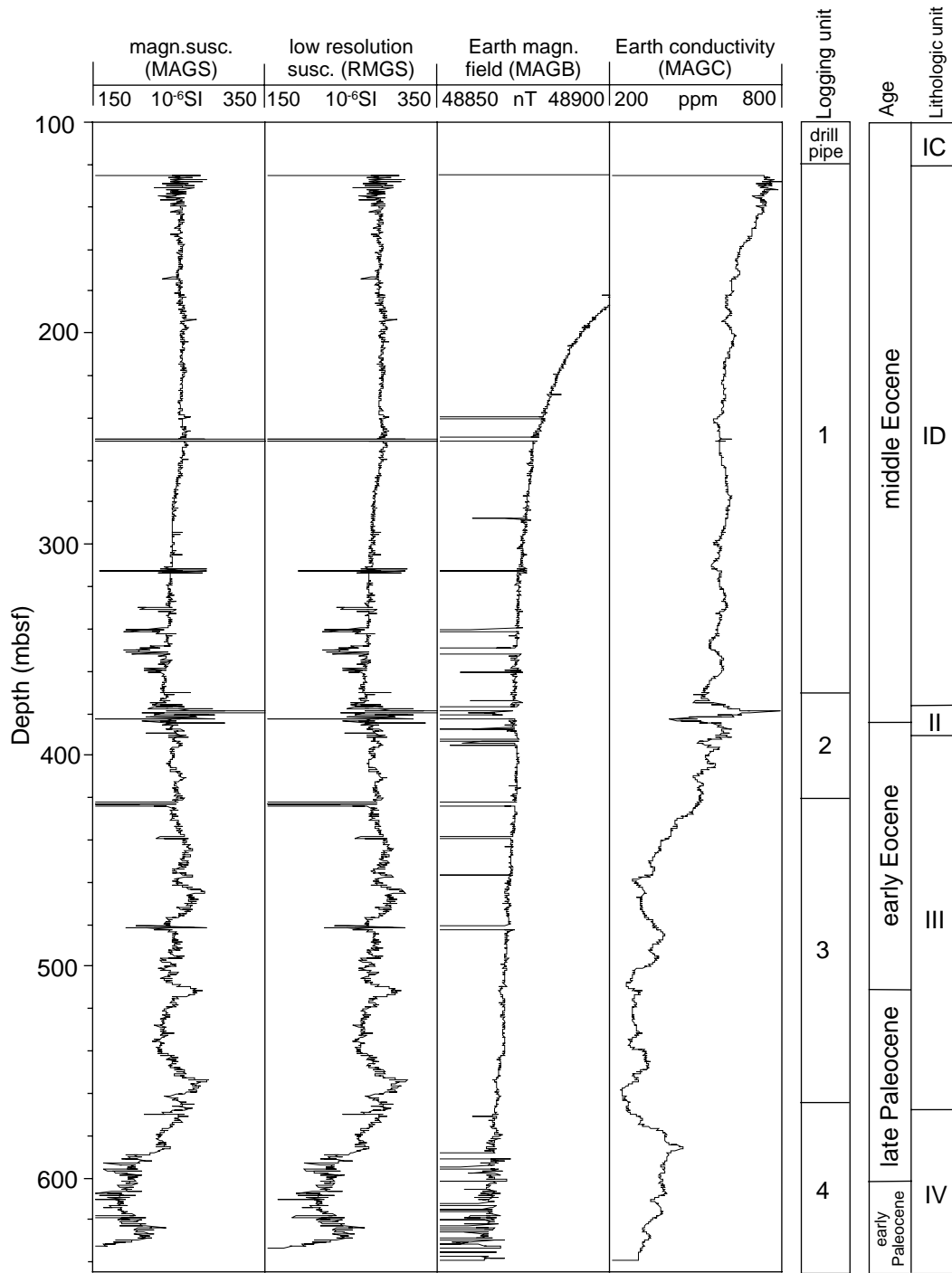
Figure 52. Selected downhole logs from the GHMT tool string for the interval 100–644 mbsf in Hole 1051A. From left to right, the tracks are magnetic suscep-tibility (MAGS), low-resolution susceptibility (RMGS), Earth's magnetic field (MAGB), and Earth's conductivity (MAGC). The logging units are discussed in the "Downhole Logging" section (this chapter); the lithologic units and ages are discussed in the "Lithostratigraphy" section (this chapter).
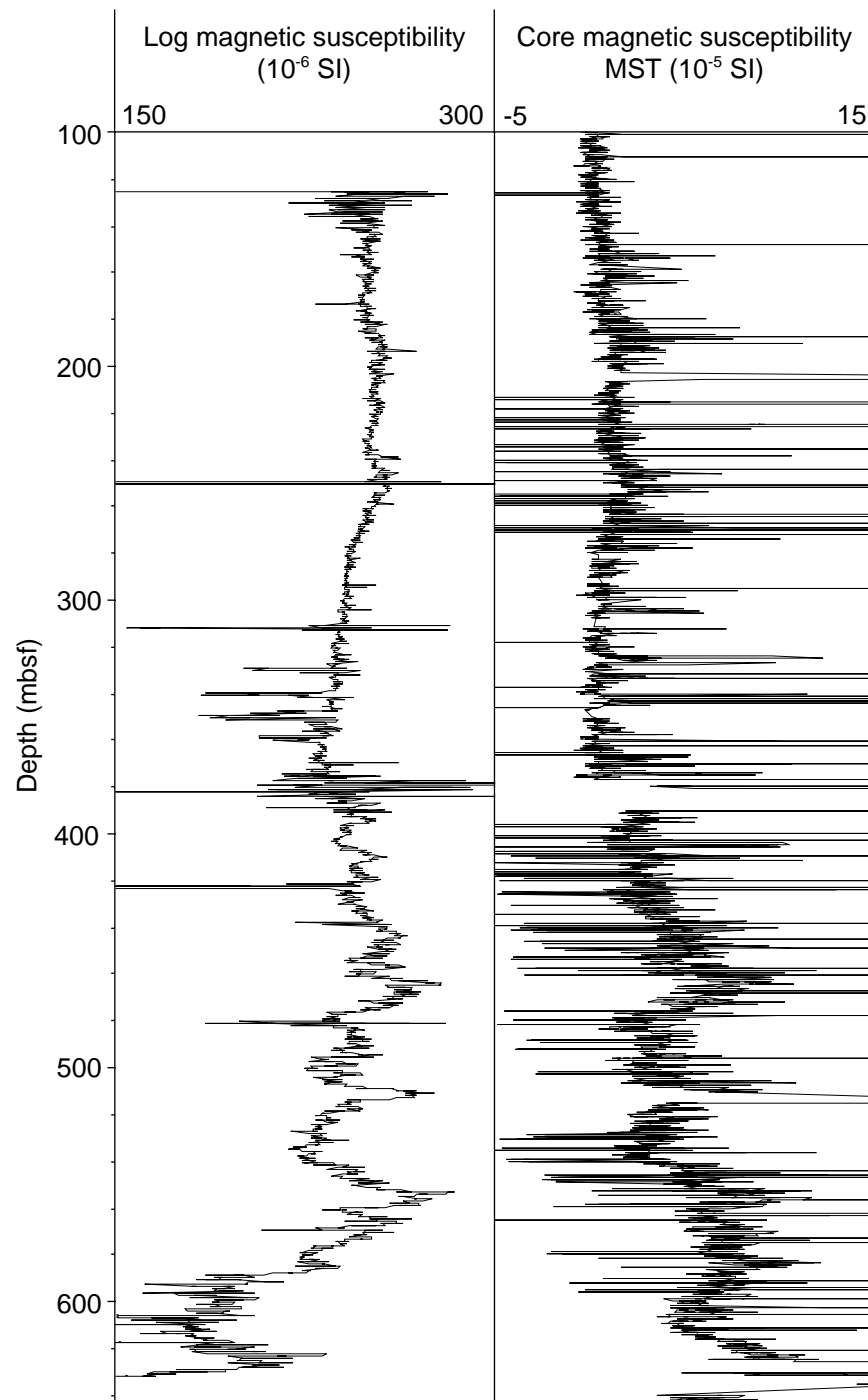
Figure 53. Comparison of log magnetic susceptibility data and core susceptibility measurements (MST; see "Physical Properties" section, this chapter) from Hole 1051A. Note the overall excellent correlation between the data sets.
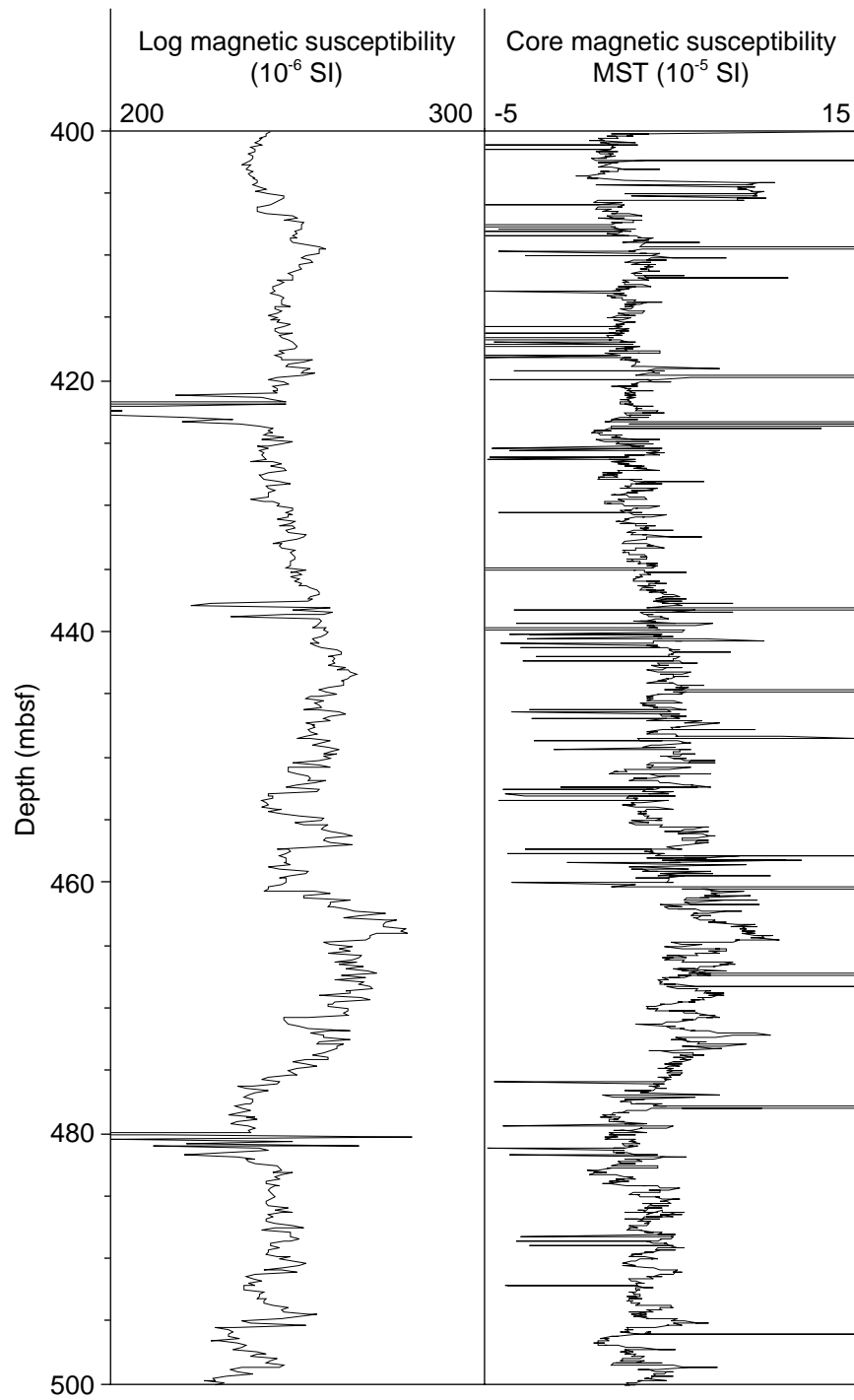
Figure 54. Comparison of log magnetic susceptibility and core magnetic susceptibility measurements (see "Physical Properties" section, this chapter) between 400 and 500 mbsf in Hole 1051A.
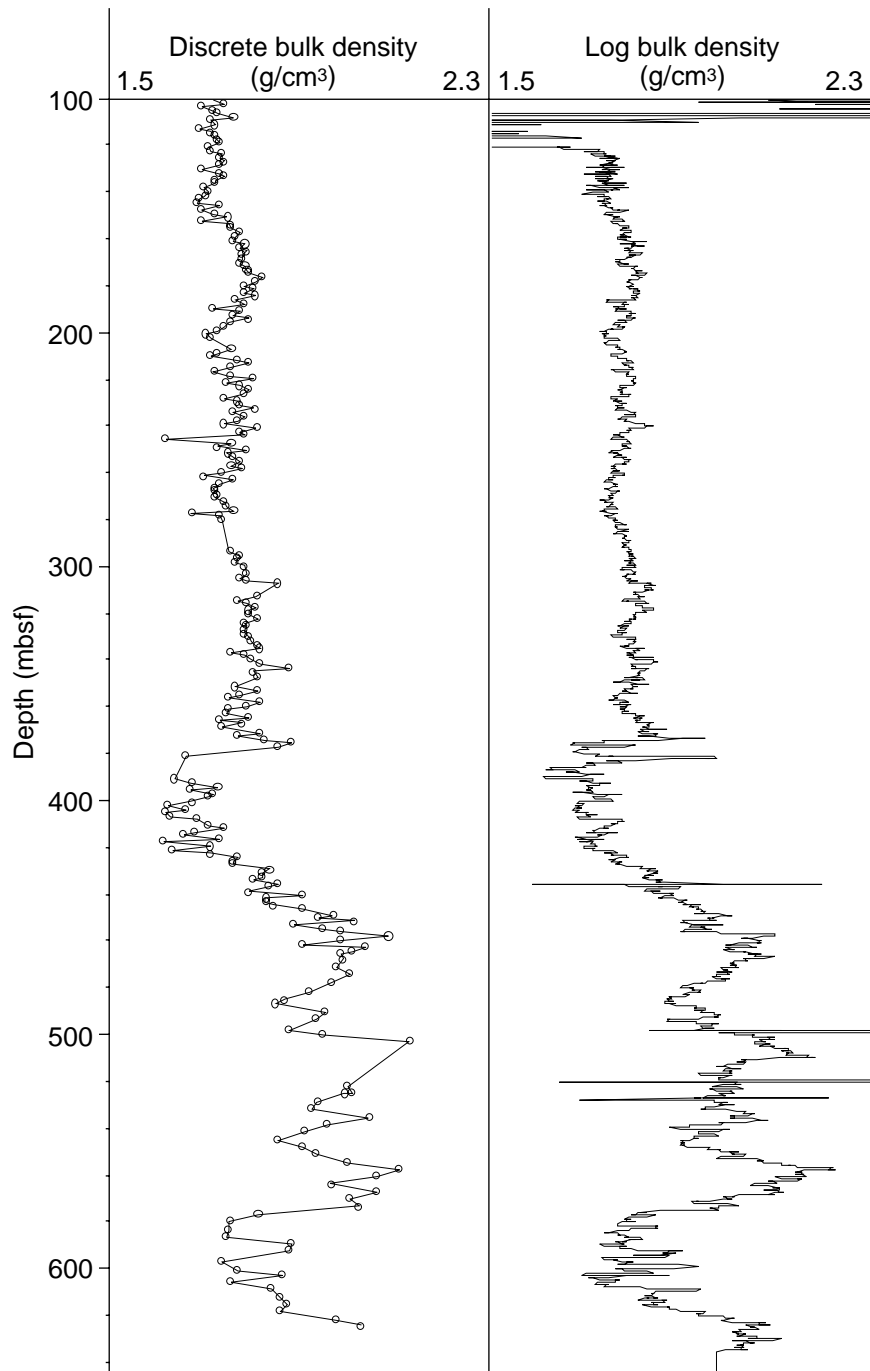
Figure 55. Comparison of core discrete bulk density (g/cm^3; see "Physical Properties" section, this chapter) and log bulk density data from Hole 1051A.